IDENTIFYING THE SEDIMENT SOURCE OF THE LOWER CENOMANIAN MANESS SHALE

By

JOSHUA ESCOBEDO DAVIDSON

Bachelor of Science, 2017
Texas Christian University
Fort Worth, Texas

Submitted to the Graduate Faculty
of The College of Science and Engineering
Texas Christian University
In partial fulfillment of the requirements
for the degree of

Master of Science

December 2023

IDENTIFYING THE SEDIMENT SOURCE OF THE LOWER CENOMANIAN MANESS SHALE

By

Joshua Escobedo Davidson

Thesis approved:

Major Professor

For The College of Science and Engineering

Acknowledgments

I would like to extend my heartfelt gratitude to the TCU department of Geological Sciences for the opportunities and support that cultivated my journey through both my undergraduate and graduate studies. My time at TCU began nearly a decade ago, and my involvement in this program has not only enriched my understanding of geology and its broader applications but also shaped my character in ways I never anticipated. I will forever treasure the bonds I have formed, the relationships I have made, and the knowledge I have gained through this program.

I would like to personally thank my advisor, Dr. Richard Denne, for taking a chance on me and giving me the opportunity to come on as one of his graduate students. His patience, guidance, and willingness to mentor me, despite my unconventional background, has been truly irreplaceable and instrumental in bringing me to this point in my academic and professional journey. I extend my sincere appreciation to Dr. Helge Alsleben for his guidance and wisdom, which have profoundly shaped both my graduate and undergraduate studies. I would also like to extend my gratitude to Dr. Omar Harvey, Dr. Arthur Busbey, Dr. Richard Hanson, Dr. John Holbrook, Dr. Nowell Donovan, and Dr. Esayas Gebremichael for the knowledge and insights I gained from their expertise in their respective fields throughout my experiences at TCU.

I am truly grateful for the assistance and mentorship provided by my friend, Skyler Wheeler, as his guidance as an industry professional greatly contributed to getting me where I am today. I would like to thank Marissa English and Sam Patterson for their contribution to this project by allowing me to utilize their data from previous studies. I would also like to thank my fellow graduate students, with special mention to Clayton Freimuth and Blake Bezucha, my peers who have shared this academic journey with me. Through our collective experiences at this institution, I am confident that these two individuals will remain as my close friends in the years to come. Lastly, I would like to thank my family for their unwavering love, support, and emphasis on the importance of education, which has been the cornerstone of my academic journey.

Table of Contents

List of Figures

List of Tables

I. Introduction:

The Maness Shale is a mudrock that was deposited during the Lower Cenomanian in the east Texas portion of the Gulf Basin that has only been identified in the subsurface (Fg. 1). Prior studies indicate that the Maness marks a major transition in depositional systems in the northern Gulf Coast, evolving from a predominantly oxygenated carbonate system, typified by the underlying Buda Limestone, to poorly oxygenated siliciclastic and mud-dominated systems, represented in Texas by the overlying Woodbine Sandstone and Eagle Ford Shale (Denne et al., 2016). Extensive siliciclastic deposition occurred in the East Texas Basin due to a major drop in sea-level, along with tectonic activity that uplifted surrounding topographic highs (Stehli et al., 1972; Laubach and Jackson, 1990).

Unconventional production of the Eagle Ford generated increased recognition of the Maness (Hentz and Ruppel, 2010; Hentz et al., 2014). Due to its clay rich composition, the Maness has been associated with complications during horizontal drilling of the overlying Eagle Ford near the San Marcos Arch (Patterson, 2018). However, recent studies have shown that Maness presence can be advantageous to operators as it can act as a fracture barrier between the Eagle Ford and underlying water-bearing strata (Patterson, 2018; Denne and Patterson, 2019). Denne et al. (2016) stated that the Maness Shale and the TOC-rich lower Eagle Ford were deposited under similar bottom water conditions, suggesting that the Maness Shale possesses source rock potential in some regions.

Certain characteristics of the Maness are still not fully understood, particularly the sediment source. Denne and Breyer (2016) constructed a thickness map of the Maness that suggests that the sediment source was from a location to the northeast of their study area near the San Marcos Arch. In a more recent study, thickness trends from an isochore map of the Maness constructed by English (2020) that extended previous maps by Denne and Breyer (2016) and Patterson (2018) to the central

Sabine Uplift suggested that this uplift is the most likely sediment source of the Maness Shale. English (2020) also tested the hypothesis that the Maness Shale is a potential source rock in the type area.

The purpose of this study is to develop a stronger understanding of the depositional source of the Maness Shale in east Texas and to determine if the Maness shale is a potential source rock. Using petrophysical well log data, this study mapped the thickness and lithofacies of the Maness to the south and west of the Sabine Uplift to determine its depositional trends. The analyses started in the East Texas Basin and extended farther east over the crest of the Sabine Uplift, and then to the south near the Edwards and Sligo Shelf margins. Previous studies by Anderson (1979), Denne and Breyer (2016), and English (2020) suggested that the Sabine Uplift is the potential source of the Maness because it was episodically active during the Cenomanian and Turonian. To this end, the current study was designed to test the following hypotheses:

1. The Maness Shale was sourced from the Sabine Uplift.
2. The Maness Shale contains source rock potential.

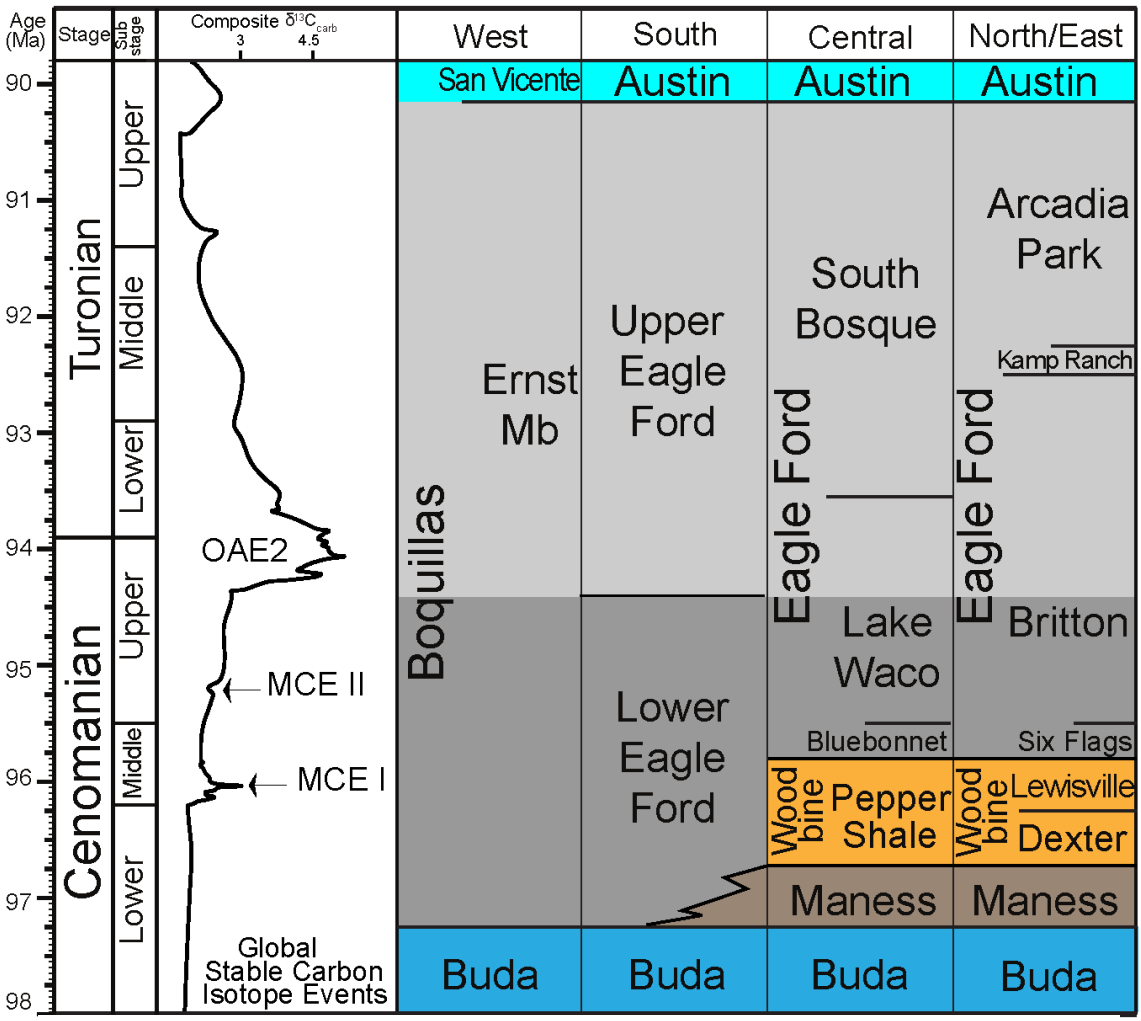

Figure 1. This figure depicts a stratigraphic column of the Cenomanian section in the East Texas and Brazos basins, with a carbon isotope curve documenting environmental changes over time. Provided by Denne (2023).

II. Regional Geology

The present study area is to the south, west, and southwest of the Sabine Uplift within the greater East Texas Basin of the Gulf Basin (Fig. 2). The northern limits of the Gulf Basin, including the Ouachita Uplift to the north of the study area, are a series of highs produced during collision and suturing between the Laurentia and Gondwana plates during the late Paleozoic (Leach and Rowan, 1986) (Fig.2). The north-south trending Mexia-Talco fault zone, which forms the western limits of the East Texas Basin, is also associated with the Paleozoic suture zone (Walthall and Walper, 1967). Subsequent seafloor spreading and crustal extension during the breakup of Pangaea culminated in the formation of the Gulf of Mexico during the Late Triassic- Jurassic (Galloway, 2008; Dennen and Hackley, 2012).

The process of halokinesis played a significant role in the structural and stratigraphic development of the East Texas Basin. The Louann Salt was deposited across rift-fill and Paleozoic basement rocks that were subaerially exposed during the Late Triassic-Early Jurassic (Seni and Jackson, 1984). Late Jurassic sedimentation triggered evaporite withdrawal that generated topographic salt structures such as pillows, diapirs, and post-diapirs (Seni and Jackson, 1984; Mondelli, 2011). This syn-depositional salt movement continued to modify the East Texas Basin from the time of deposition throughout the Cretaceous (Seni and Jackson, 1984).

The Sabine Uplift is a post-Jurassic tectonic feature that was episodically active during the Cenomanian and strongly influenced the development of the east Texas embayment. This uplift is a large, flat-topped, anticlinal structure located on the Texas-Louisiana border that defines the eastern boundary of the greater East Texas Basin (Powers, 1920). The rise of the Sabine Uplift did not begin until the Cenomanian, as Lower Cretaceous rocks either thicken or show little variation in

thickness across the structure (Tye, 1988; Laubach and Jackson, 1990). An angular unconformity between Upper and Lower Cretaceous deposits suggests tilting and subaerial exposure of Jurassic and Lower Cretaceous rocks related to purported upward movement of the structure during the Early Cenomanian, whereas thinning of Upper Cretaceous and Paleogene rocks across the Sabine Uplift indicate that it was a sporadically positive feature after the Early Cenomanian. Similarly, the San Marcos Arch, which forms the southwestern limits to the greater East Texas Basin, is also thought to have been a positive structure at that time (Murray, 1961; Luttrell 1977; Laubach and Jackson, 1990). The Angelina-Caldwell Flexure, located along the southern margin of the Sabine Uplift and oriented in an east-west direction, marks the boundary line between two different geological processes induced by Cenozoic sediment loading. To the north of the flexure, there was flexural uplift and erosion, while to the south, there was flexural subsidence (Glawe 1989; Ewing 2009; Pearson et al., 2012).

Two major Lower Cretaceous reef systems formed along the outer edge of the Texas shelf during the Barremian (Sligo) and Albian (Stuart City), enabling the development of vast carbonate platforms (Galloway, 2008; English, 2020).These reefs acted as sills for the Texas shelf throughout much of the Cretaceous, periodically restricting water mass movement and reducing oxygen levels to anoxic and euxinic conditions (Arthur and Sageman, 2005; Lowery et al., 2014; Phelps et al., 2014; Denne et al., 2016). In the current study, the Sligo and Stuart City shelf margins represent the southernmost boundary of the study area (Fig. 2).

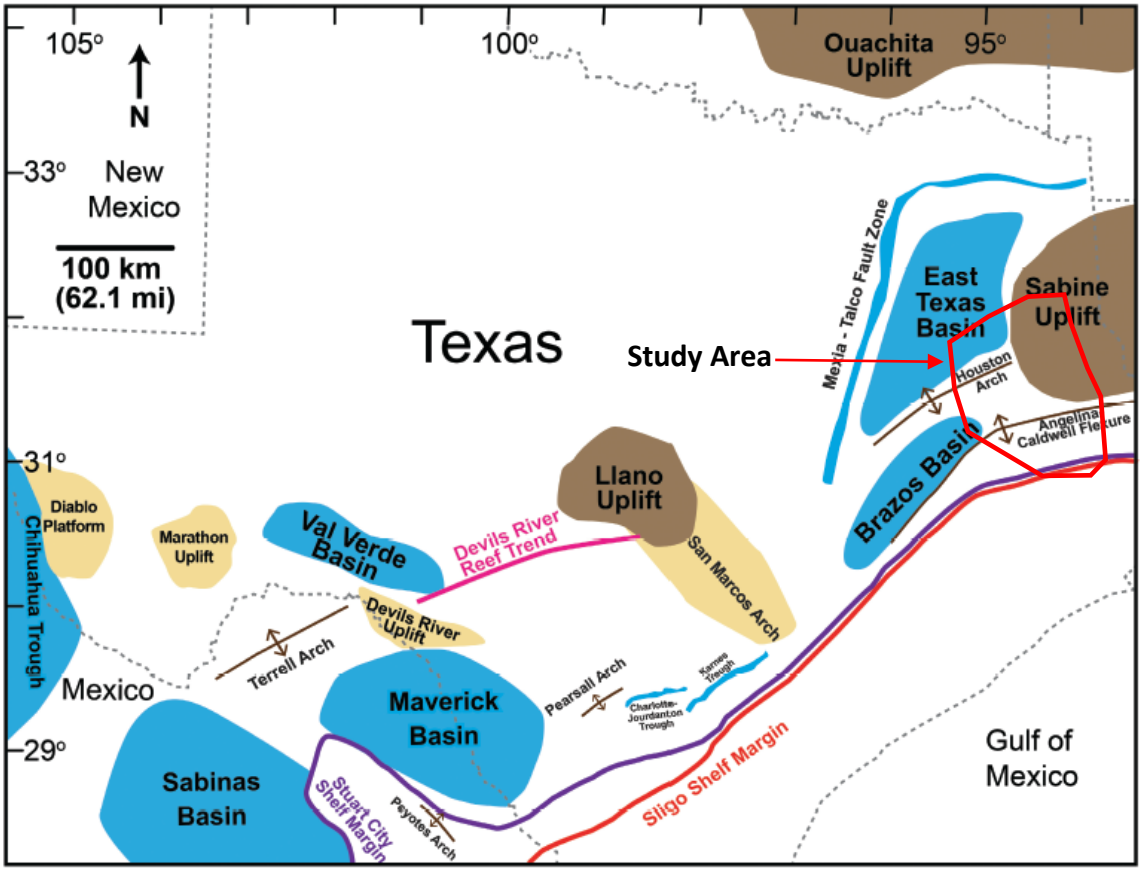

Figure 2. This map displays the structural features that influenced sediment deposition on the Texas shelf during the Early Cenomanian-Turonian period, including uplifts (shaded in brown), submarine platforms and arches (tan), and basins (blue). The Sligo margin is highlighted in red, whereas the Stuart City margin is in purple. The study area polygon is outlined in red. This figure is adapted from Denne and Breyer (2016).

III. Stratigraphy

Washita Group – Buda Limestone: The Upper Albian-Lower Cenomanian Washita Group in the East Texas Basin comprises the Kiamichi, Georgetown, Grayson, Buda Limestone, and the Maness Shale (Fig. 3). The Lower Cenomanian Buda Limestone occurs between the Grayson Shale and Maness Shale in east Texas, and between the Del Rio and Maness Shale in south Texas (Hentz et al., 2014), and extends from the Maverick Basin and Trans-Pecos region in southwest Texas to the Sabine Uplift in northeast Texas.

The Buda was deposited in a moderately shallow sea, with water depth less than 130 ft (40 m) deep (Valencia et al., 2021). Deposition occurred on the vast, flooded continental shelf of Texas, inland from the surviving remnant of the Sligo and Stuart City reef-complexes. Absence of Buda deposition occurs beyond these reef margins in deeper waters, likely due to reduction of the carbonate factory. A drop in eustatic sea level produced subaerial exposure of broad portions of the Gulf Basin during the Early Cenomanian after deposition of the Buda (Ruppel et al., 2012).

Washita Group - Maness Shale: The Maness Shale occurs between the base of the Woodbine and top of the Buda within the east Texas region of the greater East Texas Basin and between the Lower Eagle Ford Group and top of the Buda in South Texas. In its type well, Shell Oil's Maness Well No. 1 in Cherokee County, Texas (Fig. 4) (Bailey et al., 1945), the Maness is most easily identified by a sharp drop in the resistivity log from the overlying Woodbine Sandstone. Along with its clay-rich composition, the Maness is also recognized by its laminated to massive layering and the presence of calcium carbonate in this region (Bailey et al., 1945). It earned the nickname, "the bronze shale" of the East Texas Field because of its faint bronze or copper and gray splotches (Bailey et al., 1945). This can be seen in the Kinney 25 core from English (2020), which is nearby the Maness Well No. 1 (Fig. 5).

The deposition of the clay-rich Maness Shale occurred after the termination of Buda Limestone deposition (Denne and Breyer, 2016). After Maness deposition, sediment starvation occurred in the southernmost part of the basin near the San Marcos Arch, which resulted in deposition of a phosphatic lag at the top of the Maness Shale. This phosphatic lag is representative of a maximum flooding surface and condensed section and can be correlated from south Texas into the Brazos Basin (Denne et al., 2016). Additionally, the Lower Cretaceous reef systems in the East Texas Basin restricted seaway passage and produced predominantly anoxic bottom waters during Maness deposition (Denne et al., 2016). Beyond these drowned reef complexes where the Buda is absent due to carbonate factory reduction, Maness sediments were likely deposited on top of older carbonate rocks.

Woodbine Group: In east Texas, the Woodbine Group was deposited during the Middle Cenomanian, and occurs between the older, limestone-dominated Washita Group and the younger Eagle Ford Group (Hentz and Bonnaffe, 2010; Denne et al., 2016). Deposition of the Woodbine took place during a major sea-level regression that impacted the Gulf Coast Basin's depositional processes on a large scale (Salvador, 1991; Mancini and Pucket, 2005; Hentz and Bonnaffe, 2010).

The Woodbine is a sand-rich, fluvial-deltaic complex dominated by coarse, siliciclastic deposits in the East Texas Basin (Hentz and Bonnaffe, 2010). Woodbine sedimentation was controlled by structural highs, such as the Paleozoic Ouachita uplift in southern Oklahoma and Arkansas, the Sabine Uplift in northeast Texas and northwest Louisiana, and the Llano uplift with the associated, southeast trending San Marcos Arch in south-central Texas (Fig. 2) (Vallabhanemi et al., 2016; Denne and Breyer, 2016). Sediment transport from the Ouachita Uplift and Arbuckle Mountains contributed to much of the Woodbine deposition (Denne and Breyer, 2016). Also, Woodbine sediments were eroded and redeposited during Eagle Ford deposition due to the concurrent, upward movement of the Sabine Uplift (Halbouty and Halbouty, 1982; Denne and Breyer, 2016).

Extensive studies have been conducted on the Woodbine, as it has proven to be one of the most prolific conventional hydrocarbon reservoirs in the East Texas Basin. The Woodbine's thickness is approximated to be 890 ft (272 m) in the basin depocenter and gradually thins towards the Sabine Uplift, where it is as much as 250 ft (77 m) thick (Hentz and Bonnaffe, 2010). In the East Texas Basin, the Woodbine consists of two progradational sand units known as the Dexter and Lewisville formations (Denne and Breyer, 2016). Deposition of the Dexter was a result of a post-Maness relative sea level fall. After this regression, a minor transgression flooded the fluvial-deltaic Dexter and subsequently resulted in deposition of the upper Woodbine Lewisville Formation in the East Texas Basin (Denne and Breyer, 2016).

In the outer shelf to slope, the deltaic sediments of the Woodbine grade into a finer-grained facies, known as the Pepper Shale, which is present in the more distal regions of the East Texas Basin, such as the Brazos Basin (Adams et al., 2014). Similarities of the Maness and Pepper shales coupled with lack of biostratigraphic data from them, have caused these two shales to be misidentified as the same unit. Because Woodbine deposition did not reach the south Texas region of the Gulf Basin, the Maness Shale is overlain by the lower Eagle Ford in the producing region.

Eagle Ford Group: Deposition of the organic-rich Eagle Ford Shale occurred from the Middle Cenomanian through Upper Turonian in east Texas (Hentz et al., 2014; Denne et al., 2016). The Eagle Ford Group is vertically constrained by the underlying Woodbine and the overlying Austin Chalk in the East Texas Basin. In this region, the Eagle Ford Group consists of reworked Woodbine sediments generated from the upward movement of the Sabine Uplift that subaerially exposed Woodbine sediments and resulted in the erosion and redistribution of the mud-dominated Eagle Ford sediments in the East Texas Basin during the Upper Cenomanian (Hentz et al., 2014; Denne and Breyer, 2016).

During deposition of the lower Eagle Ford, anoxic to euxinic bottom-water conditions dominated in deeper regions of the East Texas Basin. This was a product of the Sligo and Stuart City reef systems acting as sills and restricting bottom water circulation (Denne et al., 2014; Lowery et al., 2014). The Late Cenomanian to Early Turonian marked the onset of Oceanic Anoxic Event 2 (OAE2) contemporaneously with a significant transgression (Arthur and Sageman, 2004; Denne and Breyer, 2016). The organic-lean upper Eagle Ford was deposited during and after this transgression when oxygenated waters flooded the Western Interior Seaway and the Texas shelf (Denne et al., 2016).

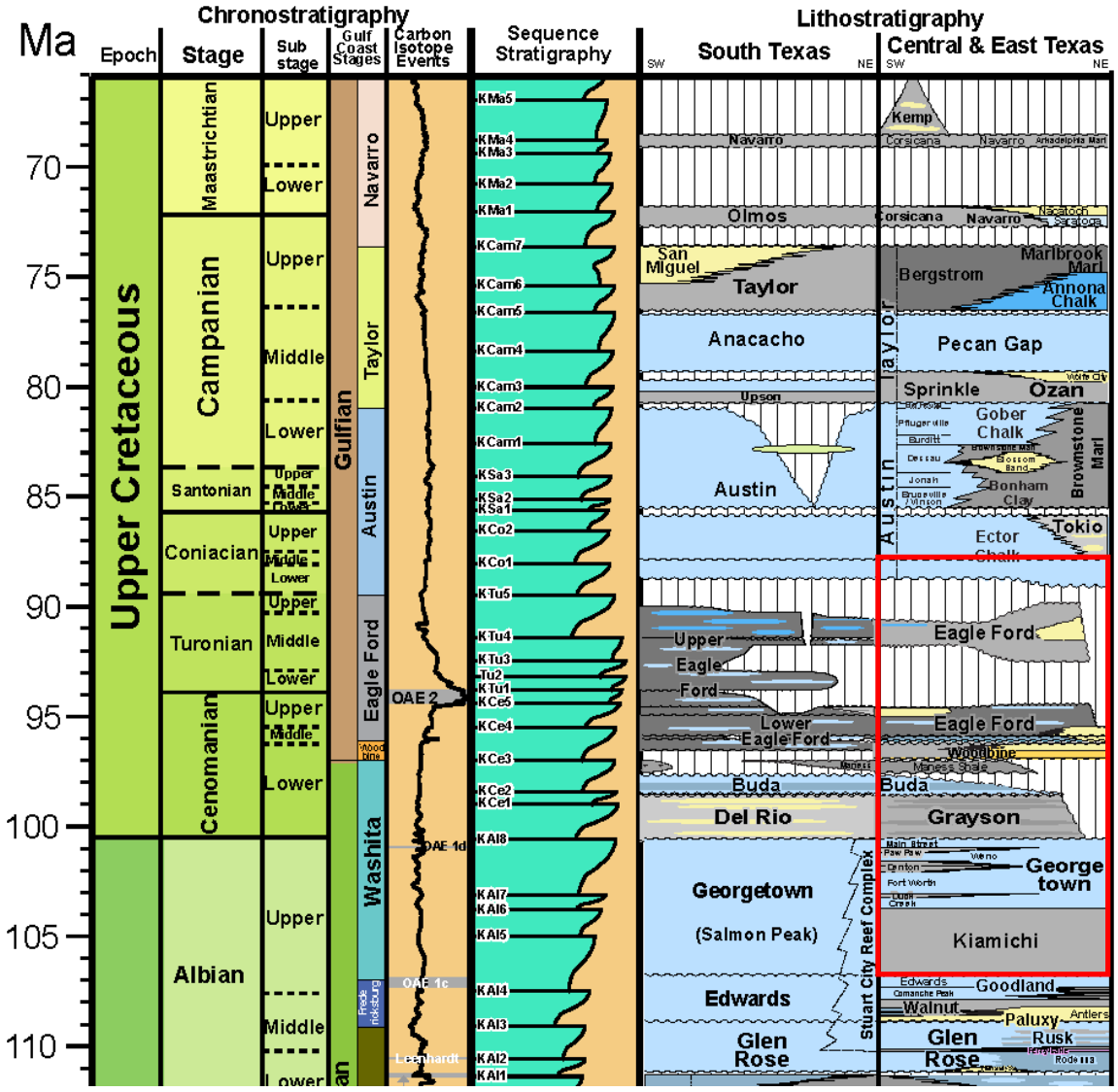

Figure 3. Chrono- and lithostratigraphic column depicting the geological history of South, Central, and East Texas in the Greater Gulf Coast Basin, spanning from the Middle Jurassic through the Upper Cretaceous, provided by Denne (2023). The red rectangle on the column delineates the interval under investigation in this study.

IV. Previous Studies

The Lower Cenomanian Maness Shale was first identified by Bailey et al. (1945) in the subsurface of the East Texas Field. It was initially recognized in a core from the Maness Well No. 1 in eastern Cherokee County drilled by Shell Oil Company. At its type locality, the Maness is constrained by the Woodbine at the top and Buda at the base. Depths of this mudrock in the Maness Well No. 1 occur at 4,705 feet to 4,766 feet (1434-1453 m) (Fig. 4) (Bailey et al., 1945).

Throughout historical literature, the Maness has been subject to varying interpretations, with different perspectives presented in publications by various authors (Ambrose et al., 2009; Ambrose and Hentz, 2010; Hentz and Bonaffe, 2010; Hentz et al., 2014; Hudson, 2014; Denne et al., 2016; English, 2020). Lozo (1951) described the misidentification of the Maness in Cherokee County, where it was erroneously correlated with the basal Woodbine Clay, Del Rio Clay in south Texas, and the Grayson Marl in north Texas. The Maness Shale does not crop out, therefore, much of the miscorrelations made in previous work can be attributed to data limitations. Notably, Lozo (1951) made a significant stride by being the first to describe and illustrate the foraminifera found within the Maness.

Subsequently, Anderson (1979) used well logs to construct a cross section from Rains County through Van Zandt, Smith, Cherokee, Anderson, Leon, and Madison counties in his study for the Louisiana Geological Survey (Fig. 6). During his mapping in the southern and southeastern regions, Anderson (1979) observed a shift in facies within Anderson and Leon counties. This shift prompted him to modify the nomenclature, renaming the Maness Shale as the “Malvern Shale.”

Barrett and Goodson (2006) tested the reservoir-quality of nine Eagle Ford/Woodbine sandstone wells in Tyler County, Texas. The methods in their study involved analyzing foraminiferal abundances and diversity changes in 10-ft (3 m) cuttings from the base of the Austin Chalk through

the top of the Buda Limestone. Their findings show that the Maness displays fining-upward sandstone patterns, which are interpreted as distributary settings in this region (Fig. 7) (Barrett and Goodson, 2006).

Ambrose et al. (2009) and Hentz et al. (2014) have contributed to our understanding of the Maness Shale deposition. Ambrose et al. (2009) developed a sequence stratigraphic framework in the East Texas Field, characterizing the Woodbine succession, which encompasses the Maness Shale. They identified the lower Maness as a regionally transgressive, upward-fining, retrogradational unit and the upper Maness as a regressive, upward-coarsening, progradational unit (Fig. 8). Both authors recognized the presence of a third-order maximum flooding surface (MFS) that delineates the upper and lower Maness systems. Ambrose et al. (2009) identified the Maness interval as the lower Woodbine in their study. However, the framework used in their study categorizes the Maness interval as the initial sequence within the broader Woodbine succession. This reinforces its classification as Maness despite not being explicitly designated as such in Ambrose et al. (2009)'s description at that time. Hentz et al. (2014) extended these observations into more distal regions of the East Texas Basin, including Leon, Houston, and Madison counties (Fig. 9) They confirmed the characteristics of the lower and upper Maness units as described by Ambrose et al. (2009).

Bunge (2007) integrated seismic stratigraphy in the downdip region of the current study area in Polk County south of the Edwards Reef and Sligo Shelf Margin (Fig. 10). The purpose of this study was to create new and more in-depth depositional models for the Woodbine Formation in east Texas. Although the Woodbine shows thinner sediment packages along the ramp margin, downdip packages display a thickness of up to 2500 ft (760 m) (Bunge 2007) (Fig. 10). Bunge (2007) made no reference of the Maness Shale in this paper. However, the Maness corresponds to the equivalent lower Woodbine, Sequence A, B shown in the Rice University No. 1 type log (Fig. 11).

Denne et al. (2016) attempted to resolve the stratigraphic issues in previous geologic literature and generated consistency in the stratigraphic nomenclature of the Maness, Woodbine, and Eagle Ford. These misunderstandings were due to complex facies changes across the San Marcos Arch as well as data limitations. Their study included biostratigraphic, geochemical, X-ray diffraction (XRD) mineralogical, X-ray fluorescence (XRF) elemental, and petrographic analyses with well logs that were used to interpret the Maness in the south Texas region of the Gulf Basin, adjacent to the San Marcos Arch (Jennings and Antia, 2013; Denne and Breyer, 2016; Denne et al., 2016). Cores and thin sections acquired from locations near the San Marcos Arch identified ammonites, foraminifera, and calcareous nannofossils that constrained the age of the Maness in that location to the mid to Early Cenomanian (Denne et al., 2016). The elemental analyses identified significant amounts of molybdenum, vanadium, and uranium. These redox proxies suggest that the Maness was deposited in a restricted basin with anoxic to euxinic bottom water conditions (Denne et al., 2016). They also identified a unique gamma ray spike that was interpreted as a phosphate lag that was interpreted as a maximum flooding surface (Denne et al., 2016) (Fig. 12).

Denne and Breyer (2016) were the first to create an isochore map of the Maness Shale. This map revealed a thickness trend from northeast to southwest (Fig. 13), suggesting that sediment deposition originated from a northern source (Denne and Breyer, 2016).

Patterson (2018) and Denne and Patterson (2019) performed thickness, geomechanical, and elemental analyses of the Maness within regions near the San Marcos Arch in south Texas. The intent of their studies was to determine if the Maness Shale acted as a fracture barrier that separates the organic rich Eagle Ford Group from underlying water-wet carbonates. Mineralogic (XRD) and geomechanical analyses were performed on conventional cores taken from two wells in Lavaca and Fayette Counties. Patterson (2018) focused heavily on geomechanics to understand the mechanical response of the Maness Shale. She found that the Maness is more clay rich than the

Eagle Ford, thus making it a weaker mudrock (Patterson, 2018). Patterson (2018) also correlated four horizons across 345 wells to create structure and isochore maps throughout her study area. The isochore map trends suggest that the Maness sediments were transported from regions to the northeast of her study area (Patterson 2018).

English (2020) conducted the most recent research, which consisted of well log correlations, core descriptions, and sample analyses. The purpose of her study was to determine the sediment source and paleoenvironment of the Maness in its type area. Core analyses involved two conventional cores from Gregg and Rusk counties. Sample analyses included petrographic, biostratigraphic, mineralogic (XRD), elemental (ICP-MS and ICP-OES), and organic geochemical analyses. The study found that the Maness in its type area is the same age as the Maness of the San Marcos Arch. Based on her elemental analyses, the bottom waters of the Maness were found to be oxic to suboxic. However, there was evidence of a shift towards increasing anoxia in the upper parts of the Maness interval, as indicated by the accumulation of redox proxies. Using TOC measurements as a criterion, organic geochemical analysis indicated that the Maness possesses minor source rock potential within the East Texas Field, with an average total organic carbon (TOC) measurement of 2.8% in the two cores studied by English (2020). Interpretation of isochore maps based on log correlations from the Brazos Basin to the East Texas Field suggested that the Sabine Uplift was a likely source of the Maness Shale (Fig. 14).

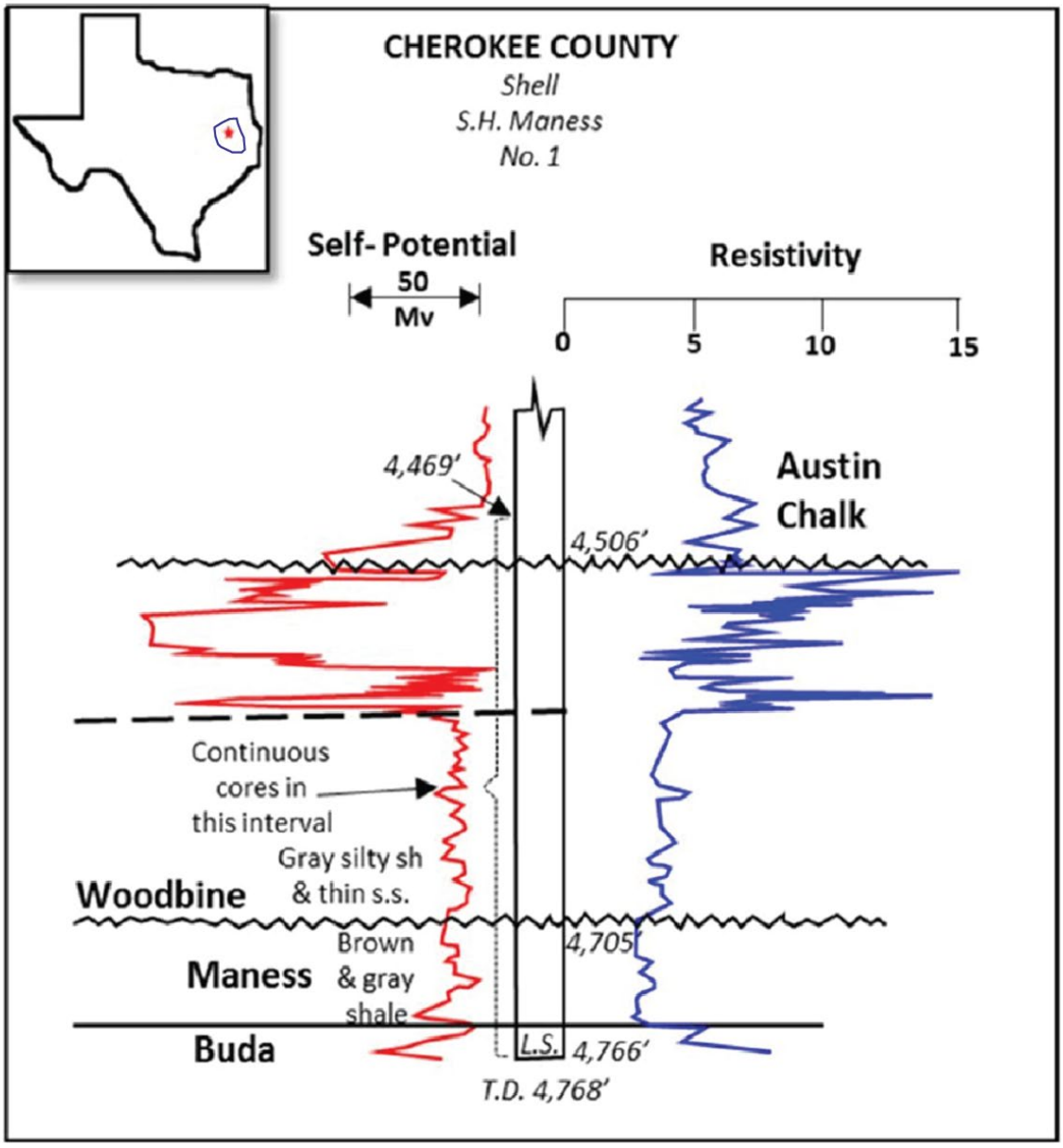

Figure 4. Well log from the S.H. Maness No. 1, which was the first to identify the Maness Shale in Cherokee County, Texas (indicated by the red star) using spontaneous potential and resistivity. The study area is outlined in royal blue. This figure is an adaptation from Bailey et al. (1945), Patterson (2018), and English (2020).

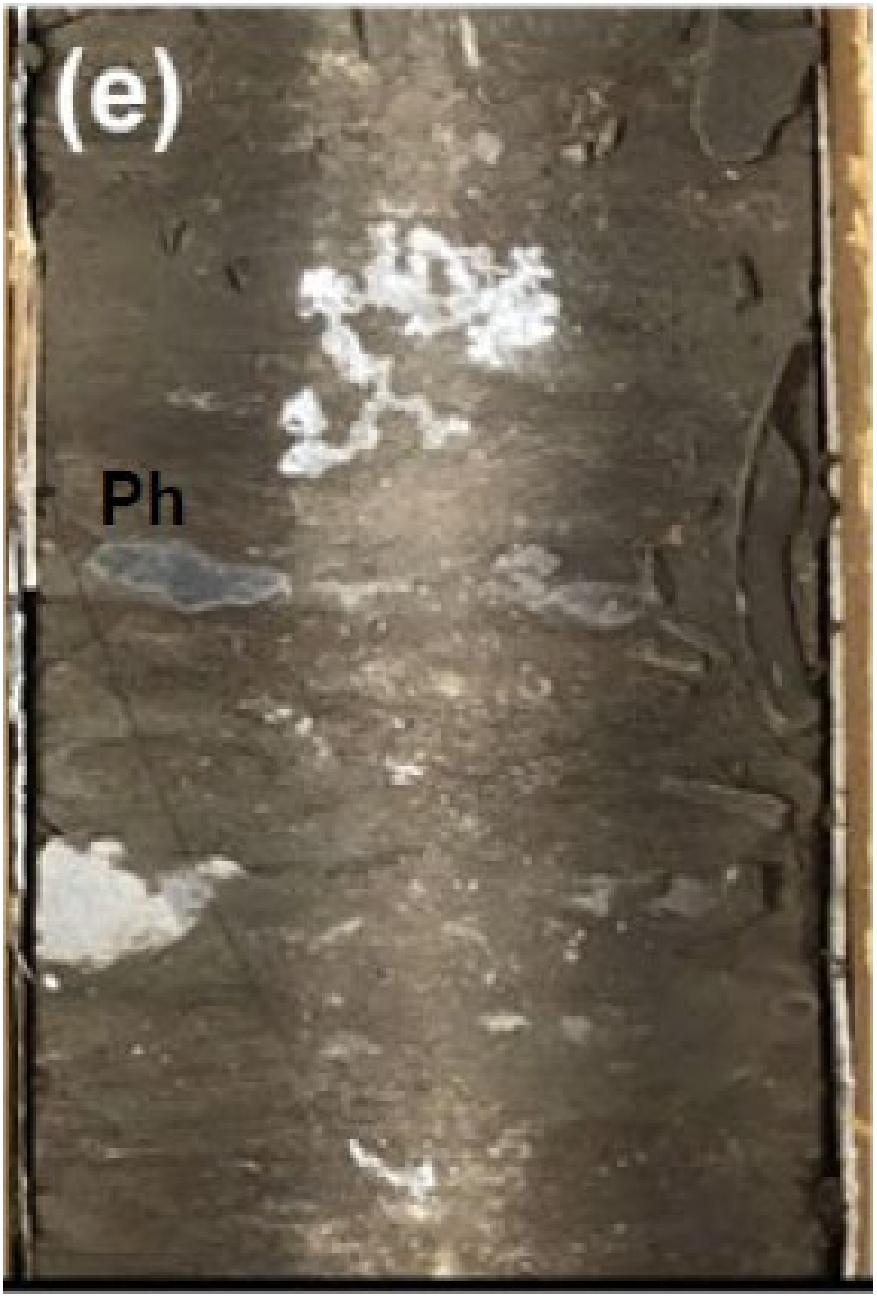

Figure 5. Core photograph of the Kinney 25 core from English (2020) displaying a phosphate (Ph) concretion within the copper-colored Maness shale as described in the type location in Cherokee County (Lozo, 1951).

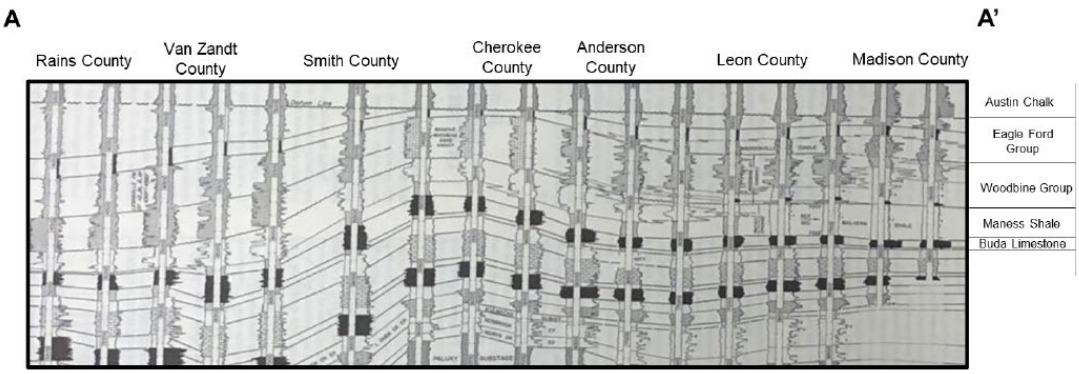

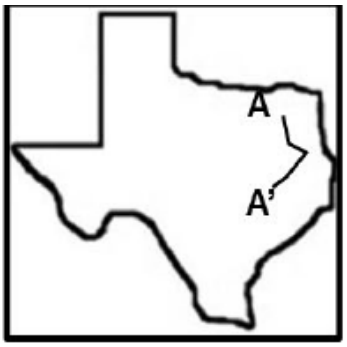

Figure 6. Cross section extending from north Texas to the Brazos Basin, based on interpretations made by the Louisiana Geological Survey. The cross section includes correlations for several stratigraphic units, namely the Buda Limestone, Maness Shale (also referred to as Malvern Shale in Anderson (1979)'s study, Woodbine Group, Eagle Ford Group, and Austin Chalk. The location of the cross section is indicated on the map from point A to point A'. The figure has been adapted from Anderson (1979).

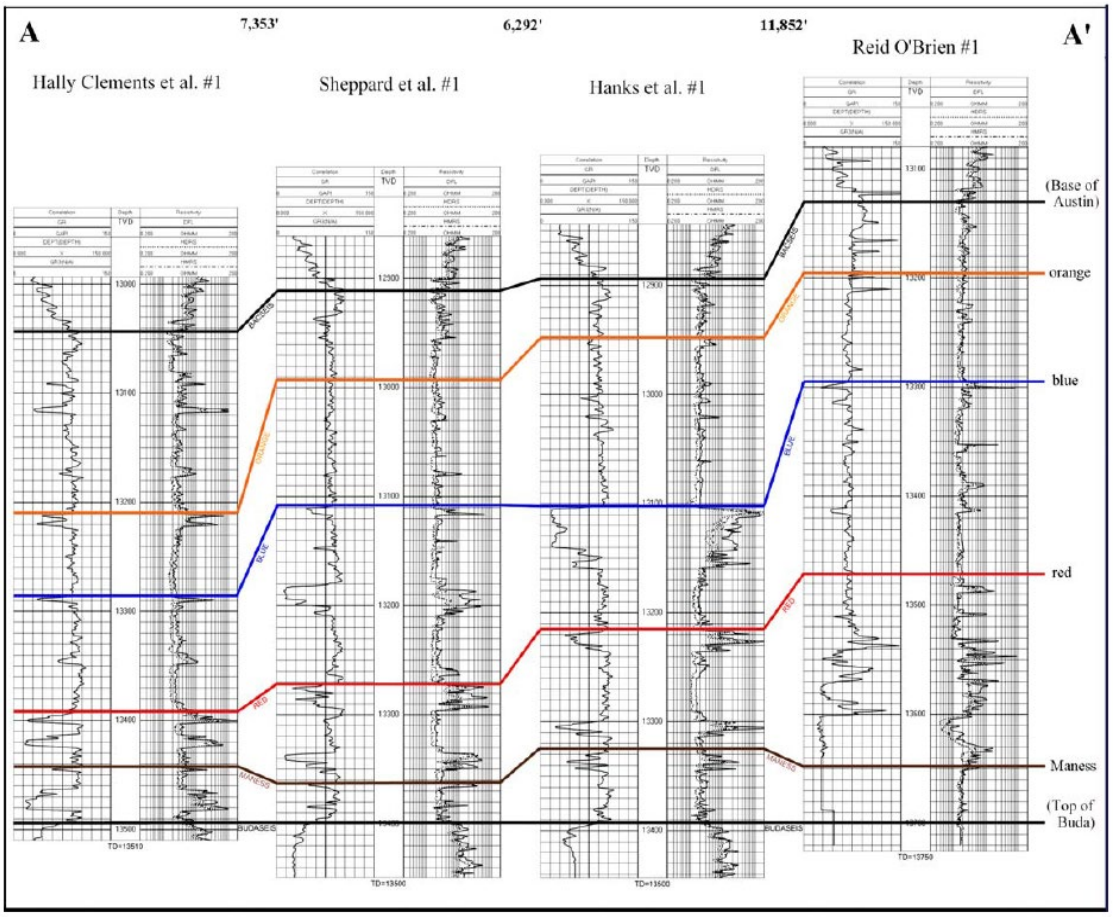

Figure 7. Representative log correlation for the stratigraphic interval from the base of the Austin Chalk to the top of the Buda (indicated by the two black lines) taken from Barrett and Goodson (2006). The top of the Maness, as interpreted in this study, is denoted by the brown line. The Hanks et al. #1 well was used as one of the three type logs in the current study.

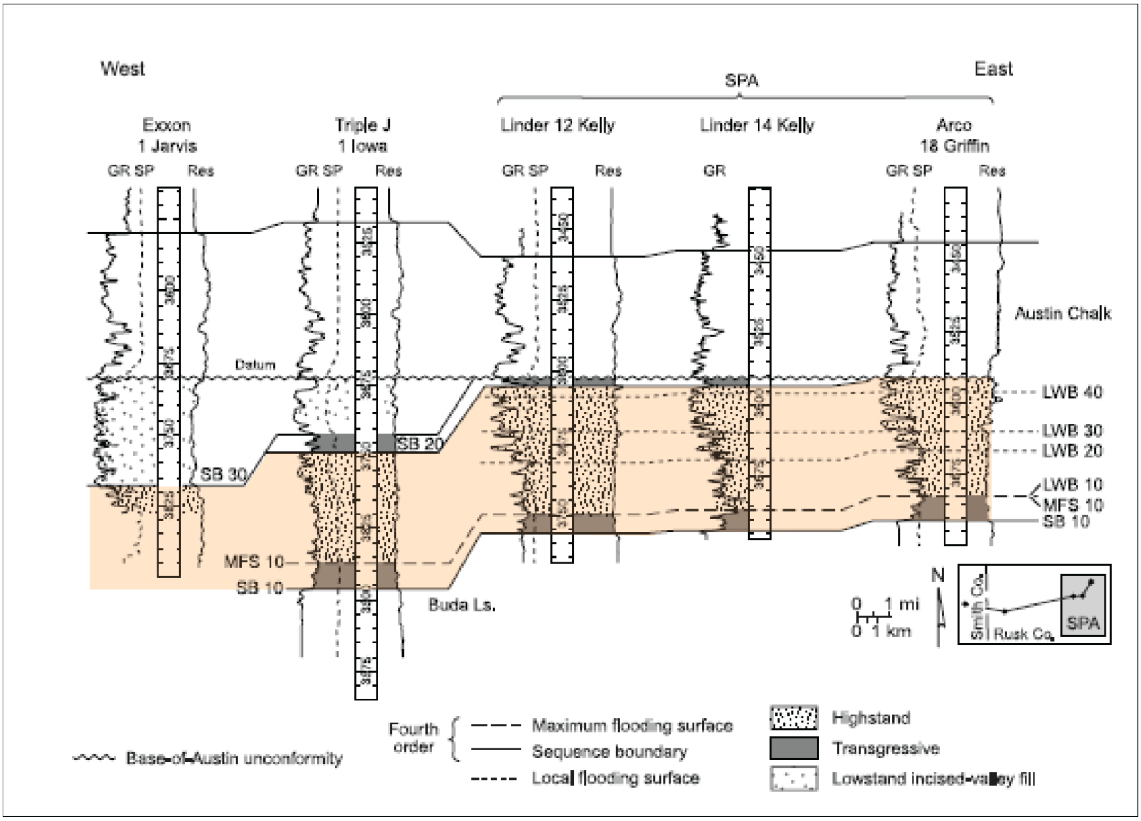

Figure 8. Cross-section modified from on Ambrose et al. (2009) in the East Texas Field, illustrating fourth-order sequences and systems tracts from the top of the Buda Limestone to the base of the Austin Chalk. The Maness interval is designated as the transgressive (lower-Maness) and highstand (upper-Maness) units, positioned below SB 20 and the base of the Austin Chalk unconformity, highlighted in orange. MFS 10 marks the intra-Maness, with the datum set at the base of the Austin unconformity. I is important to note that in Ambrose et al. (2009)'s study, the Maness interval is referred to as the lower Woodbine.

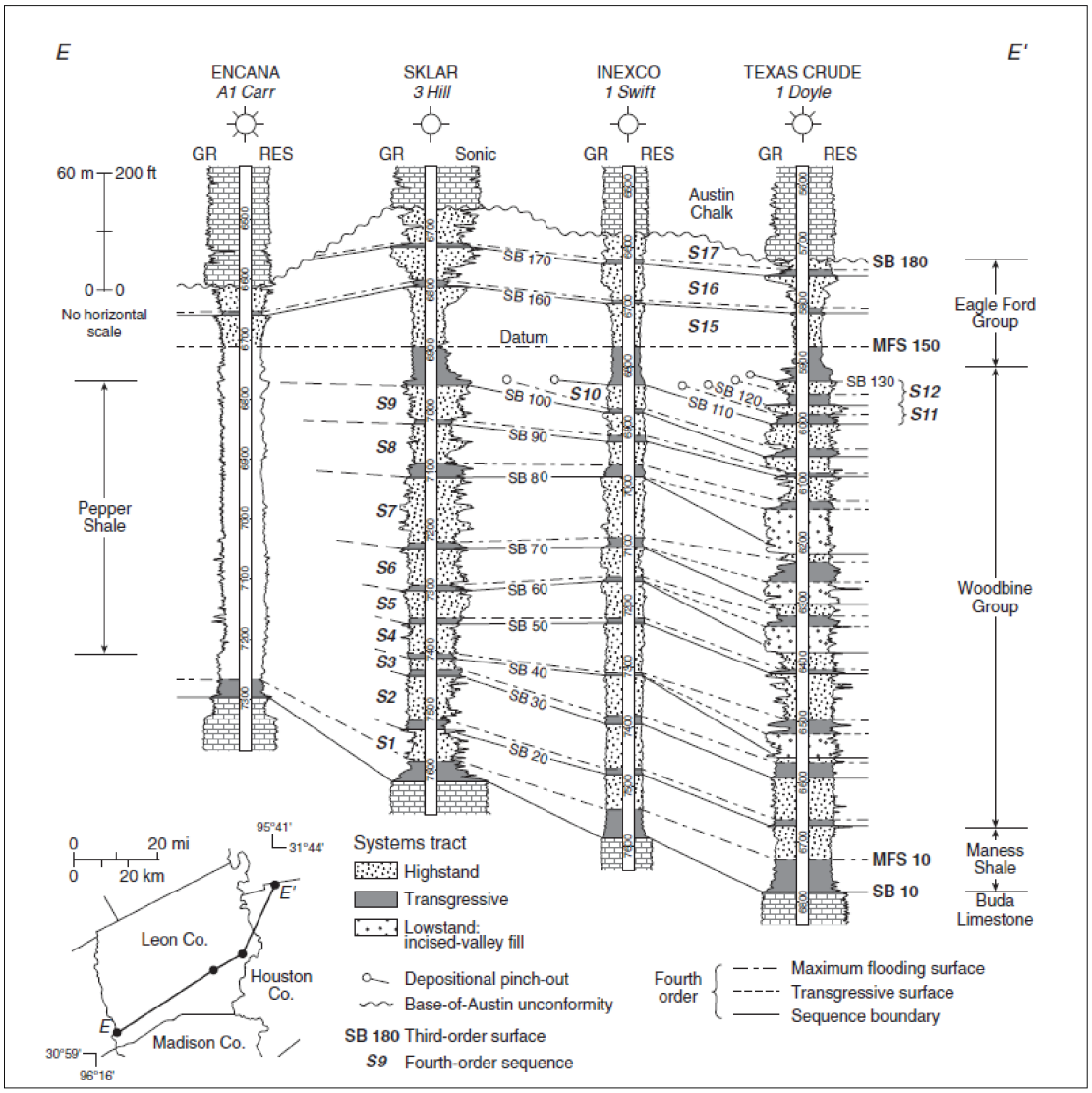

Figure 9. This cross-section from Hentz et al. (2014) in the southern part of the East Texas Basin illustrates fourth-order sequences and systems tracts spanning from the top of the Buda Limestone to the base of the Austin Chalk. Within this representation, the entire Maness interval is designated as S1, signifying the initial sequence among a total of 17 fourth-order sequences within this entire stratigraphic interval. The intra-Maness is marked by MFS 10 in this cross-section. The Maness interval is positioned beneath SB 20, and the datum is set at MFS 150, near the base of the Eagle Ford Group.

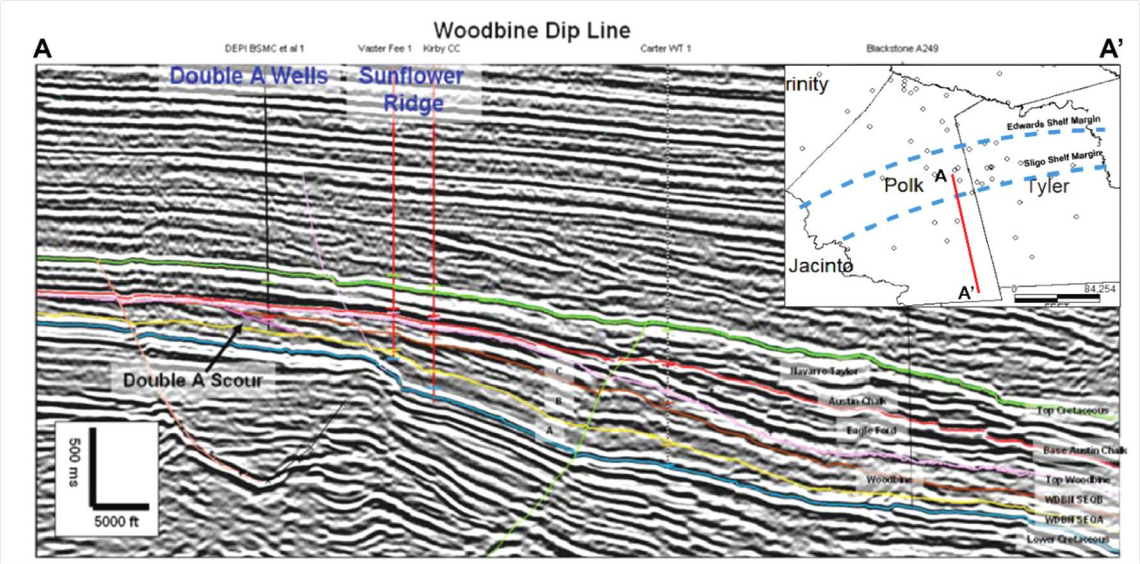

Figure 10. Seismic line from the Knight Survey in Polk County constructed by SAI (Seismic Assistants Inc.) and modified from Bunge (2007). This seismic survey displays the depositional episodes of Cretaceous aged sediments that occur along the shelf-slope break. Horizon picks are as follows: top of the Upper Cretaceous is in green, base of the Austin Chalk is in red, top Woodbine sequence C is in pink, top Woodbine sequence B is in brown, top Woodbine sequence A is in yellow, and the top of the Lower Cretaceous is in blue (Bunge, 2007).

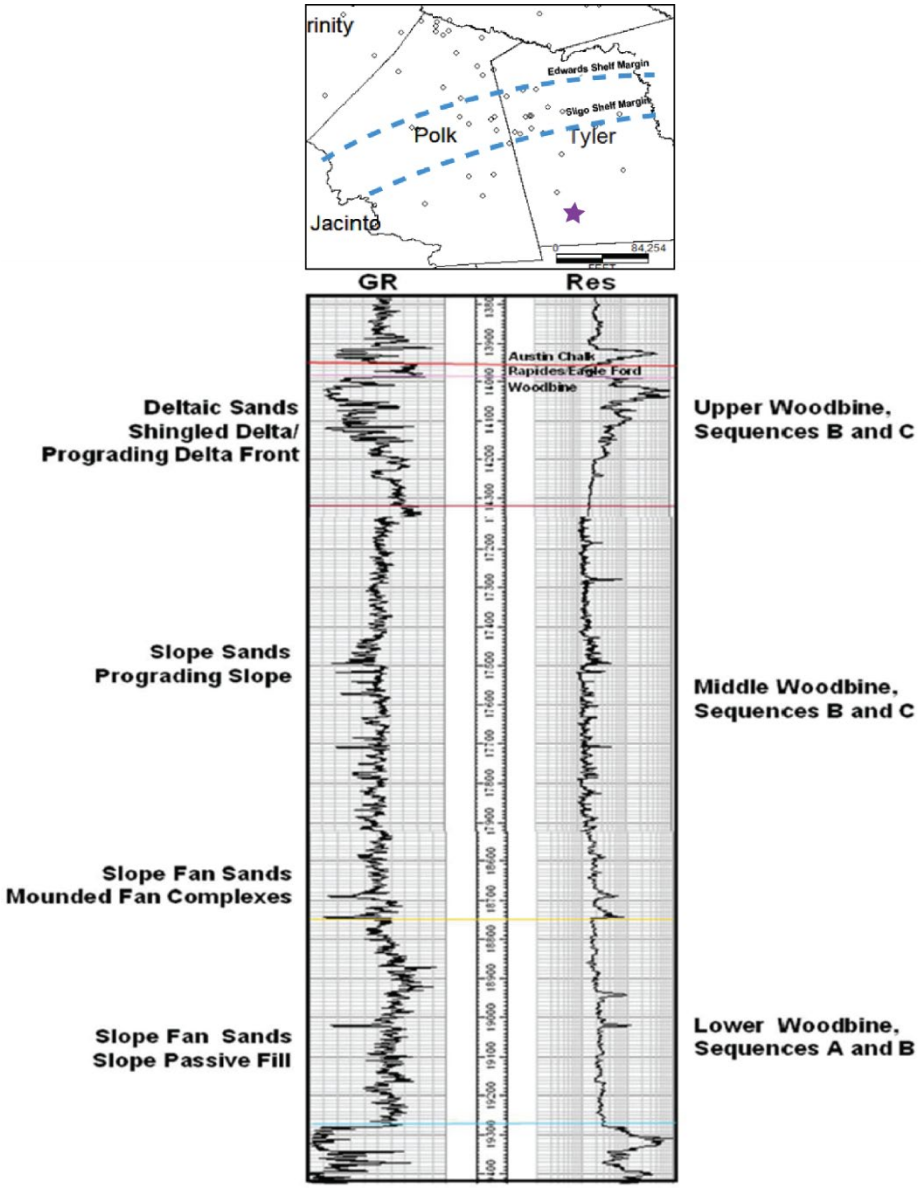

Figure 11. Downdip type log modified from Bunge (2007). This type log is from the Rice University No. 1 well (purple star) operated by Arco Oil & Gas Company in the southern part of Tyler County. The stratigraphic interval displayed in this log ranges from the base of the Austin Chalk to the top of the Lower Cretaceous.

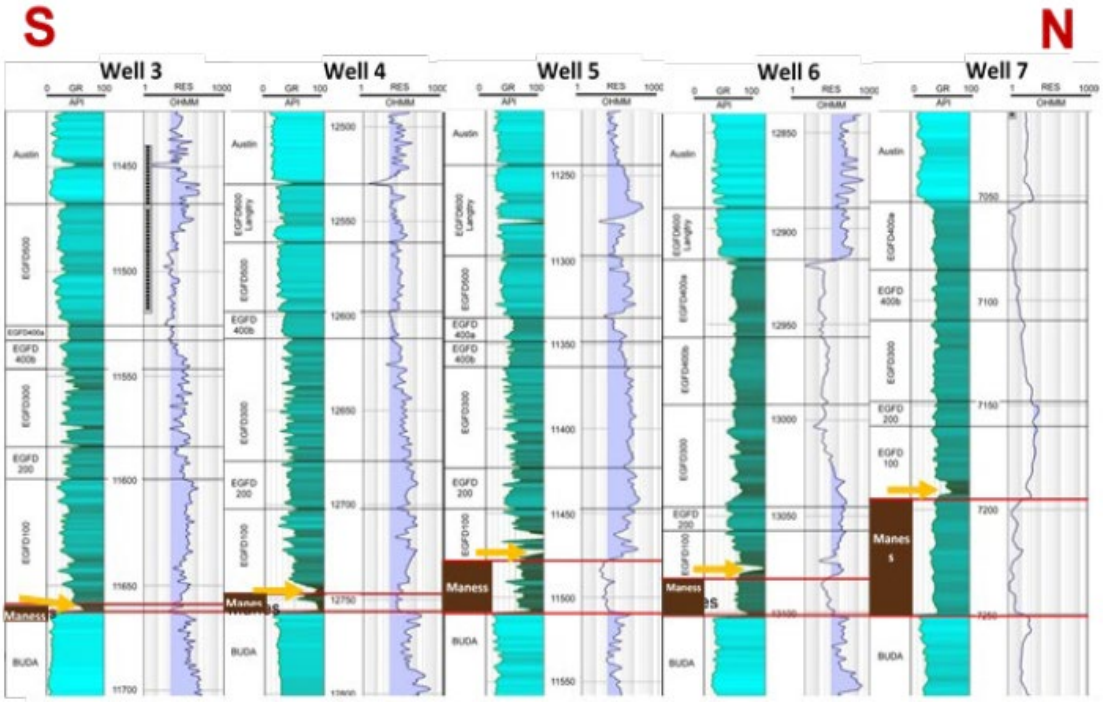

Figure 12. This figure depicts well log correlations based on the seven depositional episodes identified by Denne et al. (2016). The isopach map in figure 12 identifies each of the wells with a pink star. The reference point is positioned at the boundary between the top of the Buda and base of the Maness. The yellow arrows highlight a distinctive high gamma ray spike that corresponds to the phosphate-lag at the top of the Maness. This spike is observed to correlate consistently across the San Marcos Arch and into the East Texas Basin. This log correlation confirms the isopach map's depiction from figure 12 of the Maness interval thickening to the northeast. Image from Denne and Breyer (2016) and modified by English (2020).

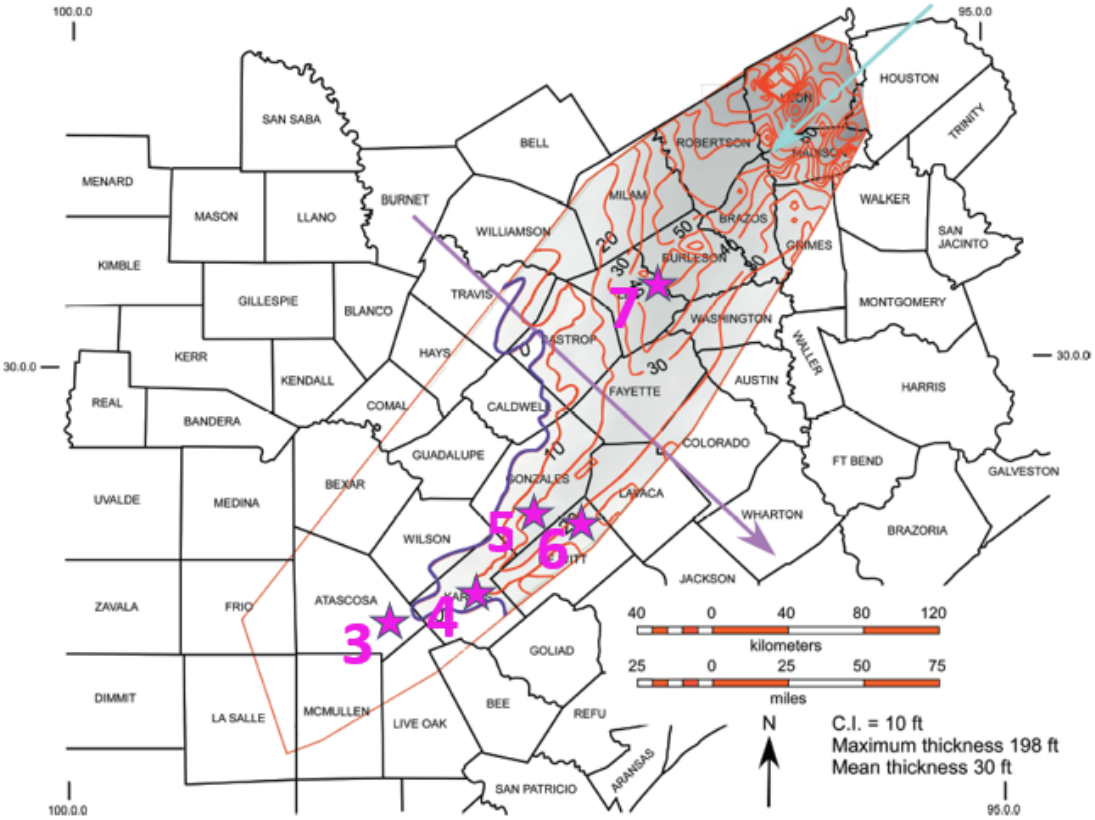

Figure 13. Isochore map by Denne and Breyer (2016). This map depicts thickness variations of the Maness Shale extending from the south Texas producing region to the northeast, crossing the San Marcos Arch (indicated by the purple arrow), and into the East Texas Basin. The inferred direction of deposition is represented by the blue arrow.

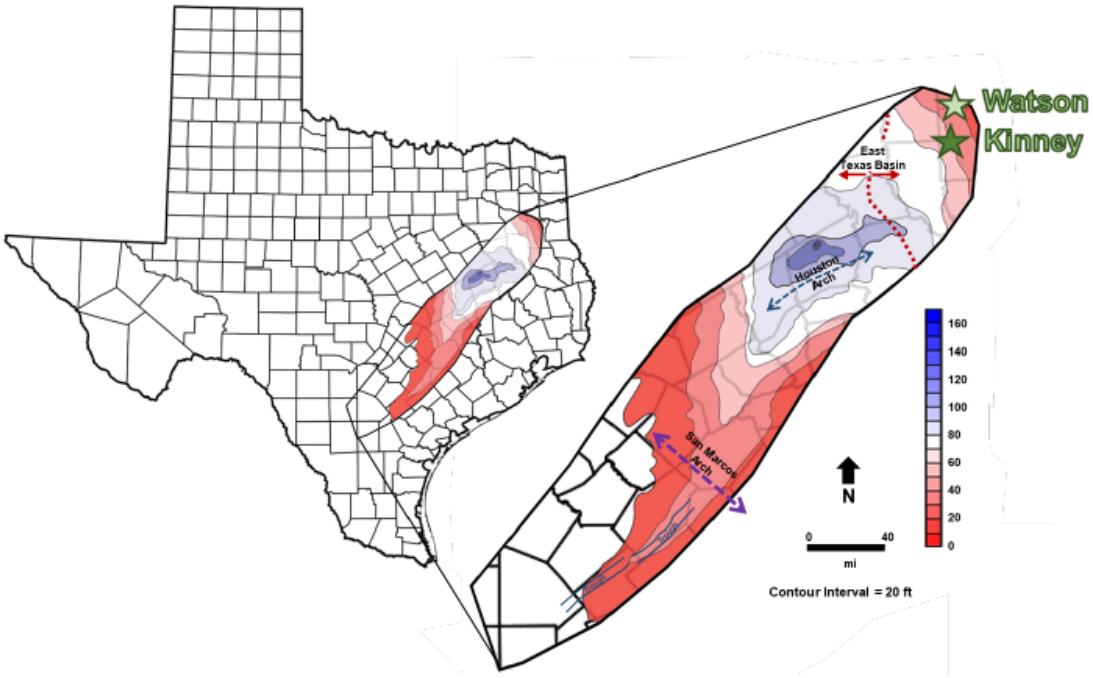

Figure 14. Composite Maness isochore map constructed by English (2020) spanning from the East Texas Basin touching the crest of the Sabine Uplift and extends southwestward to the south Texas producing region. This combined map integrates isochore maps from Patterson (2018) and Denne & Breyer (2016). Structural features such as the San Marcos Arch (purple), the Houston Arch (blue), and the axis of the East Texas Basin (red) are shown. This map further suggests that the direction of sediment transport is from the northeast.

V. Methods and Materials

V.I Mapping

The purpose of this study is to develop a better understanding of the Maness interval in proximity to the Sabine Uplift, with a particular emphasis on identifying its source origins and assessing its potential as a source rock. This study is primarily focused on regions situated to the south and east of the East Texas Basin, with a particular emphasis on the crest of the Sabine Uplift, spanning Rusk, Nacogdoches, and Angelina counties. Furthermore, it extends its scope to encompass areas located to the south of the Sabine Uplift, encompassing Trinity, Tyler, and Polk counties (Fig. 15). Additionally, this study incorporates regions that overlap with the research conducted by English (2020) within the East Texas Basin, encompassing Cherokee, Anderson, Houston, and Leon counties.

A database of 338 raster logs was developed using Enverus' Drilling Info and imported into IHS Petra. Of these raster logs, three type logs were used (Fig. 16): Hanks, L.B. et al #1H in Tyler County, Trinity County Lumber Company #1 in Trinity County, and the Galan White #11 in Rusk County that was used by English (2020). These logs demonstrated the variability of depositional patterns that occurred within the study region in basins adjacent to the Sabine Uplift. Four horizons ranging from the Lower Cenomanian to the Upper Turonian were correlated and used to establish trends throughout the study area. These horizons consisted of the top of the Buda, the Intra-Maness marker, top of the Maness Shale, and base of the Austin Chalk. This study relied on gamma ray, resistivity, and spontaneous potential to correlate these logs.

The Buda Limestone acts as the lower boundary for the mapped interval, which encompasses the top of the Buda, Maness, Woodbine, Eagle Ford, and the base of the Austin Chalk, all of which are analyzed in this study. This Lower Cenomanian carbonate reveals a consistent log response of low gamma ray (20-30 API) and high resistivity. In some portions of the study area the False Buda

overlies the Buda. The False Buda is a clay rich limestone that is oftentimes identified as part of the Buda and is thus correlated as the top Buda (Anderson, 1979; Hentz et al., 2014). However, this argillaceous limestone contains different facies than the Buda and displays higher gamma and lower resistivity log signatures. In the study by English (2020), it was identified as the initial Maness facies. Although the False Buda was seldom encountered across the study area, it was correlated in regions where it was observed but did not undergo extensive mapping or in-depth investigation.

The intra-Maness marker has a higher gamma ray (75-90 API) and lower resistivity signature, and it is often recognized by an abrupt change in resistivity. English (2020) defined the top of the Maness by a sharp drop in resistivity from the overlying Woodbine Sandstone. However, this distinguishing feature is less apparent across most of the study area, particularly in regions located to the south of the Sabine Uplift. In previous studies within the East Texas and adjacent basins, the Maness interval was defined using a sequence stratigraphic framework. This framework identified a lower segment characterized by a fining-upward (retrogradational) trend, followed by an upper section displaying a coarsening-upward (progradational) trend. These two segments are distinctly separated by a third-order maximum flooding surface (Ambrose et al., 2009; Hentz et al., 2014). In the context of this study, the correlation of the Maness interval throughout the study area heavily relied on the utilization of this sequence stratigraphic approach. Lastly, the base of the Austin Chalk served as the upper benchmark used to identify trends in this study. This chalk vertically constrains the Buda-to-Austin Chalk interval in the greater on-shelf Gulf Basin (Hentz et al., 2014).

Six north to south and east to west trending, stratigraphic cross-sections were created with the Buda Limestone as the datum (Fig. 15). Cross-section A-A' trends N-S through the western segment of the study area through the axis of the East Texas Basin, tying to the Trinity County Lumber Company #1 type log (Fig. 17). Cross-section B-B' runs N-S along the western flank of the Sabine Uplift and the eastern margin of the East Texas Basin down into the southernmost portion of the

study area off the Stuart City and Sligo Shelf Margins. This cross-section correlates the Galan White #11 type log to the deepest portion of the study region in Polk County (Fig. 18). Cross-section C-C' trends N-S, traversing the crest of the Sabine Uplift and passing through the Hanks, L.B. et al. #1 type log to the southernmost portion of Tyler County (Fig. 19). Cross-section D-D' trends E-W from the axis of the East Texas Basin through the Galan White #11 type log and into the easternmost part of Rusk County (Fig. 20). Cross-section E-E' trends E-W and starts at the southern margin of the East Texas Basin and passes over the crest of the Sabine Uplift in Nacogdoches County (Fig. 21). Lastly, Cross-section F-F' also runs E-W connecting the southernmost portion of the East Texas Basin in Trinity County to Hanks, L.B. et al. #1 in Tyler County (Fig. 22). Additionally, cross-sections C-C' and E-E' were reproduced as structural cross sections to exhibit some of the structural trends within the study region (Figs. 23 and 24).

Using formation tops picked throughout the study area and illustrated in cross-sections A through F, a total of four isochore maps, two structure contour maps, and three net sandstone maps were generated to provide insights into the depositional environment, stratigraphic relationships, and structural features pertaining to the units under study. The isochore maps generated in this study depict the thickness of the lower Maness, upper Maness, entire Maness interval, and the top of the Buda to the base of the Austin Chalk (encompassing Maness, Woodbine, and Eagle Ford). The two structure maps focus on the top of the Maness and the top of the Buda. The net sandstone maps, which were generated using a gamma ray cutoff of 60 API, depict the thickness and distribution of the siliciclastic rocks, predominantly sandstone, within the lower Maness, upper Maness, and the entire Maness stratigraphic interval. Finally, a composite isochore map of the Maness was created, covering the current study area, and extending northwest into the East Texas Basin, as well as southwest into the South Texas producing region. This map compiled geophysical log interpretations from Denne and Breyer (2016), Patterson (2018), English (2020), as well as the current study.

V.II Modeling for Organic Richness

Passey et al. (1989) formulated the Δ log R technique as a method for estimating the organic richness of various types of source rocks across a wide spectrum of maturation levels. Their visual method utilizes the sonic and resistivity curves, which are scaled so that 100 microseconds/ft (328 microseconds per meter) correspond to two logarithmic resistivity cycles (Passey et al., 1990). The baseline for the plot of the two curves is an organic-lean shale. Intervals with higher organic carbon content are identified by the separation of the two curves, as organic-rich shales are typically slower than organic-lean shales (Passey et al., 1990).

The present study employed Passey's Δ log R method to estimate the total organic carbon (TOC) in five wells: the AFGRD 4 and W.L. Green 1 in Houston County, Cameron Mineral Trust 1 and W.T. Carter 3 in Polk County, and Fitzgerald 1 in Leon County (Fig. 15). The digitized values were exported to Microsoft Excel and plotted against their corresponding depths. The scaling was adjusted to achieve a relative scaling of 150 microseconds per foot (492 microseconds per meter) per 3 logarithmic resistivity cycles (50 microseconds per foot for every one logarithmic cycle). Δ log R values were then calculated algebraically at every depth using the following equation from Passey et al. (1990):

$$\Delta \log R = \log10(R/R_{baseline}) + 0.02 \times (\Delta t - \Delta t_{baseline})$$

where Δ log R signifies the separation of the sonic/resistivity curve, R denotes resistivity measured in ohm-m, Δt represents the sonic value measured in microseconds per foot, $R_{baseline}$ and $\Delta t_{baseline}$ denote the respective resistivity and sonic values when the two curves are baselined in an organic lean shale, and the value of 0.02 is derived from the relationship between the sonic and resistivity cycles discussed above.

Upon deriving Δ log R values, subsequent computations involved the determination of Level of Organic Metamorphism (LOM) values. This entailed the utilization of the method introduced by Hood et al. (1975), incorporating both maximum temperature (T_{max}) and effective heating time (T_{eff}) parameters, quantified in millions of years, specific to the Maness Shale. Hood et al. (1975) established an integrated approach to project LOM in petroleum source rocks by combining these parameters. Hood et al. (1975) inferred that the temporal span (T_{eff}) throughout which a given rock experiences a temperature within 15°C (27°F) of its peak temperature (T_{max}) presents a pertinent measure of effective heating time, graphically represented in their T_{max} versus T_{eff} graphs (Appendix B).

To acquire the LOM values, it was essential to determine temperature and effective heating time. Temperature in degrees Celsius was sourced from the SMU Node of the National Geothermal Data System (http://geothermal.smu.edu/gtda/). The data were then utilized to construct geothermal gradients for each county by plotting the corrected bottomhole temperature against depth (Appendix A). The temperature of the Maness was subsequently calculated by inputting its depth in meters into the calculated geothermal gradient, yielding the value of T_{max}. Effective time was found using approximate ages from surface rocks, sourced from the United States Geological Survey's Pocket Geology of Texas website (https://txpub.usgs.gov/txgeology/). The most recent coastal deposits on the Gulf Coast Plain are situated at the surface due to the southeastward progression of the coastline as the Gulf of Mexico underwent sedimentation. As a result, the time period for which the Maness has remained at its current depth is at minimum as long as the age of the surface deposits. This implies that the effective heating time aligns with the approximate age of the surface deposits within this geographical area. After completing the process of determining temperature and effective heating time for all five wells, each well's data points were plotted on Hood et al.

(1975)'s LOM to maximum temperature and effective heating time graph (Appendix B). This graph provided the Level of Organic Metamorphism (LOM) values for each well.

Upon obtaining the LOM, Total Organic Carbon (TOC) was determined using Passey et al.'s (1990) empirical equation:

$$TOC = \Delta \log R \times 10^{(2.297 - 0.1688 \times LOM)}$$

The TOC measurements were expressed in weight percentage (wt.%) and subsequently plotted on a graph corresponding to the Maness interval. Additionally, gamma ray values were incorporated into these graphs for perspective. A gamma-ray cutoff was applied in the TOC wt.% graphs to eliminate elevated values attributed to anomalous Δ log R separation that could occur in hydrocarbon reservoirs, or due to adverse borehole conditions, unconsolidated sediments, and low-porosity (tight) intervals (Passey et al., 1990).

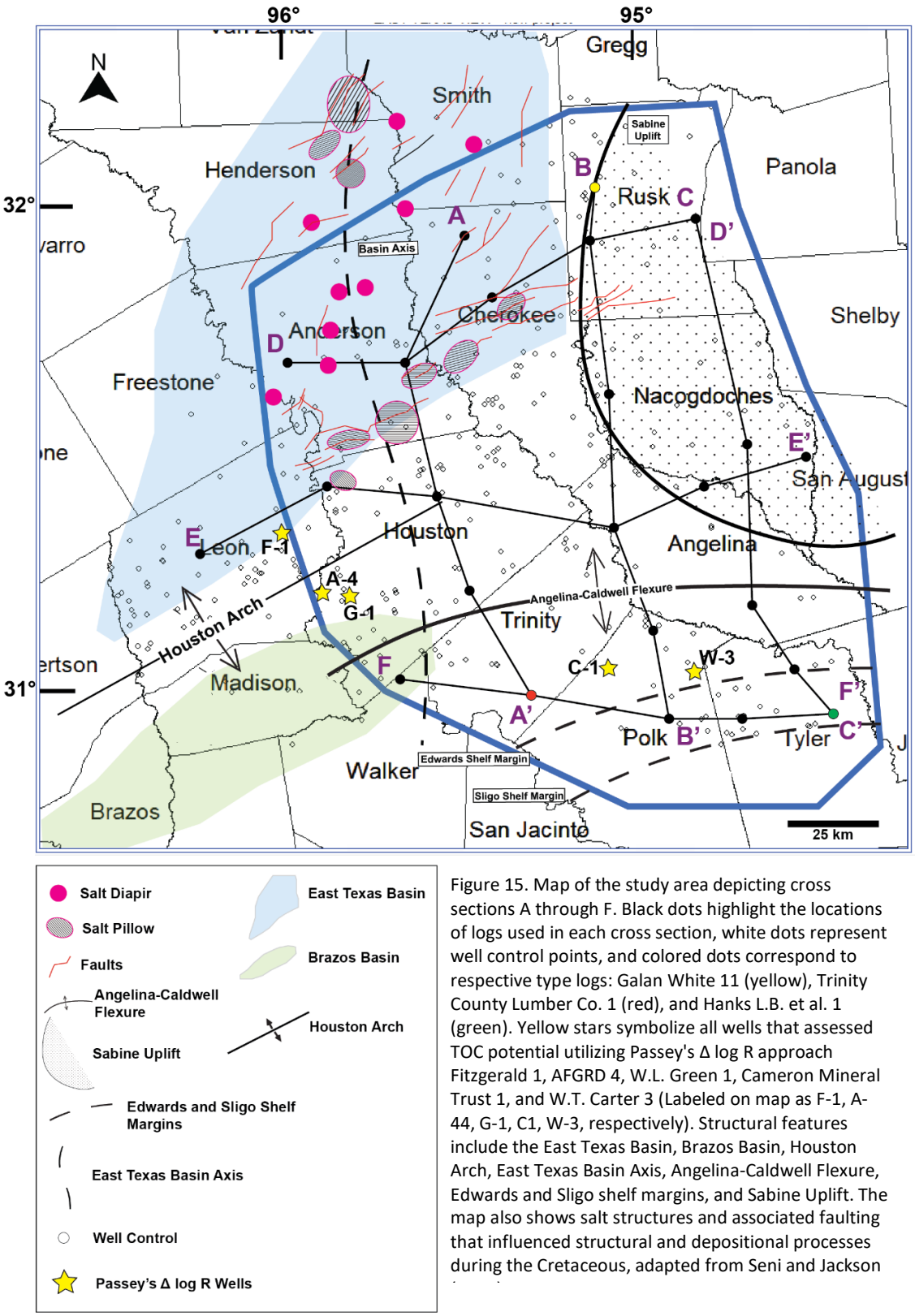

Figure 15. Map of the study area depicting cross sections A through F. Black dots highlight the locations of logs used in each cross section, white dots represent well control points, and colored dots correspond to respective type logs: Galan White 11 (yellow), Trinity County Lumber Co. 1 (red), and Hanks L.B. et al. 1 (green). Yellow stars symbolize all wells that assessed TOC potential utilizing Passey's Δ log R approach Fitzgerald 1, AFGRD 4, W.L. Green 1, Cameron Mineral Trust 1, and W.T. Carter 3 (Labeled on map as F-1, A-44, G-1, C1, W-3, respectively). Structural features include the East Texas Basin, Brazos Basin, Houston Arch, East Texas Basin Axis, Angelina-Caldwell Flexure, Edwards and Sligo shelf margins, and Sabine Uplift. The map also shows salt structures and associated faulting that influenced structural and depositional processes during the Cretaceous, adapted from Seni and Jackson

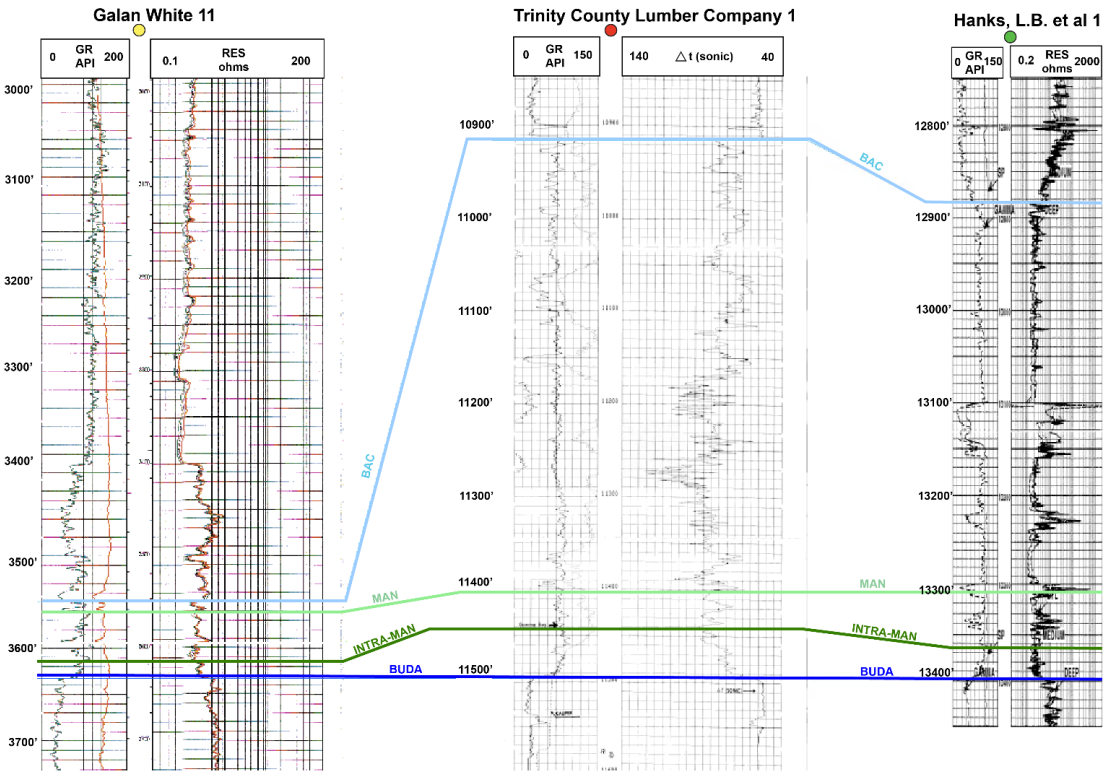

Figure 16. Type log cross section that illustrates the correlated formation tops throughout the study area, including the base of the Austin Chalk (BAC), the top of the Maness (MAN), the top of the Intra-Maness (INTRA-MAN), and the top of the Buda (BUDA). For type log locations, refer to Figures 14.

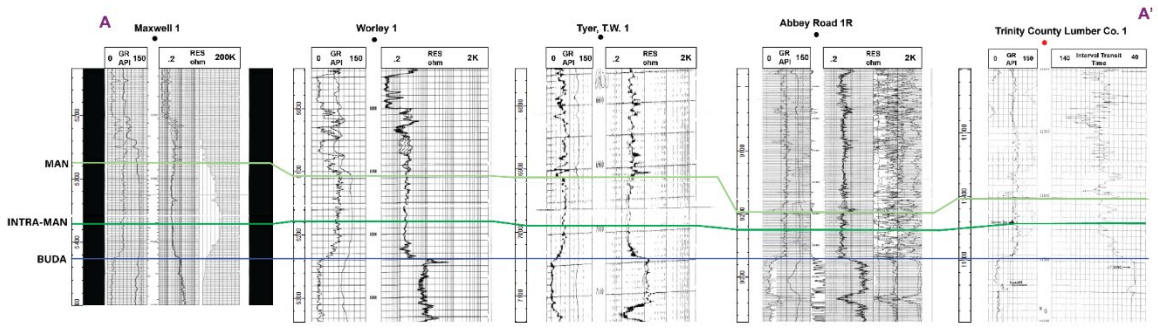

Figure 17. Cross section A-A’ extends from the northernmost part of Cherokee County to the Trinity County Lumber Co. No. 1 type log in the southernmost part of Trinity County, trending in a north-south direction. The top of the Buda is indicated by a dark blue color, the top of the Intra-Maness by a dark green color, and the top of the Maness by a lime green color. The absence of the base of the Austin Chalk in this cross section is attributed to elevated thicknesses of the Maness, Woodbine, and Eagle Ford intervals, causing the Austin Chalk to be positioned at a higher stratigraphic level. Refer to the base map (Fig. 14) for cross section location.

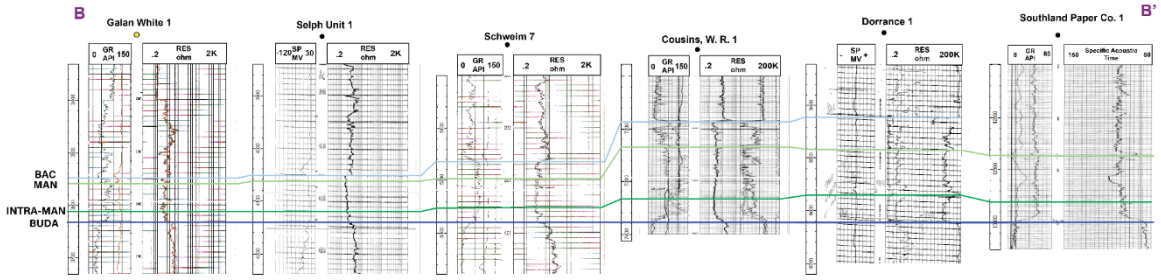

Figure 18. Cross section B-B' spans the study area from the Galan White 1 type log in Rusk County to the Sligo Shelf Margin in Polk County, extending in a north-south direction. The top of the Buda is represented by a dark blue color, the top of the Intra-Maness by dark green, the top of the Maness by lime green, and the base of the Austin Chalk by light blue. Refer to the base map (Fig. 14) for cross section location.

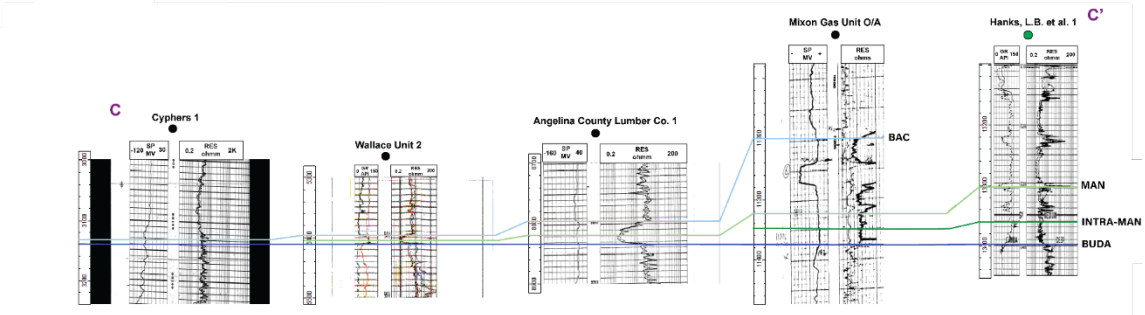

Figure 19. Cross section C-C' trends in a north-south direction from the east-central part of Rusk County, traversing the crest of the Sabine Uplift, and continuing into Tyler County at the Hanks, L.B. et al. 1 type log near the Sligo Shelf Margin. The cross-section displays the top of the Buda as dark blue, the top of the Intra-Maness as dark green, the top of the Maness as lime green, and the base of the Austin Chalk as light blue. Refer to the base map (Fig. 14) for cross section location.

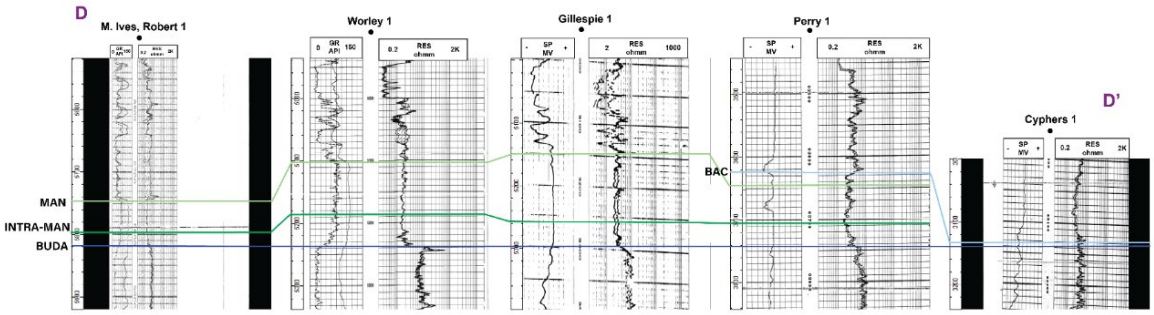

Figure 20. Cross section D-D' depicts a west-east trend starting from Anderson County in the East Texas Basin and extending into Rusk County on the crest of the Sabine Uplift. The dark blue indicates the top of the Buda, dark green represents the top of the Intra-Maness, lime green shows the top of the Maness, and the light blue denotes the base of the Austin Chalk. Refer to the base map (Fig. 14) for cross section location.

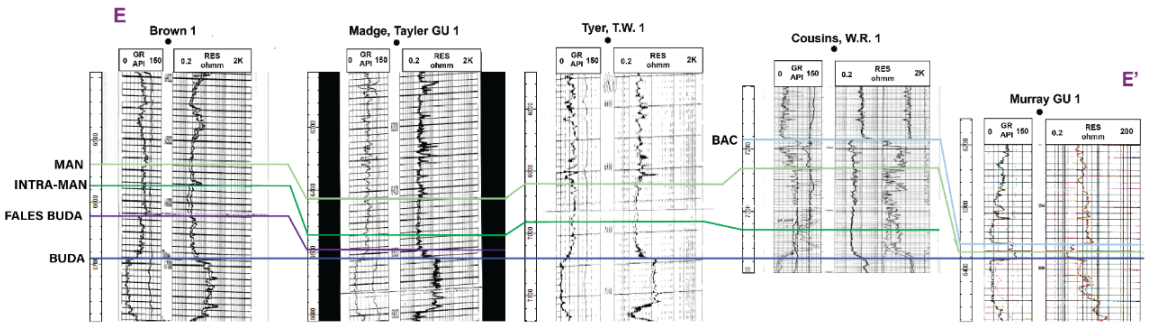

Figure 21. Cross section E-E' trends in a west-east direction and extends beyond the boundary of the current study area to the west into the study area of English (2020) in Leon County, in the East Texas Basin. This cross section continues to the east into Nacogdoches County near the southern flank of the Sabine Uplift. The top of the Buda is indicated by a dark blue line, the top of the Intra-Maness by a dark green line, the top of the Maness by a lime green line, and the base of the Austin Chalk by a light blue line. In certain regions of the study conducted by English (2020), the top of the False Buda, which represents the basal facies of the Maness, is denoted by a purple line. The False Buda was not discussed in detail in the current study since it was not present in the study area. Refer to the base map (Fig. 14) for cross section location.

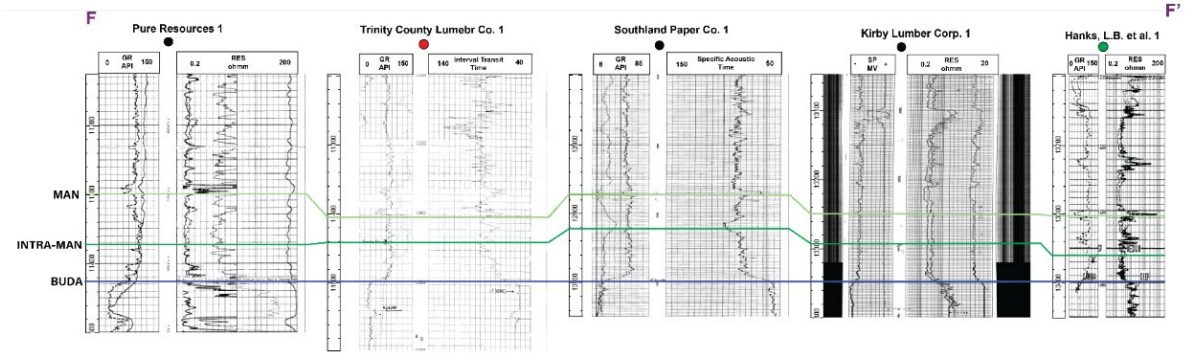

Figure 22. Cross section F-F' trends in a W-E direction along the southern boundary of the study area. It starts from the northern edge of Walker County and extends through the Trinity County Lumber Co. 1 type log before continuing east to the Hanks, L.B. et al. 1 Type log near the Sligo Shelf Margin. The top of the Buda is denoted by the dark blue line, the top of the Intra-Maness is represented by the dark green line, and the top of the Maness is shown by the lime green line. The absence of the base of the Austin Chalk in this cross section is attributed to elevated thicknesses of the Maness, Woodbine, and Eagle Ford intervals, causing the Austin Chalk to be positioned at a higher stratigraphic level. Refer to the base map (Fig. 14) for cross section location.

VI. Results

VI.I. Structural Trends

The depositional patterns within the study area were influenced by structural features that include the Sabine Uplift to the north, the Louann Salt structures within the East Texas Basin, the Angelina-Caldwell Flexure in the central region, and the Edwards and Sligo shelf margins to the south (Fig. 15). The Sabine Uplift is an anticlinal structure that trends northwest-southeast, serving as the eastern boundary of the East Texas basin (Powers, 1920). The syn-depositional Louann Salt had a profound impact on the structure of the East Texas Basin, resulting in the deformation of the sediment above it and the creation of salt domes, anticlines, and faults in the region (Seni and Jackson, 1983). The Angelina-Caldwell Flexure, oriented in an east-west direction and located along the southern boundary of the Sabine Uplift within the study region, separates two different geological provinces produced by Cenozoic sediment loading; to the north, there was flexural uplift and erosion, whereas to the south there was only flexural subsidence (Glawe 1989; Ewing 2009; Pearson et al., 2012). This low-relief fold is also regarded as the boundary separating the East Texas structural embayment from the Gulf Coast Basin (Stehli et al., 1972; Ambrose et al., 2009). The Edwards shelf margin lies to the south of the Angelina-Caldwell flexure and marks the edge of the Woodbine depositional shelf. The area to the south of this margin, extending to the Sligo Margin, is known for several fields producing from deep, Woodbine/Eagle Ford equivalent, slope turbidite facies, which includes the Seven Oaks (Polk County) and Sugar Creek (Tyler County) fields (Siemers, 1978; Foss, 1979; Ambrose et al., 2009).

Structural maps of the study area revealed consistent deepening trends of the Buda and Maness (Figs. 25 and 26). The depths of the top of the Buda ranged from -3,000 to -15,000 ft (-914 to -4572 m) subsea true vertical depth (SSTVD). The shallowest part of the study area is near the flanks and

crest of the Sabine uplift in Rusk and Nacogdoches counties, where the Buda top ranged from -3,000to -5,000 ft (-762 to -1,524 m). To the west of the Sabine uplift is the East Texas Salt Basin, where Buda depths ranged from -5,000 to -7,000 ft (-1,524 to -2,134 m). To the south, across the Angelina-Caldwell Flexure and towards the Edwards and Sligo Margins, Buda depths drastically increased from -7,000 to -14,000 ft (-2,134 to -4,267 m) in Polk and Tyler counties (Figs. 23 and 25). The depths of the top of the Maness exhibited similar trends to the Buda, consistently deepening towards the southern region (Fig. 26). Within the study area, Maness depths varied from -3,500 to -13,500 ft (-1,067 to -4,115 m), with the greatest depths observed in distal regions situated between the Edwards and Sligo shelf margins

VI.II Thickness Trends

In the study area, the identification of the Maness interval relied on previous sequence stratigraphic interpretations of its lower section, which features upward-fining sediments, and its upper section, which shows upward-coarsening sediments (Hentz et al., 2014). The lower, retrogradational section of the Maness is identified as a third-order transgressive systems tract (TST) that occurred after a regional sea-level fall. This relative sea level fall is evidenced by a hiatus in deposition on the underlying Buda Limestone (Ambrose et al., 2009; Hentz et al., 2014). The upper part of the Maness interval is characterized by progradational features, marking the onset of lower Woodbine deposition. The transition from the lower to the upper Maness interval is marked by a third-order maximum flooding surface (MFS) (Hentz et al., 2014). This MFS is represented in the current study as the “intra-Maness” marker.

The Maness interval exhibits varying thicknesses across the study area, with the thinnest occurrences observed in regions around the flanks of the Sabine Uplift where it is completely absent on the crest (Fig. 27). The thickness ranges from 0 to 50 ft (0 to 15 m) on the western flank and from

0 to 20 ft (0 to 6 m) on the southern flank, extending from the crest. To the west of the Sabine Uplift, the Maness interval thickens significantly, reaching up to 200 ft (61 m) in the East Texas Salt Basin in northern Cherokee County. In northern Houston County, just south of the East Texas Salt Basin, there is a zone that abruptly thickens to 220 ft (67 m). In a southerly direction, the Maness interval shows a significant increase in thickness, particularly south of the Angelina-Caldwell Flexure towards the Edwards and Sligo Shelf Margin, where its thickness ranges from 20 to 160 ft (6 to 49 m). Both the lower and upper Maness intervals exhibit notable thickening patterns extending westward toward the East Texas Salt Basin and southward along the shelf margins from the Sabine Uplift. In the lower Maness interval, thickness peaks at approximately 90 ft (27 m) in southeast Anderson County, west of the Sabine Uplift, and in the southern region near the Sligo Margin, straddling the Polk and Tyler County boundary (Fig. 28). The thickness pattern within the upper Maness strata closely resembles that observed in the broader Maness interval, which includes both the lower and upper Maness. However, a pronounced thick zone measuring 110 ft (34 m), is discernible along the boundary of Rusk and Smith counties, situated immediately west of the Sabine Uplift (Fig. 29). In summary, there is a general trend of increasing thickness in the Maness as one progresses further from the Sabine uplift.

Like the Maness, the thickness of the interval spanning from the top of the Buda to the base of the Austin Chalk, including the Maness, Woodbine, and Eagle Ford, follows a discernible trend of increasing thickness away from the Sabine Uplift. Notably, this interval reaches its maximum thickness, measuring up to 1300 ft (396 m), in the western extent of the East Texas Basin (Fig. 30). Additionally, an unconformity was observed on the Sabine Uplift where the top of the Buda Limestone was directly overlain by the Base of the Austin Chalk, as illustrated in the cross sections (Figs. 20 and 21).

The analysis of net sandstone thickness within the Maness interval extended beyond the study area, incorporating data from English's 2020 study in Leon County (Fig. 31). This comprehensive analysis reveals the existence of sandstones within the Maness interval, particularly in areas situated just west of the Sabine Uplift and in regions south of the Sabine Uplift near the shelf margins. The most substantial sandstone layers were identified just west of the Sabine Uplift, reaching thicknesses of up to 60 feet (18 meters). Other notable sandstone occurrences were observed in the East Texas Salt Basin in northern Cherokee County, with a thickness of 20 feet (6 meters), and along the shelf margins, where sandstone thickness reached approximately 30 feet (9 meters). However, aside from the above-mentioned locations, much of the net sandstone map showed limited to no sandstone presence within the Maness interval. In the upper Maness interval, sandstone thickness patterns closely resembled those of the entire Maness interval (Fig. 33). Conversely, the net sandstone map for the lower Maness interval exhibited sandstone occurrence measuring 20 feet (6 meters) in thickness only near the shelf margin in Tyler County (Fig. 32).

The sandstones within the Maness south of the Sabine Uplift were also illustrated by Barrett and Goodson (2006) in their cross sections generated from Tyler County, south of the Sugar Creek field between the Edwards and Sligo shelf margins (Fig. 7). Although the original cross section by Barrett and Goodson relied on foraminiferal abundances, this study adapted a sequence stratigraphic approach due to the absence of available foraminiferal data. This analysis utilized three wells from Barrett and Goodson’s (2006) cross section, resulting in a modified version that applied the sequence stratigraphic methods of Ambrose et al. (2009) and Hentz et al (2014). This cross section further revealed sand rich intervals within the Maness to the south of the Sabine Uplift.

A composite isochore map of the Maness interval was developed as a part of this study, integrating data from Denne and Breyer (2016), Patterson (2018), and English (2020) (Fig. 35), spanning from the study area to Atascosa and Live Oak counties in south Texas. The composite

isochore map revealed that the thickest occurrences of the Maness interval are in the southernmost region of the East Texas Basin (Leon County), the East Texas Salt Basin in Cherokee County, and adjacent regions in northern Houston County, as well as to the south of the Sabine Uplift near the Edwards and Sligo shelf margins (Tyler and Polk Counties). In the composite isochore map, the Maness interval exhibits a gradual decrease in thickness in regions approaching the Sabine Uplift and as it extends southwestward towards its depositional limit in Karnes County.

VI.III. Organic Richness

Organic richness was quantified using Passey's method in five distinct wells: AFGRD 4 and W.L. Green 1 in Houston County, Cameron Mineral Trust 1 and W.T. Carter 3 in Polk County, and Fitzgerald 1 in Leon County (Fig. 15). The baseline interval for each log was determined at a depth where the sonic (Δt) and resistivity (R) measurements showed clear overlap, and the organic-rich intervals were identified based on the separation between the two curves. Once the sonic/resistivity graphs were plotted, Δ log R values were calculated using the equation described in the Methods section. Subsequently, LOM values were generated based on the process outlined in the Methods Section to determine the corresponding weight percentage (wt.%) values of Total Organic Carbon (TOC) (Table 1). TOC wt.% values were then plotted against their respective depths. Figure 36 provides the graphs for the W.L. Green 1 well, serving as an example, while graphs for all other wells analyzed in this study can be found in figures 37 through 41.

The analysis of the W.L. Green 1 well indicates distinct Δ log R separation within the upper Maness, observed at depths ranging from 8495 to 8530 ft (2589 to 2600 m) (Fig. 36B). Baseline measurements at 8574 ft (2613 m) show $R_{baseline}$ of 3.1 ohm-m and $\Delta t_{baseline}$ of 81.4 microseconds per foot (277 microseconds per meter). The Maness at a depth of 8573 ft (2613 m) in this well was estimated to be at a temperature of 108°C based on the geothermal gradient for Houston County.

This, along with an effective heating time of 40 m.y., positioned the Level of Organic Metamorphism (LOM) at 10 on the LOM to maximum temperature and effective heating time graph (Appendix B). The TOC wt.% profile exhibits its peak concentrations within the upper Maness interval at a depth of 8483 ft (2586 m), with maximum values of 1.9 wt.% TOC (Fig. 36C), whereas the minimum values are found within the lower Maness at a depth of 8570 ft (2612 m), with TOC wt.% values of 0.0.

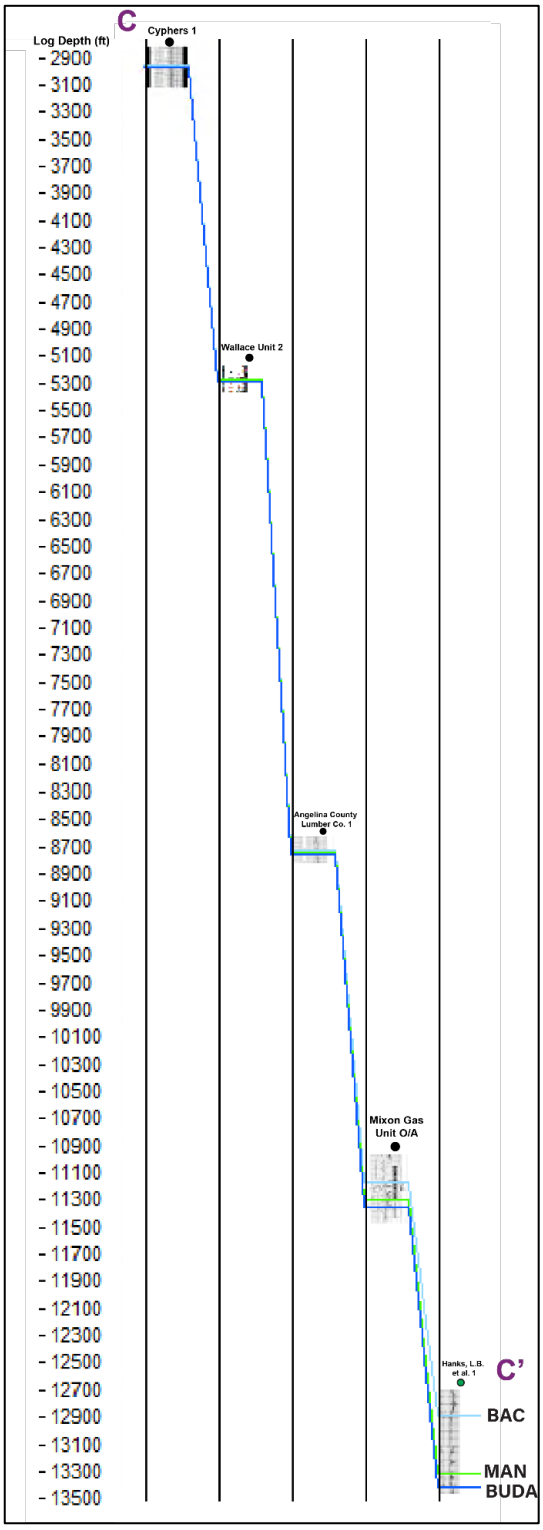

Figure 23. Structural representation of Cross-Section C-C' measured in subsea true vertical depth (SSTVD) encountering the same structural features as discussed Figure 14. This cross section displays the N-S structural trend that characterizes the study region from the crest of the Sabine Uplift and moving southward towards the Edwards and Sligo Shelf Margins.

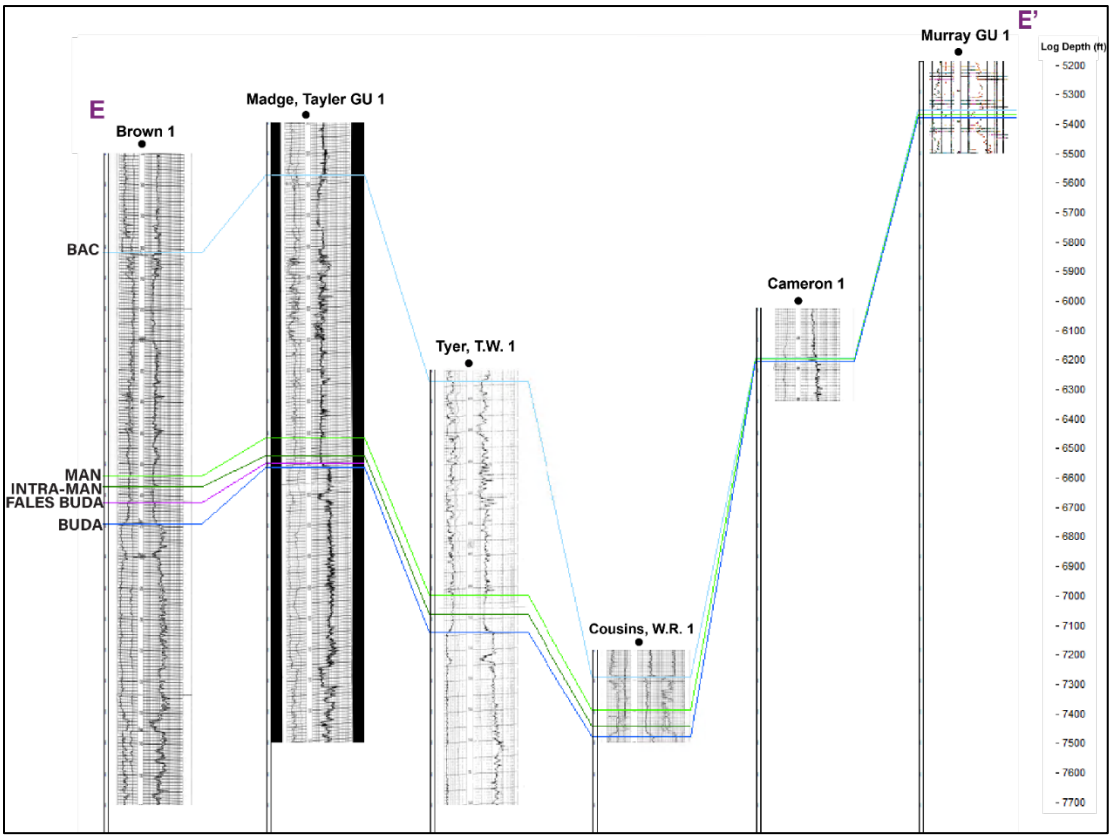

Figure 24. Structural representation of Cross-Section E-E', measured in subsea true vertical depth (SSTVD) and encountering the same structural features as discussed in Figure 14. This structural cross-section illustrates the east-to-west structural patterns that extend from the East Texas Basin to the crest of the Sabine Uplift.

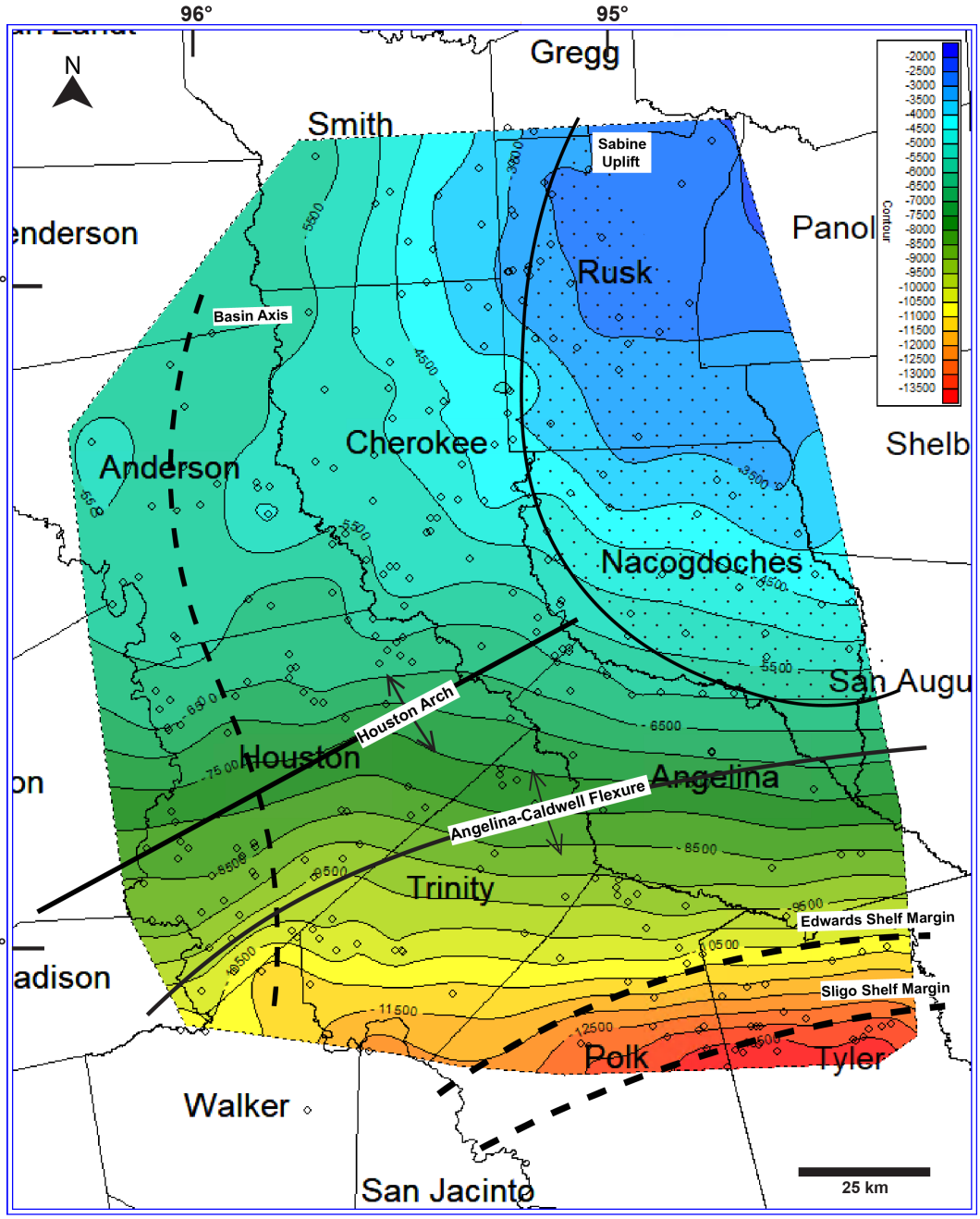

Figure 25. Top of the Buda Limestone structure map measured in subsea true vertical depth (SSTVD) presented with a 500 ft contour interval. The map includes the same structural features as those present in Fig. 14, such as the axis of the East Texas Basin, Edwards and Sligo Shelf Margins, and Sabine Uplift, superimposed for reference.

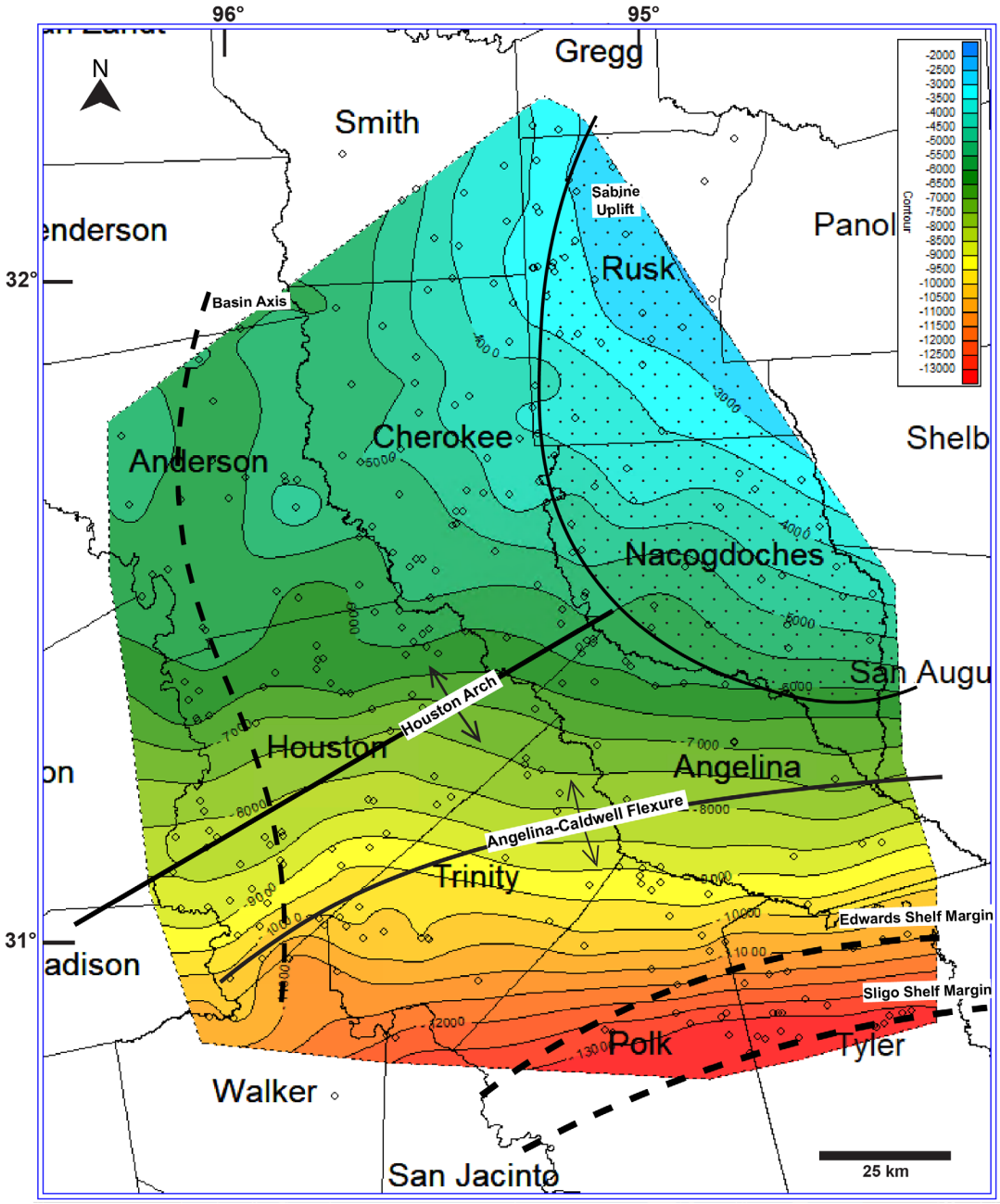

Figure 26. Top of the Maness Shale structure map measured in subsea true vertical depth (SSTVD) with a 500 ft contour interval. The same structural features are superimposed on this map as in Fig. 14, including the axis of the East Texas Basin, the Edwards and Sligo Shelf Margins, and the Sabine Uplift. The general trend of this map reflects that of the Buda.

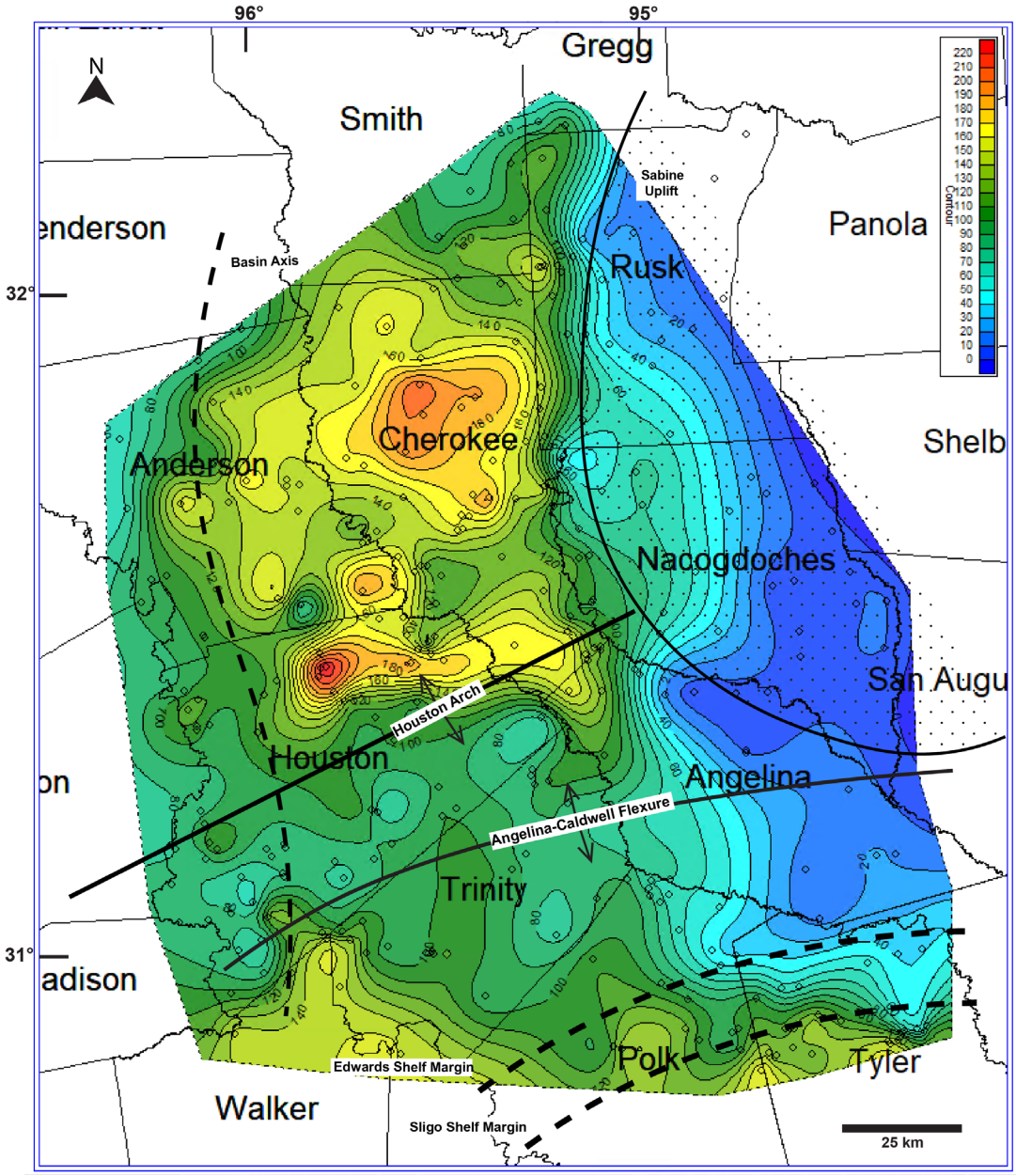

Figure 27. Isochore map illustrating the thickness interval from the top of the Buda to the top of the Maness Shale with a contour interval of 10 ft. The same structural features as in Fig. 14 are superimposed, including the axis of the East Texas Basin, the Edwards and Sligo Shelf Margins, and the Sabine Uplift.

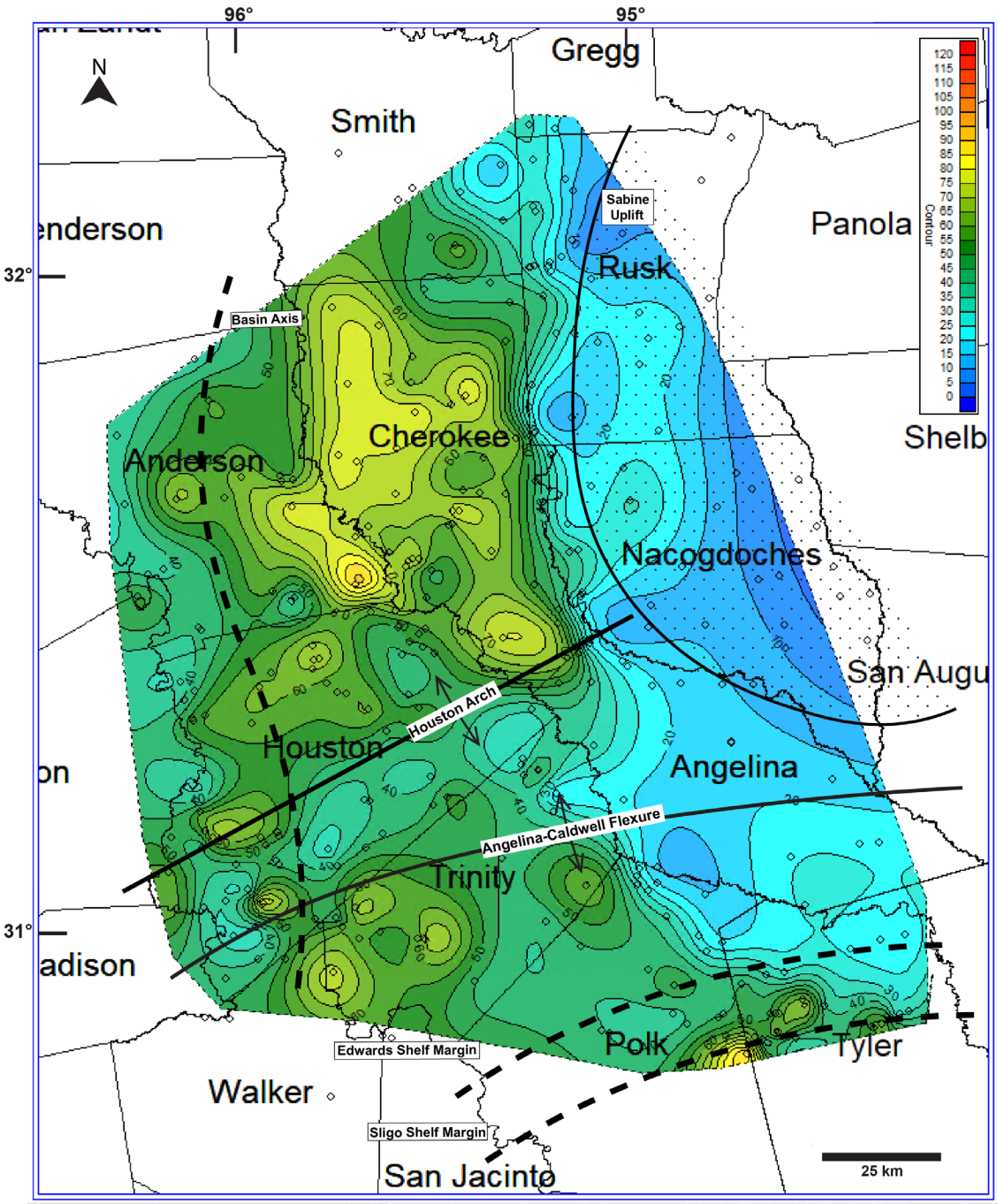

Figure 28. Isochore map displaying the thickness interval of the lower Maness with a contour interval of 5 ft. Structural features shown are the axis of the East Texas Basin, Angelina-Caldwell Flexure, Edwards and Sligo Shelf Margins, and the Sabine Uplift, which are superimposed for reference.

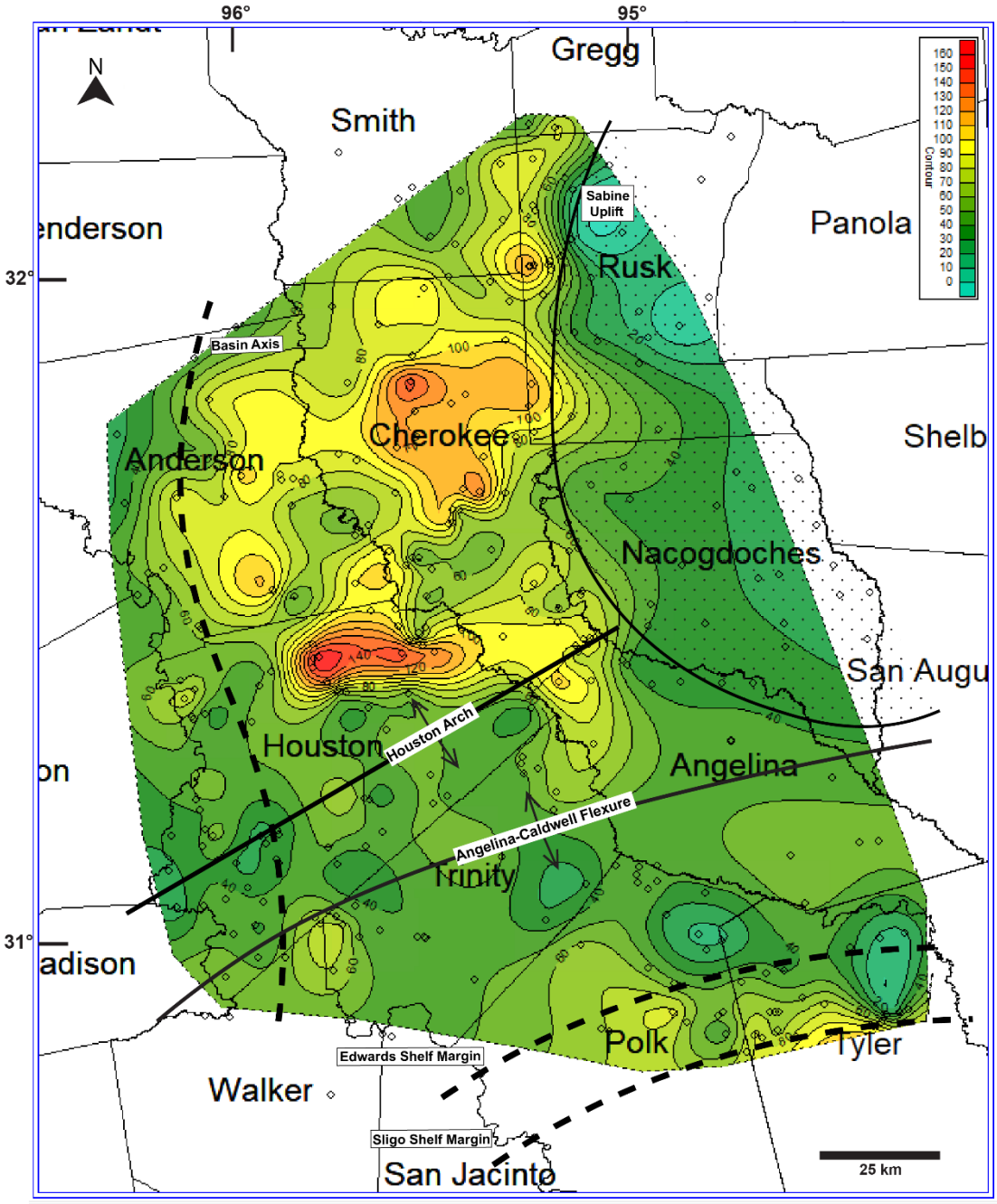

Figure 29. Isochore map displaying the thickness variation of the upper Maness with a contour interval of 5 ft. Structural features shown are the axis of the East Texas Basin, Angelina-Caldwell Flexure, Edwards and Sligo Shelf Margins, and the Sabine Uplift, which are superimposed for reference.

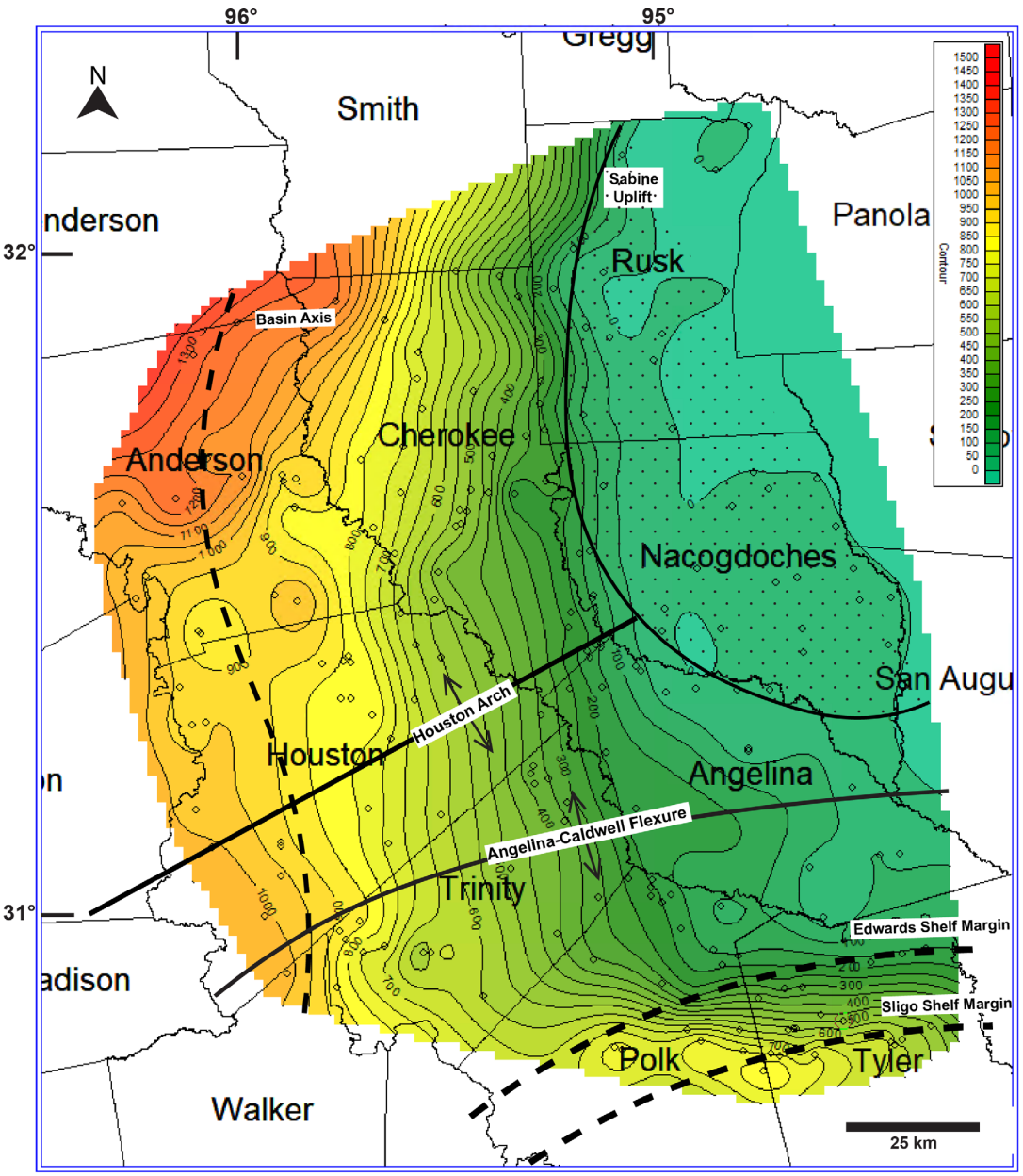

Figure 30. Isochore map showing the thickness interval from the top of the Buda to the top of the Base of the Austin Chalk with a contour interval of 50 ft. This map includes the same structural features as in Fig. 14, such as the axis of the East Texas Basin, the Edwards and Sligo Shelf Margins, and the Sabine Uplift, which are superimposed for reference.

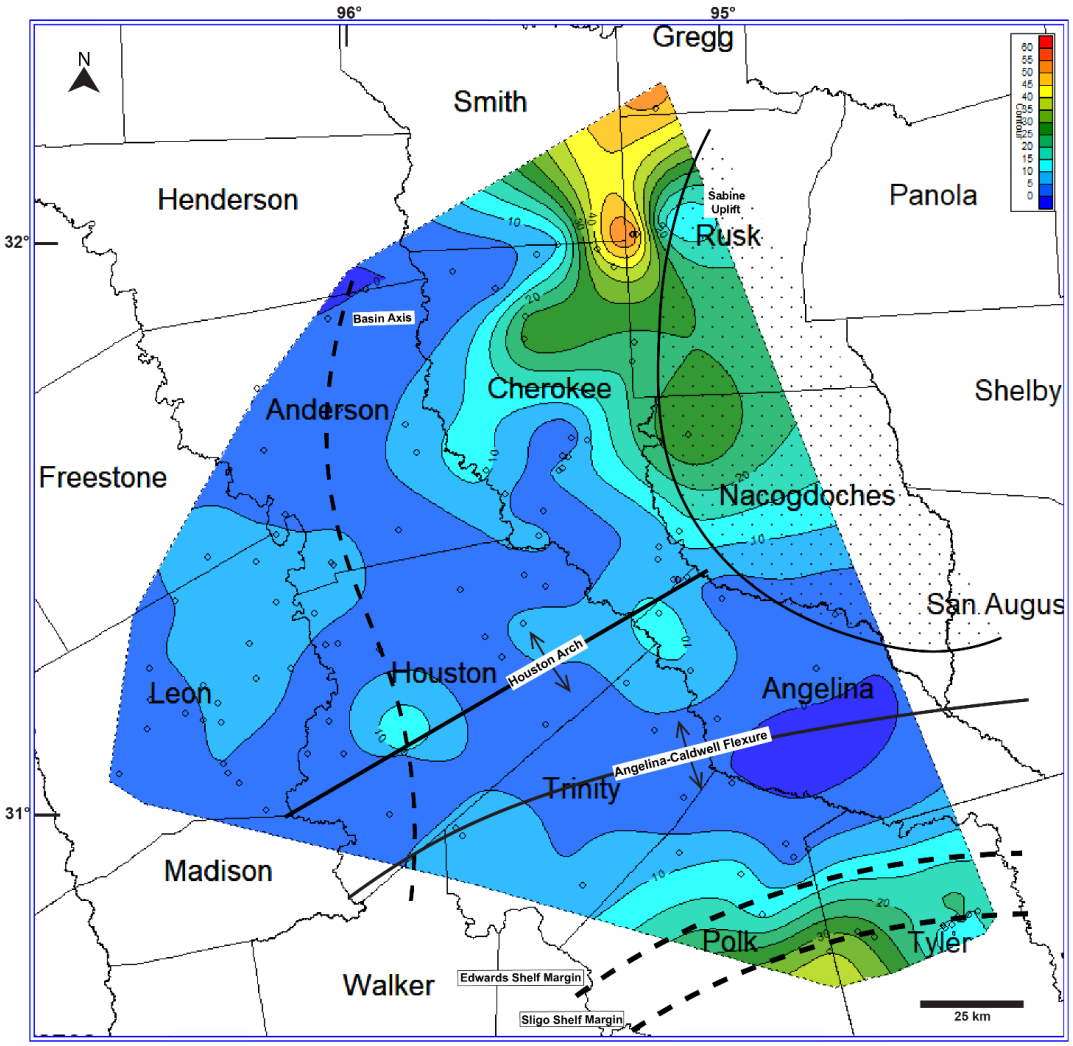

Figure 31. Maness net sandstone map generated using a gamma ray cutoff of 60 API and a contour interval of 10 ft. This map covers the study area and extends beyond its boundaries to the west and into the study area of English (2020) in Leon County. It has been overlaid with structural features such as the axis of the East Texas Basin, the Edwards and Sligo Shelf Margins, and the Sabine Uplift.

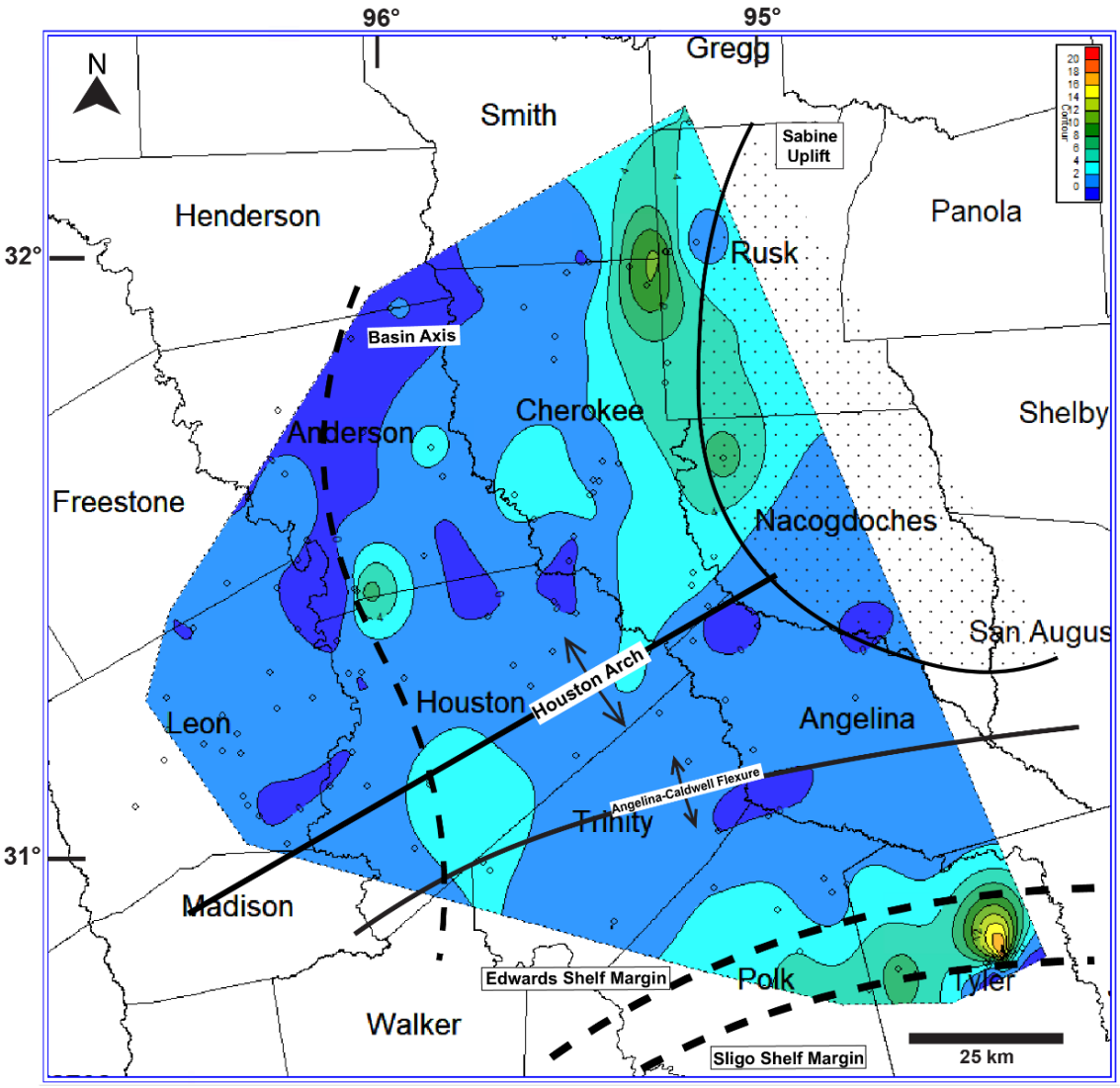

Figure 32. Lower Maness net sandstone map generated using a gamma ray cutoff of 60 API using a 5 ft. contour interval. This map covers the study area and extends beyond its boundaries to the west and into the study area of English (2020) in Leon County. It has been overlaid with structural features such as the axis of the East Texas Basin, the Edwards and Sligo Shelf Margins, and the Sabine Uplift.

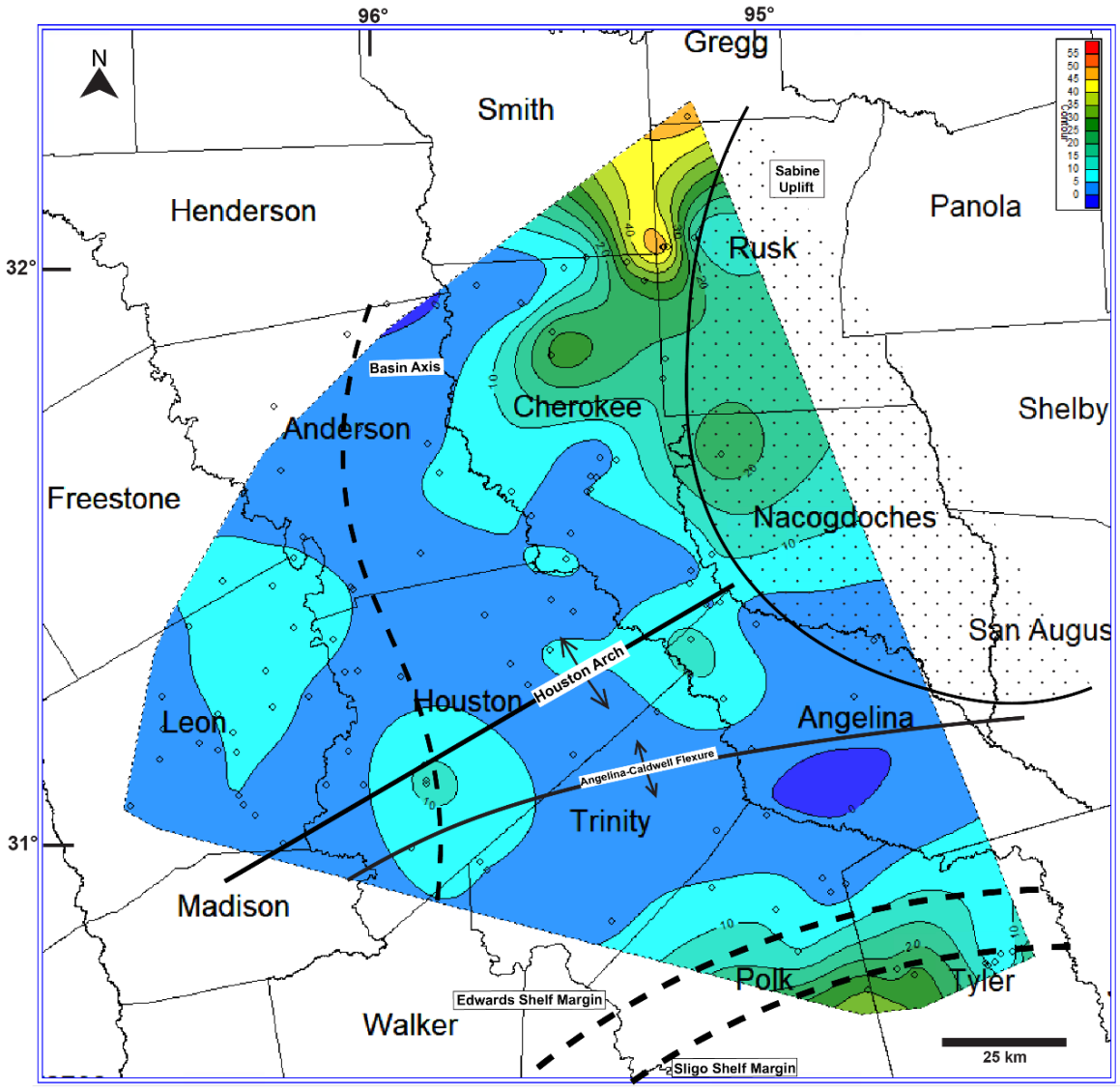

Figure 33. Upper Maness net sandstone map generated using a gamma ray cutoff of 60 API using a 5 ft. contour interval. This map covers the study area and extends beyond its boundaries to the west and into the study area of English (2020) in Leon County. It has been overlaid with structural features such as the axis of the East Texas Basin, the Edwards and Sligo Shelf Margins, and the Sabine Uplift.

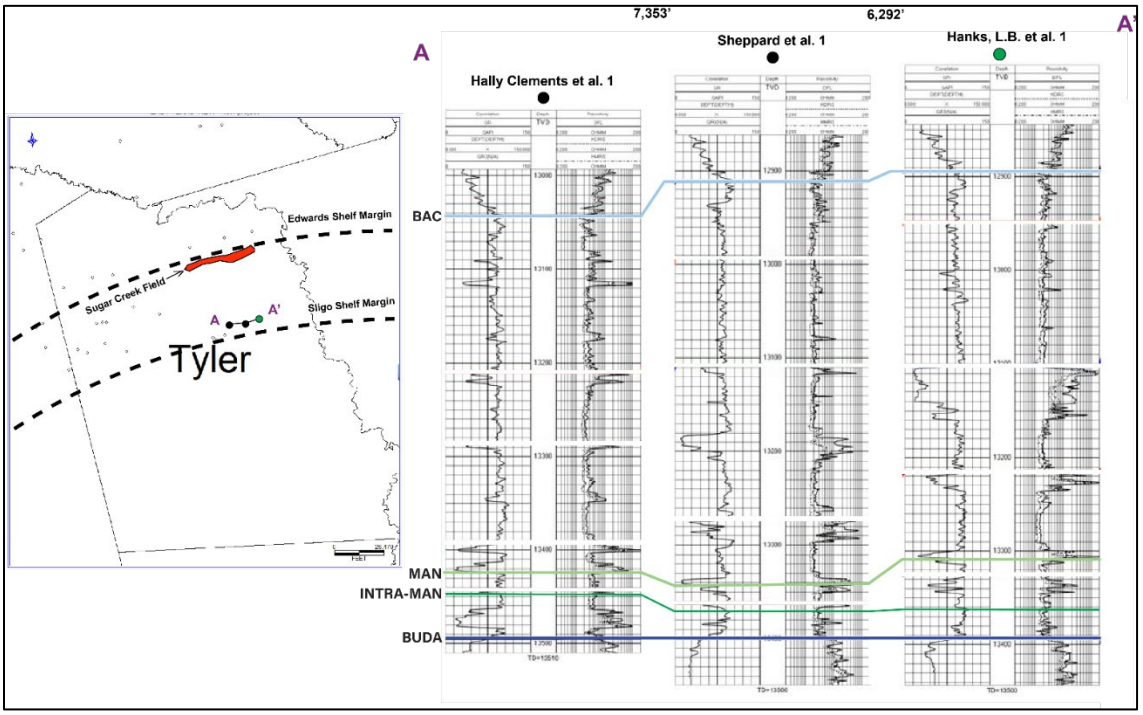

Figure 34. Tyler County Cross-Section modified from Barrett and Goodson (2006) using sequence stratigraphy rather than foraminiferal data. This cross section occurs between the Edwards and Sligo shelf margins (respective black dashed lines) and to the south of the Sugar Creek petroleum field (red polygon). Formation tops include the top of the Buda (dark blue), intra-Maness (dark green), Maness (light green) and base of the Austin Chalk (light blue). The lateral spacing between wells is represented by measurements in feet.

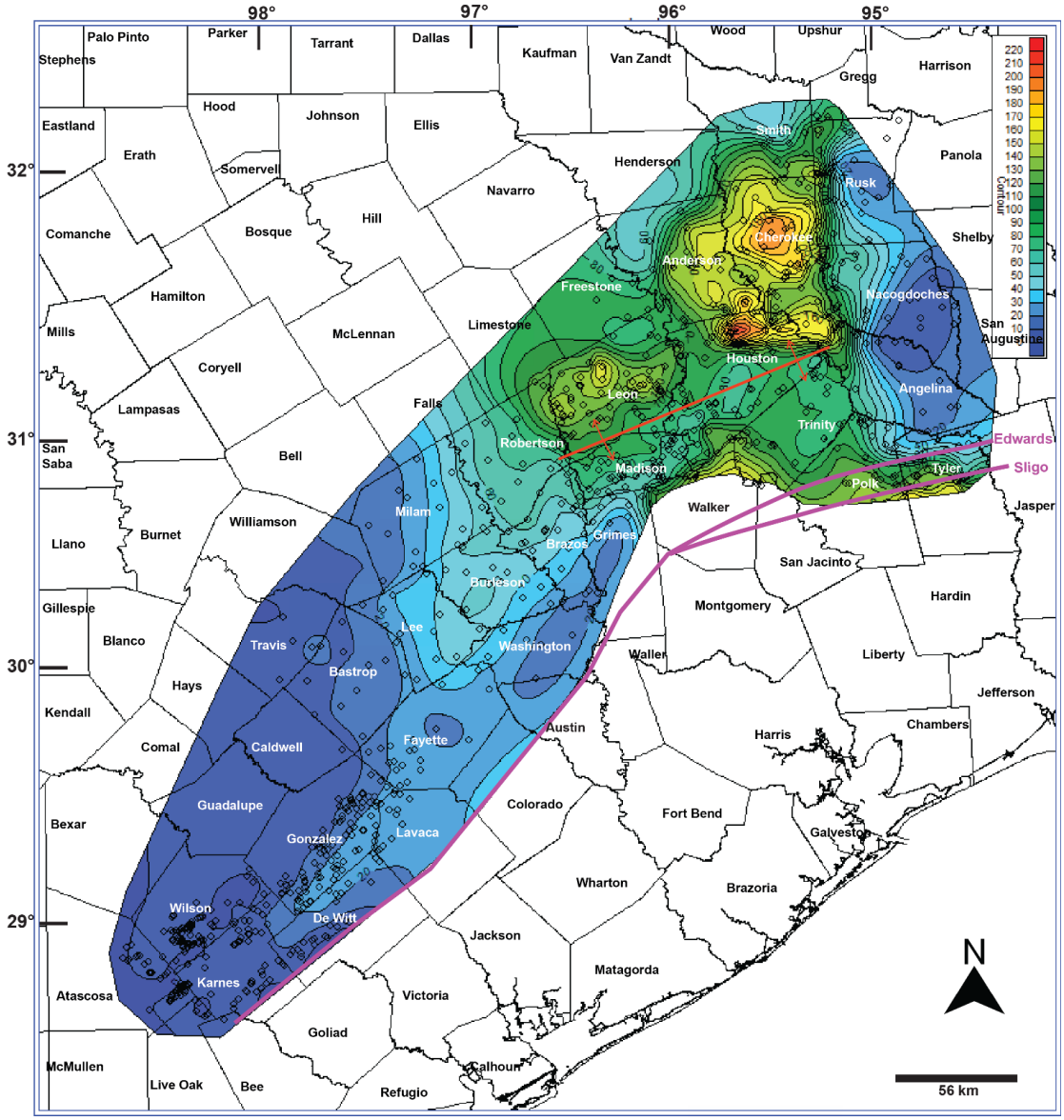

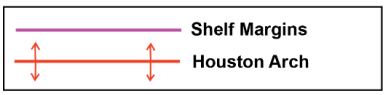

Figure 35. Composite isochore map integrating geophysical well log data from Denne and Breyer (2016), Patterson (2018), English (2020), and the present study.

Table 1. Values obtained and generated for each analyzed well in the current study based on Passey's method for estimating organic richness.

Well	County	Age at Surface	Effective Heating Time (M.y.)	Temperature (°C)	LOM	Top Maness Depth (ft)	Base Depth (ft)	Base R	Base Δ t	Maness TOC Thickness (ft) >2%
Fitzgerald (F-1)	Leon	Eocene	40	92	9	7113	7183	2.7	83.4	6
AFGRD (A-4)	Houston	Eocene	40	106	10	8337	8205	2.6	89.8	0
Green (G-1)	Houston	Eocene	40	108	10	8481	8574	3.1	81.4	7
Cameron Minerals (C-1)	Polk	Oligocene	25	129	10	10479	10304	3.1	80.9	1
W.T. Carter (W-3)	Polk	Miocene	10	137	10	10971	10882	4.0	78.5	1

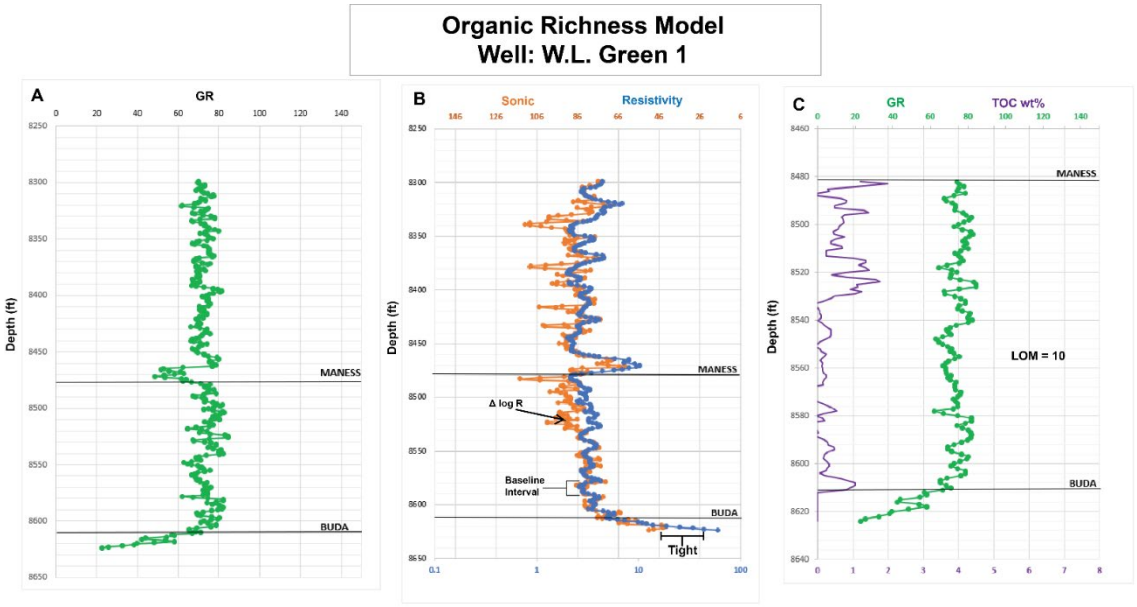

Figure 36. *W.L. Green1 Well* - Graph A depicts digitized gamma ray values. Graph B presents the sonic/resistivity overlay in the Maness and lower Woodbine intervals, revealing the potential for total organic carbon (TOC) content in the upper Maness interval (Δ log R). A baseline value of 8574 ft SSTVD is established, highlighting an organic-lean shale. A low-porosity interval occurred below the Maness-Buda contact. The orange curve represents the sonic response, while the blue curve represents the resistivity. Graphs C shows TOC wt% calculations. The purple curve depicts the TOC wt% values, and the green curve corresponds to the gamma-ray response. A gamma-ray cutoff is implemented to exclude high TOC wt% values originating from the tight Buda interval.

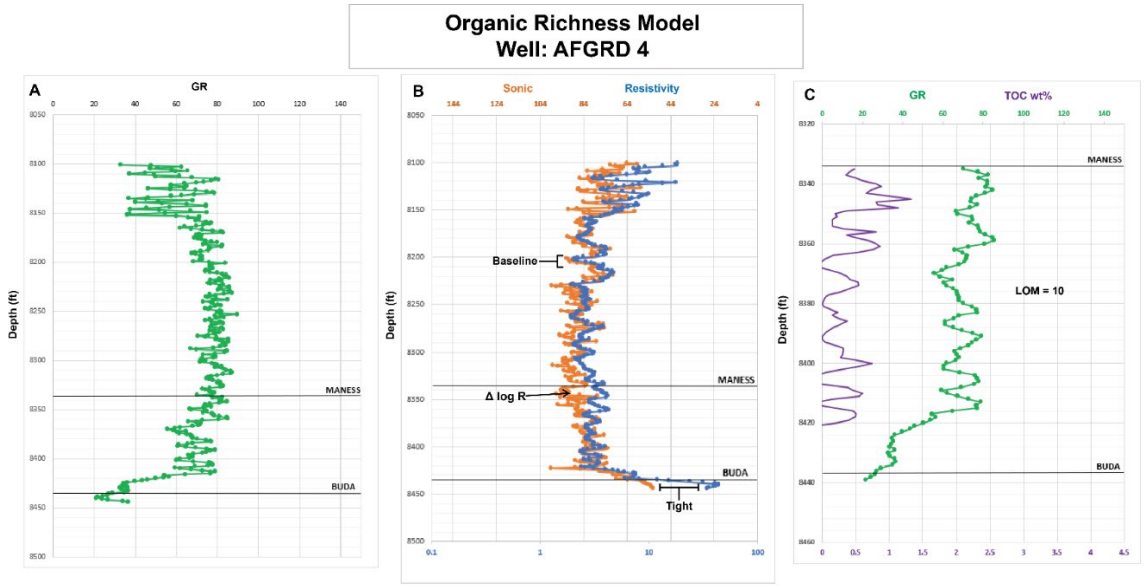

Figure 37. *AFGRD 1 Well* - Graph A depicts digitized gamma ray values. Graph B displays the sonic/resistivity overlay within the Maness and lower Woodbine, highlighting the potential for total organic carbon (TOC) content in the upper Maness interval (Δ log R). The baseline value was set at 8200 ft subsea true vertical depth (SSTVD) and a distinct tight, low-porosity interval observed below the Maness-Buda contact. The sonic response is represented by the orange curve, while the resistivity is depicted by the blue curve. Graphs C shows TOC wt% calculations. The purple curve depicts the TOC wt% values, and the green curve corresponds to the gamma-ray response. A gamma-ray cutoff is implemented to exclude high TOC wt% values originating from the tight Buda interval.

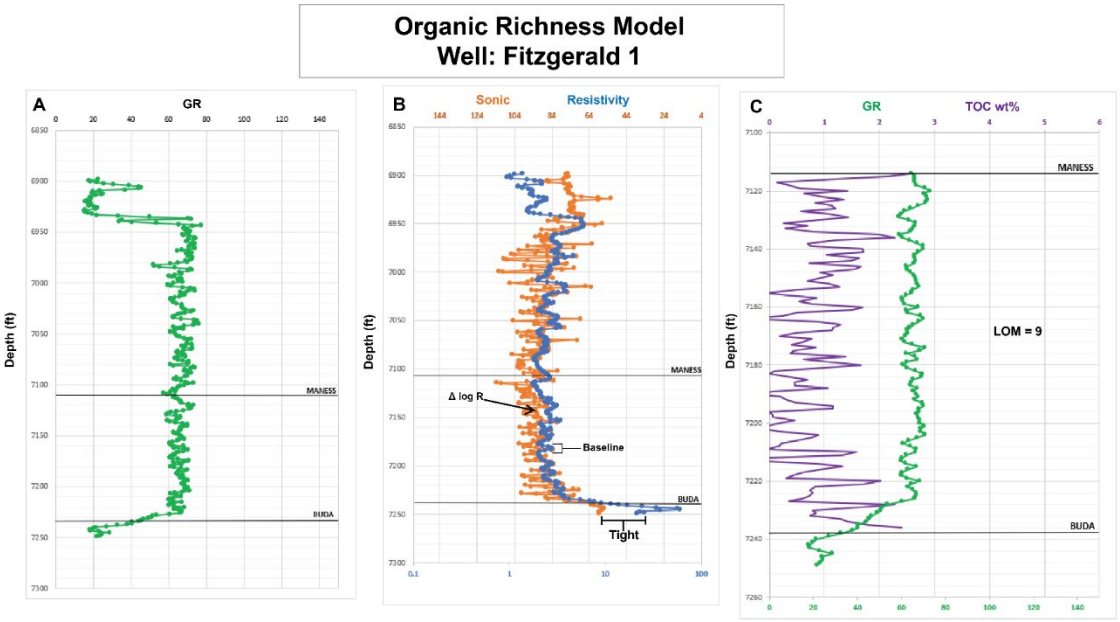

Figure 38. *Fitzgerald 1 Well* - Graph A depicts digitized gamma ray values. Graph B displays the sonic/resistivity overlay within the Maness and lower Woodbine, highlighting the potential for total organic carbon (TOC) content in the upper Maness interval (Δ log R). The baseline value was set at 7183 ft SSTVD and a distinct tight, low-porosity interval observed below the Maness-Buda contact. The sonic response is represented by the orange curve, while the resistivity is depicted by the blue curve. Graphs C shows TOC wt% calculations. The purple curve depicts the TOC wt% values, and the green curve corresponds to the gamma-ray response. A gamma-ray cutoff is implemented to exclude high TOC wt% values originating from the tight Buda interval.

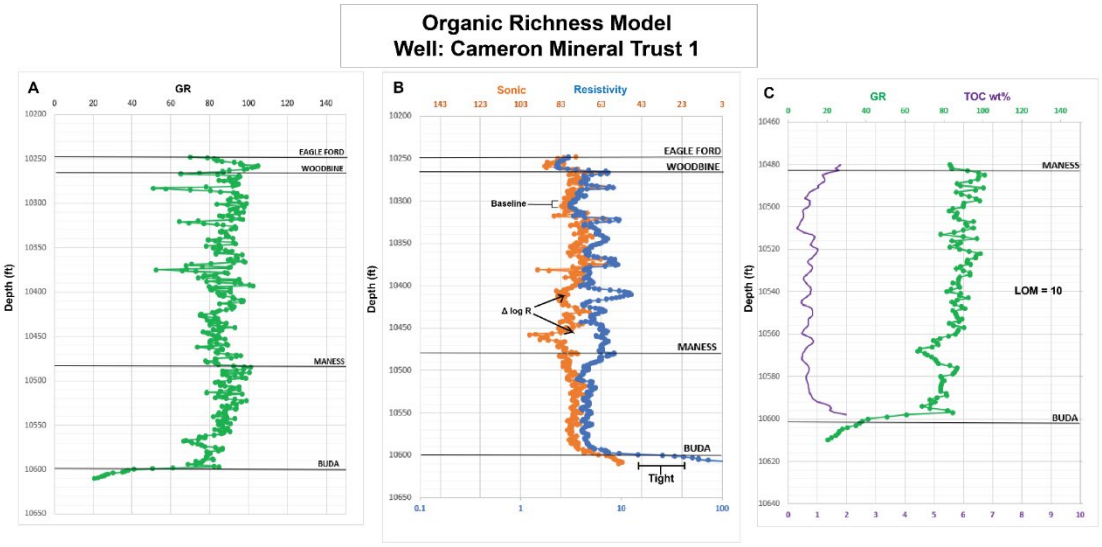

Figure 39. *Cameron Mineral Trust 1 Well* - Graph A depicts digitized gamma ray values. Graph B presents the sonic/resistivity overlay encompassing the Eagle Ford, Woodbine, and Maness intervals. Δ log R separation indicates potential total organic carbon (TOC) content, primarily within the lower Woodbine interval rather than the upper Maness. The baseline value was taken at a depth of 10304 ft SSTVD and the low porosity (tight) interval was observed at the Maness-Buda contact. The sonic response is represented by the orange curve, while the resistivity is depicted by the blue curve. Graphs C shows TOC wt% calculations. The purple curve depicts the TOC wt% values, and the green curve corresponds to the gamma-ray response. A gamma-ray cutoff is implemented to exclude high TOC wt% values.

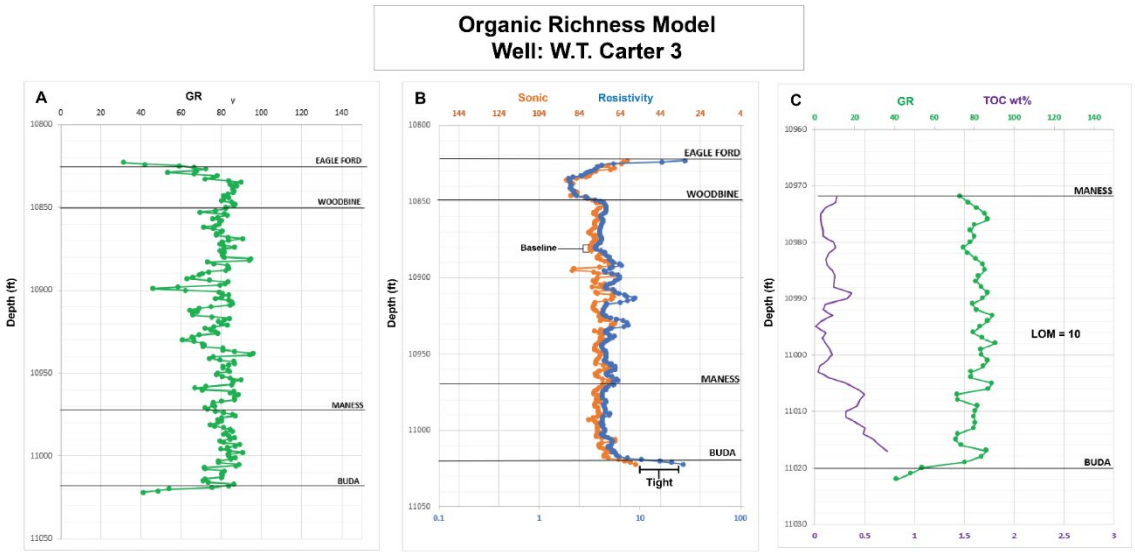

Figure 40. W.T. Carter 3 Well - Graph A depicts digitized gamma ray values. Graph B illustrates the sonic/resistivity overlay across the Eagle Ford, Woodbine, and Maness intervals. The absence of Δ log R separation suggests a lack of total organic carbon (TOC) content within this well. The baseline value was taken at a depth of 10882 ft SSTVD and a low porosity (tight) interval was observed at the Maness-Buda contact. The sonic response is represented by the orange curve, while the resistivity is depicted by the blue curve. Graphs C and D represent TOC wt% calculations within the Maness interval for two levels of maturity (LOM): LOM 7 and LOM 12, respectively. The purple curve represents the TOC wt% values, while the green curve represents the gamma-ray response. A gamma-ray cutoff was applied to exclude high TOC values that occurred within the low-porosity (tight) Buda interval.

VII. Discussion

VII.I Sediment Source

The principal objective of this thesis was to ascertain the primary clastic sediment source of the Maness Shale. This study used the sequence stratigraphic approach of Ambrose et al. (2009) and Hentz et al. (2014) to identify the Maness as a sequence. This approach broadened the perspective beyond the traditional lithostratigraphic interpretation of the Maness Shale, which had been the primary focus in prior studies, including Patterson (2018) and English (2020). Moreover, it classifies the Maness interval as the earliest among a series of sequences within the broader Woodbine succession. Ambrose et al. (2009) did not explicitly designate the upper portion of the sequence as the Maness, but instead referred to it as the S1 highstand within the lower Woodbine. Ambrose et al. (2009) identified the Maness/S1 sequence in the East Texas Field, spanning western Rusk and eastern Smith counties (Fig. 8), and Hentz et al. (2014) identified it in the southernmost region of the East Texas Basin, specifically in Leon and northwest Houston counties (Fig. 9). Both studies recognized this initial sequence as comprising a lower unit with upward fining characteristics, corresponding to the lower Maness in this study, and an upper unit with upward coarsening features, which aligns with the upper Maness in this study. These two units are separated by a maximum flooding surface (MFS), identified as the intra-Maness in this study.

This discussion will examine the upper and lower Maness intervals separately because of a potential shift in the sediment source during their deposition. The findings in the current study, alongside previous research by Denne and Breyer (2016), Patterson (2018), and English (2020), consistently suggest a northeastern origin for the sediment (Fig. 35). This study identified a deltaic sediment source within the upper Maness just west of the Sabine Uplift in Rusk and Smith counties (Fig. 33). However, this source is not evident for the lower Maness interval.

VII.I.I Upper Maness

The presence of thick sandstones was identified within the upper Maness interval, notably concentrated immediately to the west of the Sabine Uplift in the East Texas Field in western Rusk and southwestern Gregg Counties (Fig. 33). This observation strongly implies the existence of a deltaic sediment source at the southern end of the East Texas Field. Furthermore, Ambrose et al. (2009) previously noted that their S1 highstand displayed sedimentary characteristics typical of fluvial-dominated deltaic systems. This observation, based on a core from the Shell 55 Watson well in the East Texas Field and detailed mapping in Rusk County (Fig. 41), provides compelling evidence of deltaic sediments on the Sabine Uplift, which aligns with the findings of this study.

The most substantial sediment accumulations are primarily found in areas located downdip from the deltaic regions. Notably, in Cherokee County, situated within the East Texas Salt Basin, and the northernmost part of Houston County, extending westward and southwestward from the deltaic environment region (Fig. 29), these areas display significant thicknesses. However, they exhibit minimal presence of sandstones, consistent with the characteristic features of pro-deltaic mud deposits. The major thicknesses in Cherokee County can be attributed to the deposition of pro-deltaic mud within withdrawal basins adjacent to salt diapirs.

Regions of significant thickness are separated by an area characterized by thinner sediment deposition, extending from the Houston Arch to the Edwards Shelf Margin (Figs. 29, 35). This configuration, commonly referred to as a bypass zone (Fig. 42), is typically associated with areas featuring steep gradients and channelized sediment transport, where sediments are transported downslope for subsequent deposition. In the region displaying characteristics of a bypass zone, the map indicates that sediment deposition predominantly consisted of mud (Fig. 33).

South of the Sabine Uplift, in Tyler and Polk counties near the Edwards and Sligo shelf margins, there is a distinct thickening trend and the presence of sandstone packages. In this down-slope region, the interplay between increased accommodation space and the influences of debris flows and turbidity currents along the shelf slope break significantly contributes to the formation of sandstone features within the upper Maness interval (Fig. 42). Supporting this observation, Ambrose et al. (2014) documented the presence of debris-flow deposits, characterized by larger grain size, limited sorting, and disordered bedding, in a core sample extracted from the Standard No. 2 Longbell well. These deposits were identified at depths similar to the Maness interval within this region, located downdip from the Edwards Shelf margin in Tyler County. It is essential to note that Ambrose et al. (2014) did not identify this interval as the "Maness" but rather referred to it as the lower Woodbine in their study.

VII.I.II Lower Maness

Unlike the upper Maness, which displays sandstone presence in proximity to the Sabine Uplift, the lower Maness primarily consists of shale (Fig. 32). This shale layer covers the Buda Limestone throughout the entire study area, with minimal to no occurrences of sandstones. Although the deposition of the lower Maness interval is indicative of a northern to northeastern sediment source, the absence of sandstones in up-dip regions near the Sabine Uplift suggests that the source of the lower Maness is likely situated farther to the north, outside of the study area.

The thickness trends observed in the lower Maness are similar to those in the upper Maness. The thickest accumulations of sediment are situated downdip from the Sabine Uplift, particularly to the west within the pro-deltaic environment of the East Texas Salt Basin, as well as to the south near the Edwards and Sligo margins (Fig. 28). In Tyler County, to the south, the lower Maness interval predominantly comprises mud with the rare occurrence of intermittent layers of interbedded

sandstone packages (Fig. 32). The occurrence of these interbedded sandstone packages is indicative of downdip slope deposits within this region.

VII.I.III Evaluation

Hypothesis 1 proposed that the Sabine Uplift served as the principal sediment source for the Maness Shale. According to Ambrose et al. (2009), the Sabine Uplift remained stable during the deposition of the Buda Limestone and Maness Shale, which is demonstrated by the absence of significant thickness variations within these two units. The uplift subsequently began to rise after the deposition of the Maness Shale, continuing its gradual uplift throughout the Woodbine and Eagle Ford depositional periods. This study's observations regarding the lower Maness interval align with these assertions, revealing minimal to no sandstone presence (Fig. 32). In contrast, as pointed out by Ambrose et al. (2009) and supported here, the S1 highstand sequence, equivalent to the upper Maness in this study, contains sandstones immediately west of the Sabine uplift. This finding suggests that the Sabine Uplift may have contributed sediment, but it does not establish it as the primary source for the Maness.

Comparing the Sabine Uplift's potential erosion to the Harris Delta's behavior provides valuable insights. Denne and Breyer's (2016) isopach map (Figure 26 in their study) illustrates the Harris Delta's westward expansion, displaying a trend of E-W sedimentation. This indicates that sediment eroded from the Sabine Uplift extended into the East Texas Basin. Notably, the Harris Delta shows distinctive incised valley fills, clearly visible in log character. These features, however, are absent in the Maness interval. That said, the trends found in this study indicate that while the Sabine Uplift may have provided sediment, especially during deposition of the upper Maness, it was not the primary sediment source for the Maness. It is more plausible that the sediment originated from a source further north, such as the Ouachita Highlands.

VII.II Organic Richness

Another key objective of this study was to assess the source rock potential of the Maness shale. The initial plan to utilize core samples for determining TOC values was modified due to logistical constraints. Therefore, Passey's Δ log R method was applied to model organic richness in the current study. In the W.L. Green well (Fig. 36B) a discernible Δ log R separation between the sonic/resistivity log curves occurs in the upper Maness interval between 8520 to 8530 ft (2597 to 2600 m). This indicates the possible presence of source rock potential at this specific depth. Per Passey et al. (1990), the observed Δ log R separation in this instance is indicative of a mature source. The separation signifies contributions from both sonic and resistivity curves, distinguishing it from scenarios characterized solely by sonic response (indicating immature source) or resistivity response (suggesting low-porosity tight zones) (Passey et al., 1990).

However, the models for Total Organic Carbon content (TOC wt.%) (Figs. 36C through 40C) suggest limited potential for substantial TOC content within the Maness across most wells in this study. Notably, the Fitzgerald 1 well stands out as an exception (Fig. 38C), displaying TOC wt.% values exceeding 2% over a 6-foot thickness within the Maness interval. In contrast, the other wells surveyed did not exhibit TOC wt.% values greater than 2% within the Maness interval. It is worth highlighting that the Fitzgerald 1 well, despite its TOC characteristics, is distinguished by its shallower depth, lower temperature, and an LOM (Level of Organic Metamorphism) value of 9. Conversely, all other surveyed wells had estimated LOM values of 10, nearing the threshold of overmaturity, which is conventionally recognized at an LOM of 11 (Passey et al., 1989).

Through this analysis, it became evident that although the Maness Shale exhibits some evidence of TOC, it falls short of being classified as a robust source rock, particularly within the specific wells studied. However, this assessment rests on estimations derived from computational models, which

inherently bear limitations tied to data quality. Consequently, a more precise evaluation of the Maness Shale's source rock potential necessitates core analysis and a direct and empirical approach offering deeper insights into TOC content and sedimentary composition.

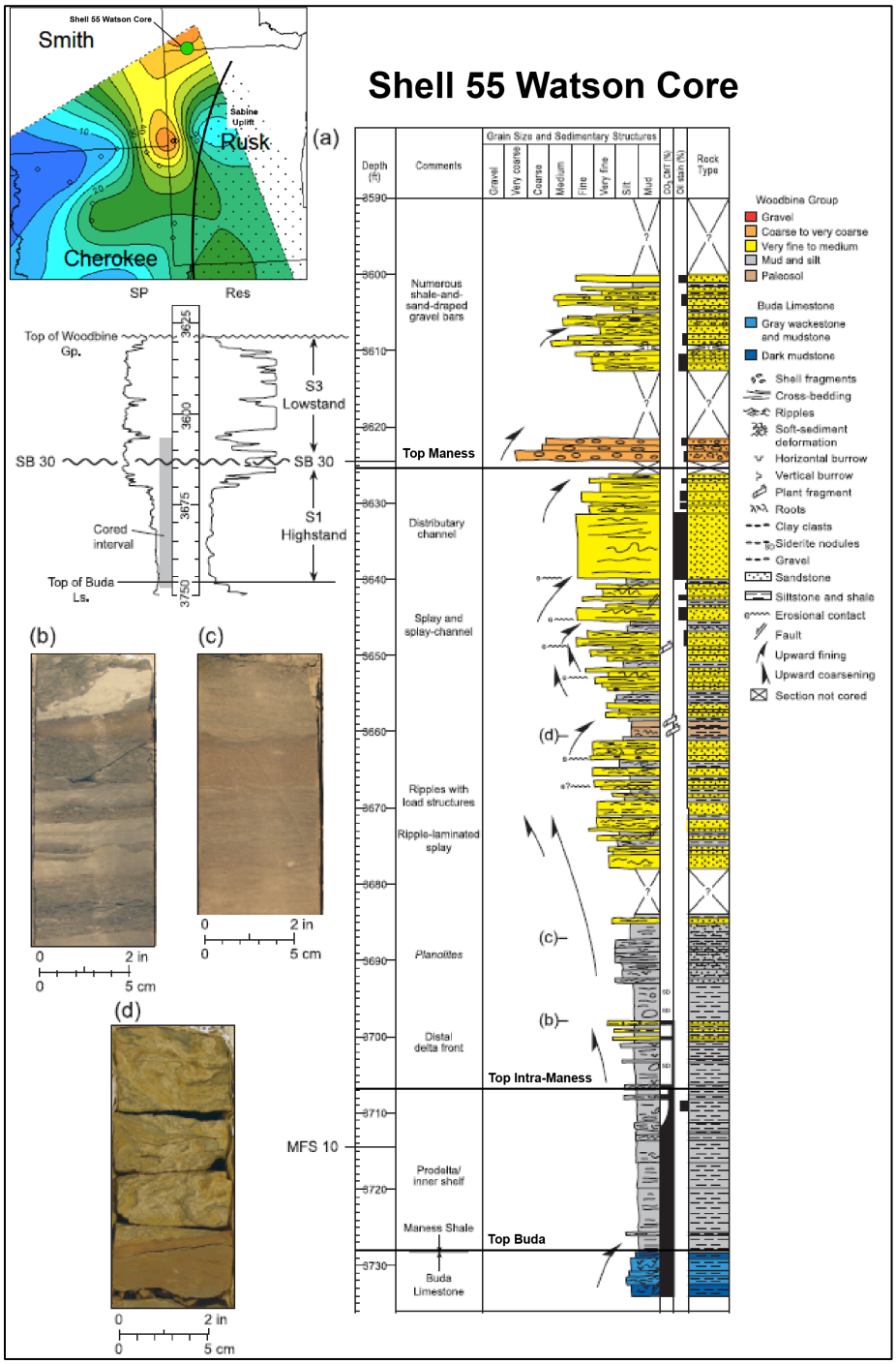

Figure 41. Core description and log response analysis of the Maness interval, also referred to as the S1 highstand, in the Shell 55 Watson well (adapted from Ambrose et al., 2009). The identification of the top of the Maness and intra-Maness was based on sequence stratigraphic trends applied in this study. A close-up view of Figure 30 shows where this core occurs and how it corresponds to the net sandstone maps of the Maness (Shell 55 Watson Core illustrated by the green dot on close-up view of Figure 30).

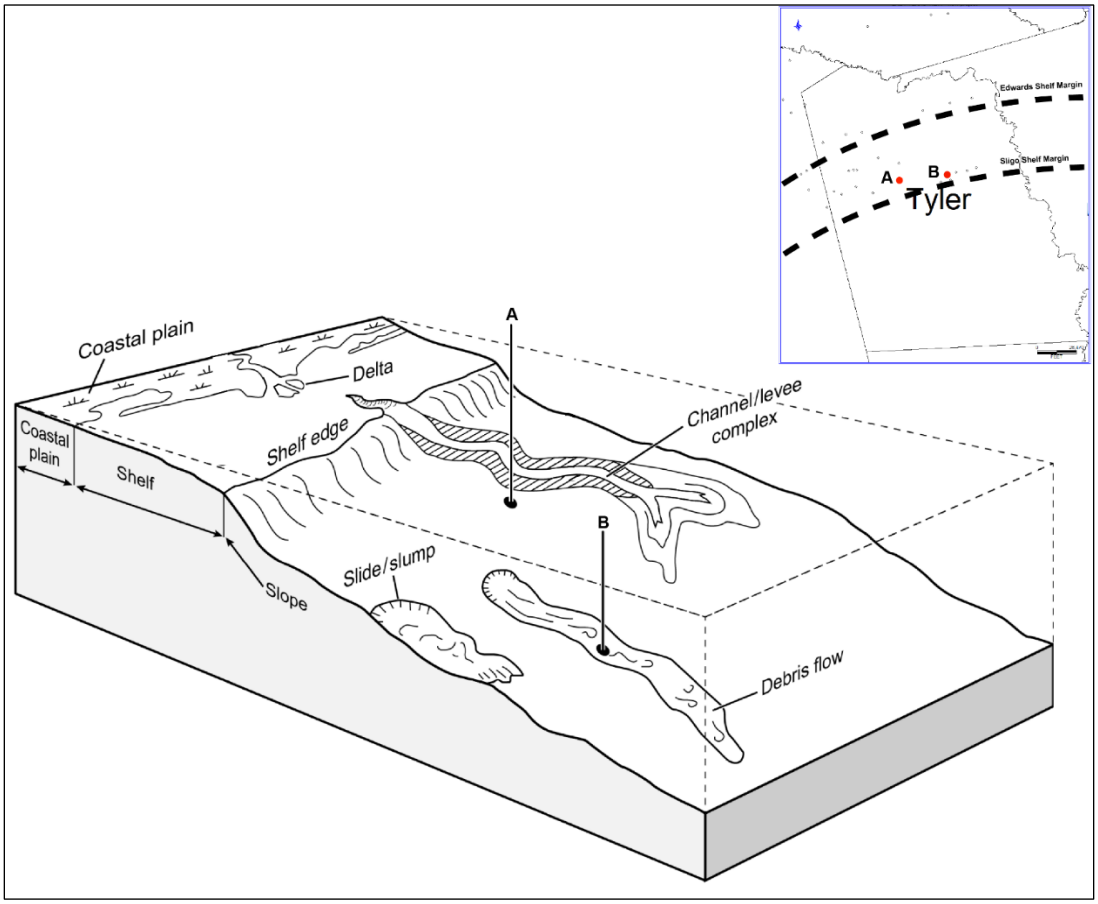

Figure 42. Block diagram modified from Ambrose et al. (2014), illustrating the depositional setting of the cores employed as analogs in their study. These cores are situated in the southern sector of the study area, adjacent to the Edwards and Sligo Margins within Tyler County. (A) pertains to the Delta No. 2 Carter well, deposited in a region marked by debris flows and turbidity currents, whereas (B) pertains to the Standard No. 2 Longbell well, deposited in a bypass zone environment. The precise locations of these cores are denoted by red dots on the map.

VIII. Summary and Conclusions

The Maness Shale, which is historically placed within the Washita Group, is a clay-rich mudrock that serves as the basal member of the Eagle Ford Shale in the south Texas producing region, and underlies the Woodbine Sandstone in east Texas. The primary objective of this study was to conduct a comprehensive investigation of the Maness Shale in east Texas, with specific focus on regions adjacent to the Sabine Uplift. The research aimed to gain a deeper understanding of this mudrock's sediment source and to estimate its organic richness and potential as a source rock. In line with this objective, the following hypotheses were tested:

1. The Sabine Uplift serves as the primary sediment source of the Maness Shale.
2. The Maness Shale is a potential source rock.

Previous studies (Denne and Breyer, 2016; Patterson, 2018; English, 2020) revealed variable thickness trends of the Maness shale across the East Texas Basin and south Texas Eagle Ford producing region. Their combined isopach maps shown in English (2020) showed that this mudrock thickens towards the west, peaking in the southern part of the East Texas Basin, and thins towards the southwest, extending across the San Marcos Arch and into Karnes and Atascosa counties. Ambrose et al. (2009) and Hentz et al. (2014) used a sequence stratigraphic approach to map the Maness sequence which comprises a lower, upward-fining retrogradational sequence, and an upper, upward coarsening progradational sequence, separated by a maximum flooding surface.

The current study utilized the approach of Ambrose et al. (2009) and Hentz et al. (2014) to correlate the Maness interval across the study area to help identify its sediment source by generating structural, isochore, and net sandstone maps as well as a composite isochore map that combined the maps from Denne and Breyer (2016), Patterson (2018), and English (2020). After the maps were generated, the present study employed Passey's Δ log R method to estimate organic

richness in 5 wells by utilizing a sonic/resistivity overlay. TOC wt.% values were then generated by utilizing the SMU Node of the National Geothermal Data System to estimate bottomhole temperature and United States Geological Survey's Pocket Geology of Texas website to estimate effective heating time which produced Level of Organic Metamorphism (LOM) values.

The net sandstone maps indicated the presence of fluvial deltaic sediments located immediately west of the Sabine Uplift within the upper Maness, suggesting a deltaic depositional environment. In contrast, the lower Maness is characterized by a predominance of mud deposits across the entire study area. Based on the isochore maps produced in this study, the thickest intervals of Maness are observed in northern Houston and Cherokee County. These regions are indicative of pro-deltaic muds influenced by salt movement in Cherokee County. Additionally, thick Maness intervals are present in Tyler and Polk counties, suggesting the influence of debris flows and turbidity currents in proximity to the shelf-slope break. These two distinctive thickness patterns are separated by a bypass zone, which is situated between the Houston Arch and the Edwards Shelf Margin.

The collective data from these maps consistently point to a northern origin for the Maness sediment source. There is no clear evidence to support the idea that the primary sediment source is related to erosion of the Sabine Uplift. In fact, it is likely that the primary sediment source came from somewhere to the north of the study area, most likely the Ouachita Highlands. Lastly, the analysis of organic richness using Passey's Δ log R method did reveal some potential within the Maness interval. However, the results provided insufficient evidence to categorize the Maness as a viable source rock within the examined wells.

References

Adams, R. L., Carr, J.P., & Ward, J.A., (2014). The lower Woodbine organic shale of Burleson and Brazos counties, Texas: Anatomy of a new old play. Gulf Coast Association of Geological Societies Transactions, v. 64, p. 3–31.

Ambrose, W.A., Hentz, T.F., Bonnaffe, F., Loucks, R.G., Brown Jr., L.F., Wang, F.P., & Potter, E.C., (2009). Sequence stratigraphic controls on complex reservoir architecture of highstand fluvial deltaic and lowstand valley-fill deposits in the upper Cretaceous (Cenomanian) 122 Woodbine Group, East Texas Field: Regional and local perspectives. AAPG Bulletin, v. 93, p. 231-269.

Ambrose, W.A., Hentz, T.F., & Smith, D. (2014). Facies variability and reservoir quality in the shelf-to-slope transition, upper Cretaceous (Cenomanian) Woodbine group, northern Tyler sands and southeastern Polk counties, Texas, U.S.A.: Gulf Coast Association of Geological Studies, v. 3, p. 1–19.

Anderson, E.G., (1979). Basic Mesozoic study in Louisiana, the north coastal region, and the gulf basin, Louisiana geological survey, mineral and energy resource program LSU, p. 58.

Arthur, M.A., & Sageman, B.B., (2004). Sea-level control on source-rock development: Perspectives from the Holocene black sea, the mid-Cretaceous western interior basin of North America, and the late Devonian Appalachian basin. SEPM Special Publication, v. 82, p. 35–59.

Arthur, M.A., & Sageman, B.B., (2005). Sea-level control on source-rock development: Perspectives from the Holocene Black Sea, the mid-Cretaceous western interior basin of north America, and the late Devonian Appalachian basin. In Harris NB (editor). The deposition of organic-

carbon-rich sediments: Models, Mechanisms, and Consequences, special publication 82: SEPM (Society for Sedimentary Geology), Tulsa, Oklahoma. p. 35–59.

Bailey, T.L., Evans, F.G., & Adkins, W.S., (1945). Revision of stratigraphy of part of Cretaceous in Tyler Basin, northeast, Texas. AAPG, 29(2), 170-186.

Barrett, M.L., & Goodson, J., (2006). High-resolution foraminiferal biostratigraphy of Cenomanian and Turonian sandstones, Tyler County, Texas.

Bunge, R.J. (2007). Woodbine formation sandstone reservoir prediction and variability, Polk and Tyler Counties, Texas.

Denne, R A., & Breyer, J.A., (2016). Regional depositional episodes of the Cenomanian–Turonian Eagle Ford and Woodbine Groups of Texas, in J.A. Breyer, ed., the Eagle Ford Shale: A renaissance in U.S. oil production: AAPG memoir 110, p. 87–133.

Denne, R.A., & Patterson, S.P., (2019). The effects of the Maness Shale on Eagle Ford water production. v. 928, p. 1-15.

Denne, R.A., Breyer, J.A., Callender, A.D., Hinote, R.E., Kariminia, M., Kosanke, T.H., Kita, Z., Lees, J.A., Rowe, H., Spaw, J.M., & Tur, N., (2016). Biostratigraphic and geochemical constraints on the stratigraphy and depositional environments of the Eagle Ford and Woodbine groups of Texas. in J.A. Breyer, ed., the Eagle Ford Shale: A renaissance in U.S. oil production. AAPG Memoir, 110, p. 1-86.

Denne, R.A., Hinote, R.E., Breyer, J.A., Kosanke, T.H., Lees, J.A., Engelhardt-Moore, N., Spaw, J.M., & Tur, N., (2014). The Cenomanian-Turonian Eagle Ford Group of south Texas: Insights on timing and palaeoceanographic conditions from geochemistry and micropaleontologic analyses. Paleogeography, Palaeoclimatology, Paleoecology, v. 413, p. 2-28.

Dennen, K.O., & Hackley, P.C., (2012). Definition of greater gulf basin Lower Cretaceous and Upper Cretaceous Lower Cenomanian shale gas assessment unit, United States Gulf of Mexico basin onshore and state waters.

English, M.M., & Denne, R.A. (2020). Stratigraphy and geochemistry of the Lower Cenomanian Maness Shale of east Texas.

Ewing, T.E. (2009). The ups and downs of the Sabine Uplift and the northern Gulf of Mexico Basin: Jurassic basement blocks, Cretaceous thermal uplifts, and Cenozoic flexure.

Foss, D.C., (1979). Depositional environment of Woodbine sandstones, Polk County, Texas: Gulf Coast Association of Geological Societies Transactions, v. 29, p. 83–94.

Galloway, W.E., (2008). Depositional evolution of the Gulf of Mexico sedimentary basin, in Andrew D. Miall, ed., sedimentary basins of the world: Elsevier, 505–549.

Geothermal Laboratory - SMU. (2023). Geothermal Data Aggregation. http://geothermal.smu.edu/gtda/.

Glawe, L.N., (1989). Stratigraphic relationships between odontogryphae thirsae beds and the big shale of the Wilcox (Paleocene- Eocene) in Louisiana. Gulf Coast Association of Geological Societies Transactions, v. 39, p. 375–383.

Halbouty, M.T., & Halbouty, J.J. (1982). Relationships between East Texas Field region and Sabine Uplift in Texas. AAPG Bulletin, v. 66, no. 8, p. 1042–1054.

Hentz, T. F., & Bonnaffe, F., (2010). Sequence Stratigraphy of the Upper Cretaceous (Cenomanian) Woodbine Group: Chronostratigraphic integration of the East Texas Basin and East Texas Field. Bureau of Economic Geology Report of Investigations, 274, p. 1-16.

Hentz, T. F., & Ruppel, S.C. (2010). Regional lithostratigraphy of the Eagle Ford shale: Maverick Basin to East Texas Basin. Gulf Coast Association of Geological Societies, 60, p. 325- 337.

Hentz, T.F., Ambrose, W.A., & Smith, D.C., (2014). Eaglebine play of the southwestern East Texas Basin: Stratigraphic and depositional framework of the Upper Cretaceous (Cenomanian-Turonian) Woodbine and Eagle Ford groups. AAPG Bulletin, v. 98, p. 2551-2580.

Hood, A., & Gutjahr, C.C.M., (1975). Organic metamorphism and the generation of petroleum. AAPG Bulletin, 59.

Jennings, D. S., & Antia, J., (2013). Petrographic characterization of the Eagle Ford shale, south Texas: mineralogy, common constituents, and distribution of nanometer scale pore types. In camp W., Diaz E., Wawak, B. (Editors). Electron microscopy of shale hydrocarbon reservoirs, memoir 102: American Association of Petroleum Geologists, Tulsa, Oklahoma, p. 101–113.

Laubach, S. E., & Jackson, M.L.W., (1990). Origin of arches in the northwestern Gulf of México Basin. Geology, v. 18, p. 595-598.

Leach, D.L., & Rowan, E.L. (1986). Genetic link between Ouachita foldbelt tectonism and the Mississippi valley–type lead-zinc deposits of the Ozarks. Geology, 14, 931-935.

Lowery, C.M., Corbett, M.J., Leckie, R.M., Watkins, D., Romero, A.M., & Pramudito, A., (2014). Foraminiferal and nannofossil paleoecology and paleoceanography of the Cenomanian–Turonian Eagle Ford Shale of southern Texas. Palaeogeography, Palaeoclimatology, Palaeoecology, v. 413, p. 49–65.

Lozo, F.E., (1951). Stratigraphic notes on the Maness (Comanche Cretaceous) Shale in F. E. Lozo, ed., the Woodbine and adjacent strata of the Waco area of central Texas, a symposium for the

1951 field trip sponsored by the East Texas Geological Society: SMU Press, Fondren Science Series 2, Dallas, Texas, p. 67-100.

Luttrell, P.E., (1977). Carbonate facies distribution and diagenesis associated with volcanic cones - Anacacho Limestone (Upper Cretaceous), Elaine Field, Dimmit County, Texas, in Bebout, D. G. and Loucks, R. G. eds., Cretaceous carbonates of Texas and Mexico: applications to subsurface exploration. University of Texas at Austin, Bureau of Economic Geology Report of Investigations No. 89, Austin, TX, pp. 260-285.

Mancini, E.A., and T.M. Puckett, (2005). Jurassic and Cretaceous transgressive-regressive (t-r) cycles, northern Gulf of Mexico, USA. Stratigraphy, v. 2, no. 1, p. 31–48.

Mancini, E.A., Obid, J., Badali, M., Liu, K., & Parcell, W. C., (2008). Sequence-stratigraphic analysis of Jurassic and Cretaceous strata and petroleum exploration in the central and eastern gulf coastal plain, United States. American Association of Petroleum Geologists Bulletin, v. 92/12, p. 1655–1686.

Mondelli, K., (2011). Salt reconstruction and study of depositional history, Upper Jurassic, East Texas Basin. M. S. thesis, University of Houston, 83 pp.

Murray, G.E., (1961). Geology of the Atlantic and gulf coastal province of North America: Harper and Brothers, New York, 692 p.

Passey, Q. R., Creaney, S., Kulla, J.B., Moretti, F. J., & Stroud, J.D., (1989). Well log evaluation of organic-rich rocks. 14th International Meeting on Organic Geochemistry. Paris, Abstract 75.

Passey, Q., Creaney, S., Kulla, J., Moretti, F. & Stroud, J. (1990). A practical model for organic richness from porosity and resistivity logs. The American Association of Petroleum Geologists Bulletin. 74(12): 1777- 1794.

McLaren, P. (1981). An interpretation of trends in grain size measures. SEPM Journal of Sedimentary Research, Vol. 51.

Patterson, S.A., (2018). The Maness Shale: a comparison of the geomechanical and mineralogical properties within the Lower Eagle Ford Formation, South Texas. M.S. thesis, Texas Christian University, Fort Worth, TX, 97 pp.

Pearson, O.N., Rowan, E.L., & Miller, J. J., (2012). Modeling the Mesozoic Cenozoic structural evolution of east Texas. Modeling the Mesozoic-Cenozoic Structural Evolution of East Texas, 1, 118–128.

Phelps, R.M., Kerans, C., Loucks, R.G., Da Gama, R.O., Jeremiah, J. & Hull, D., (2014). Oceanographic and eustatic control of carbonate platform evolution and sequence stratigraphy on the Cretaceous (Valentinian–Campanian) passive margin, northern Gulf of Mexico. Sedimentology, v. 61(2), p.461-496.

Powers, S. (1920). The Sabine Uplift. Bull. Amer. Assoc. Petroleum. Geol., vol. 4, pp. 117-36.

Ruppel, S. C., R. G. Loucks, & Frébourg, G., (2012). Guide to field exposures of the Eagle Ford-equivalent Boquillas Formation and related Upper Cretaceous units in southwest Texas: The University of Texas at Austin, BEG, Mudrock Systems Research Laboratory Field Trip Guidebook, 151 p.

Salvador, A., (1991). Origin and development of the Gulf of Mexico Basin, in A. Salvador, ed., The Gulf of Mexico Basin. Geological Society of America, Decade of North American Geology, v. J, p. 389–444.

Seni, S. J., and M. P. A. Jackson, (1983). Evolution of salt structures, east Texas diapir province, part 1: Sedimentary record of halokinesis: AAPG Bulletin, v. 67.

Seni, S. J., &, Jackson, M.P.A., (1984). Sedimentary record of Cretaceous and Tertiary salt movement, East Texas Basin. Report of Investigations No. 139, Bureau of Economic Geology, The University of Texas, Austin.

Siemers, C.T., (1978). Submarine fan deposition of the Woodbine-Eagle Ford interval (Upper Cretaceous), Tyler County, Texas. Gulf Coast Association of Geological Societies Transactions, v. 28, p. 493–533.

Stehli, F.G., Creath, W.B., Upshaw, C.F., & Forgotson Jr., J.M., (1972). Depositional history of Gulfian Cretaceous of East Texas embayment. AAPG Bulletin, v. 56, no. 1, p. 38–67.

Tye, R.S., & Coleman, J.M., (1988). Evolution of Atchafalaya lacustrine deltas, south-central Louisiana. Sedimentary Geology, v. 65, p. 95–112.

U.S. Geological Survey, Pocket Texas Geology; Texas Geological Survey, 2023, https://txpub.usgs.gov/txgeology/.

Valencia, F.L., Buatois, L.A., Laya, J.C., Mángano, M.G., Valencia, G.L., & Pope, M.C., (2021). Depositional environments and controls on the stratigraphic architecture of the Cenomanian Buda limestone in West Texas, U.S.A. Marine and Petroleum Geology, 133, 105275.

Vallabhaneni, S., Olszewski, T.D., Pope, M.C., & Heidari, Z., (2016). Facies and stratigraphic interpretation of the Eaglebine play in Central Texas. GCAGS Journal, v. 5, p. 25-46.

Walthall, B.H., & Walper, J.L., (1967). Peripheral gulf rifting in Northeast Texas. AAPG Bulletin, 51, 102-110.

Appendix A – Trendline for Bottomhole Temperature

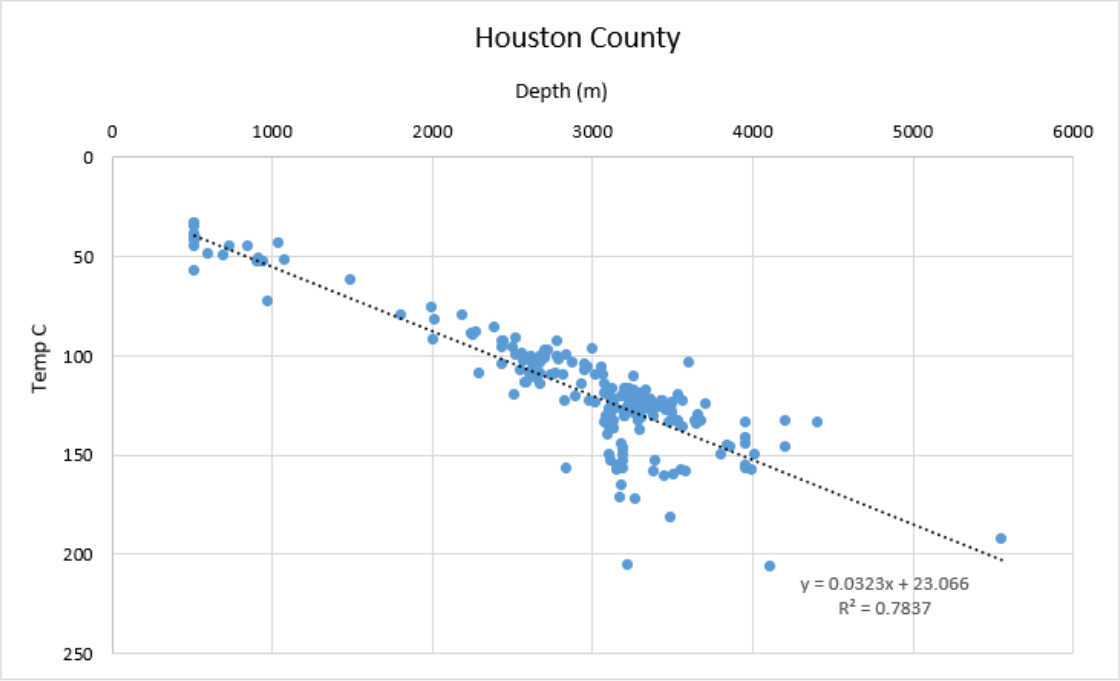

Appendix A-1. Trendline for bottom hole temperature against depth in Houston County, Texas, generated using data obtained from the SMU Node of the National Geothermal Data System (http://geothermal.smu.edu/gtda/).

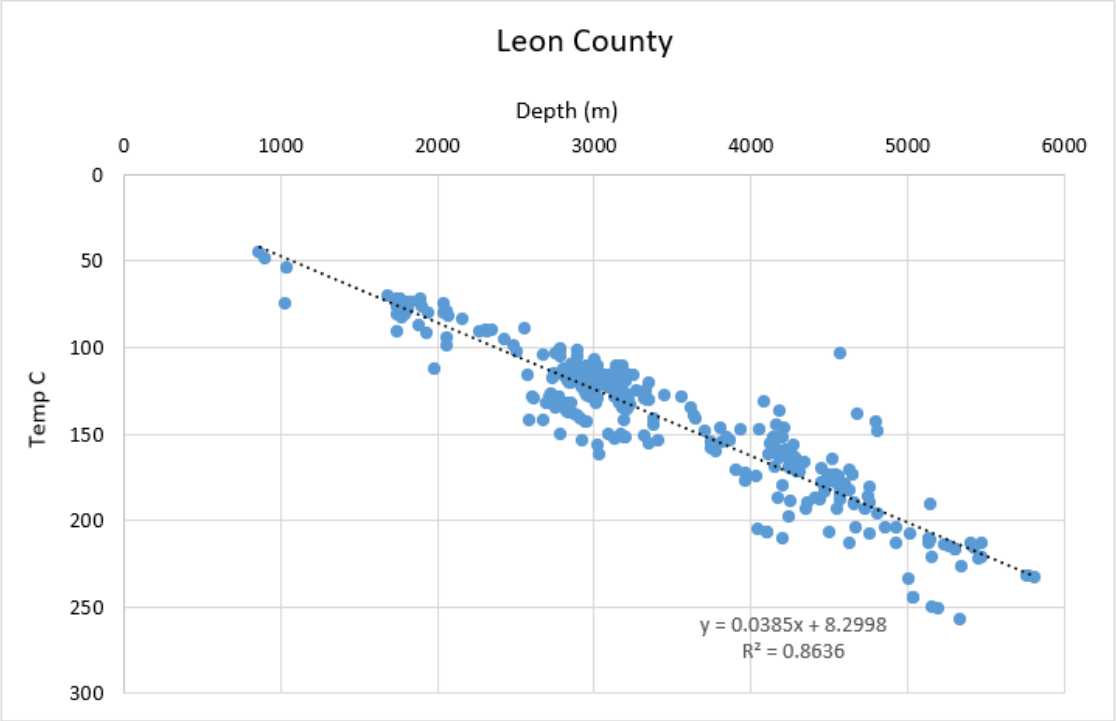

Appendix A-2. Trendline for bottom hole temperature against depth in Leon County, Texas, generated using data obtained from the SMU Node of the National Geothermal Data System (http://geothermal.smu.edu/gtda/).

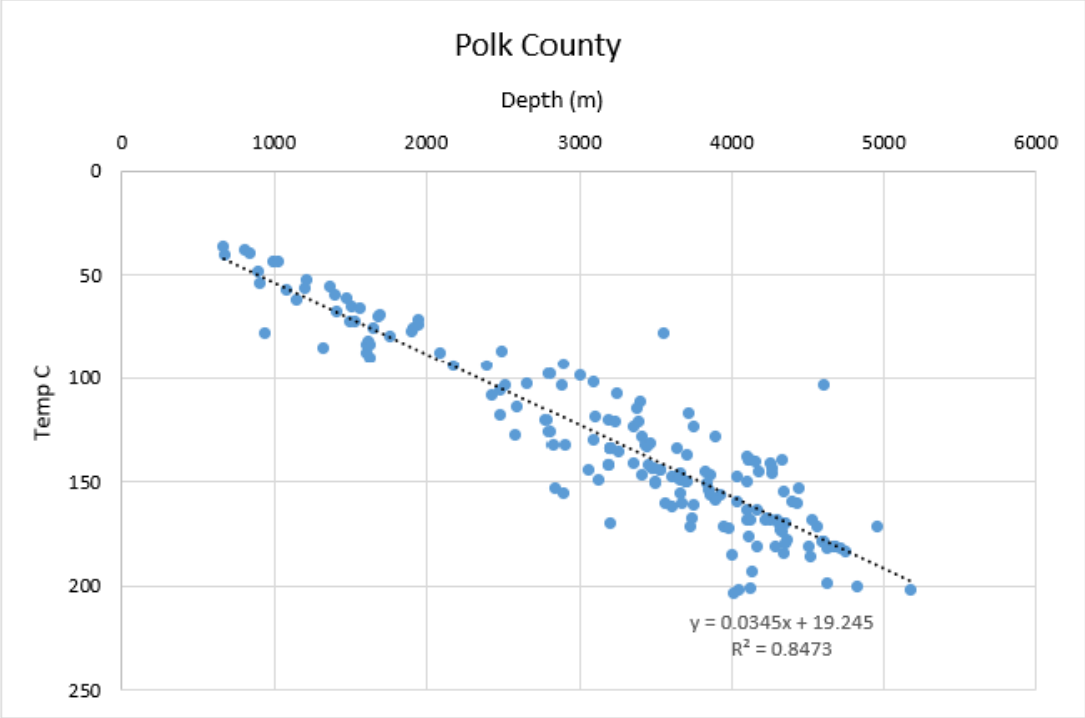

Appendix A-3. Trendline for bottom hole temperature against depth in Polk County, Texas, generated using data obtained from the SMU Node of the National Geothermal Data System (http://geothermal.smu.edu/gtda/).

Appendix B – Maximum Temperature vs. Effective Heating Time Graph

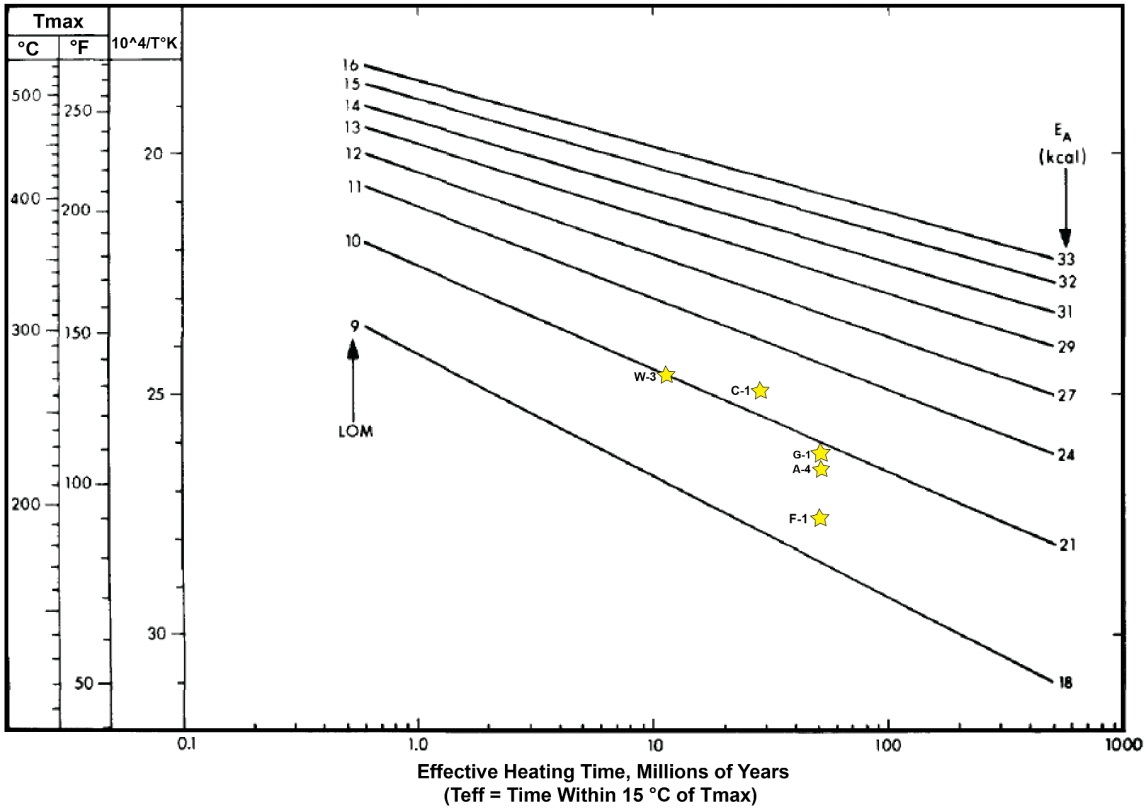

Appendix B: Relation of LOM to maximum temperature and effective heating time graph modified from Hood et al. (1975). Yellow stars on the graph represent wells from this study where organic richness was evaluated. These wells include Fitzgerald 1 (labeled as F-1), AFGRD 4 (labeled as A-4), W.L. Green 1 (labeled as G-1), Cameron Mineral Trust 1 (labeled as C1), and W.T. Carter 3 (labeled as W-3). They were plotted on the graph based on their estimated maximum temperature in relation to their effective heating time.

Appendix C – Wells Logs and Fm Tops

API Number (14 #)	Well Name	Top Maness Depth (ft)	Top Intra Maness Depth (ft)	Top Buda Depth (ft)	Maness Thickness (ft)
42401306350000	KINNEY	3627		3670	43
42225310670000	COLEMAN	8663	8692	8739	76
42395317220000	LILY HOPPESS UNIT	6751	6787	6859	108
42395313540000	LANDERS	6840	6871	6951	112
42395314580000	MCCULLOUGH B	6544	6580	6653	109
42289315720000	FOSSIL WILDMAN TRUST	6826	6865	6935	109
42289308310000	SIMMS	7062	7106	7186	125
42289318430000	ERICSON GAS UNIT	5629		5758	129
42289319630000	CAMPBELL GAS UNIT	5541		5662	122
42289319670000	HELMCAMP	6251		6355	104
42289315400000	MULLENAX, G.	5459	5502	5579	120
42289313510000	RAINBOLT RANCH A	6091		6229	138
42041313220000	WILSON, JAMES D.	8908	8927	8982	74
42041306940000	BRYAN WOODBINE UNIT	8601	8625	8685	84
42041307820000	ERCANBRACK-RAMBO UNI	8653		8738	86
42041308180000	BRYAN WOODBINE UNIT	8689	8712	8779	90
42041305230000	ADAMS, J.	8413	8441	8504	91
42041306030000	CLEAR LAKE PROPERTIE	9259		9330	71
42041306870000	RANSOM UNIT	7912	7940	8005	93
42041307040000	GRAY UNIT	8079	8107	8177	98
42395304100000	DAVISON	7534	7564	7640	106
42395309200000	PLATT GAS UNIT	4811		4926	115
42395309110000	DUNCAN GAS UNIT NO.	4898	4932	5005	107
42395309760000	LINCECUM, M. TRUST	5287		5399	112
42395312290000	T-BAR-X/TULLOUS	6423	6455	6527	104
42395316290000	HEBERT	7528	7559	7633	105
42313305050000	BAYER	8379	8413	8476	97
42313309320000	BLAZEK-PETERS	8285	8310	8377	93
42313305220000	COLE	8823	8847	8907	84
42313305060000	REDING	8975	9005	9067	92
42313302700000	FOSTER	9955	9976	10016	61
42313311010000	STERLING	9681		9753	72
42313306540000	OVERPECK, BONNIE J.	9103	9125	9185	82
42313306850000	LANG, JAMES	9140	9162	9215	75

42313303140000	HARRIS-BEVERLY	9322	9342	9388	66
42313308170000	THEISS	8539	8565	8630	91
42289318150000	CARR-NAVASOT UNIT	7235	7274	7336	100
42289310490000	DOUTHITT	7175	7209	7283	108
42289318420000	FOSSIL DONELSON GAS	6807	6844	6921	114
42289318080000	LITTLE 4 RANCH	7204	7236	7308	104
42289314060000	FOSSIL CHENEY GAS UN	6521	6556	6632	111
42289311350000	ALBRECHT, MAUDE ESTA	7165		7298	133
42289311340000	JOHNSON, WALLACE	7184		7307	123
42289311310000	GERALDINE BAIN ET AL	7184		7307	123
42289311300000	AFGRD UNIT	7700		7822	122
42289311280000	AFGRD UNIT	7861		7992	131
42289311250000	SAM KNIGHT UNIT D	7094		7204	110
42289311120000	AFNU	7351		7479	128
42289311070000	AFGRD UNIT	7635	7682	7758	123
42289311060000	COOK B	7173		7300	127
42289308550000	AFGRD UNIT	7806		7923	116
42289308360000	AFGRD UNIT	7764		7879	115
42289319800000	RED RANCH GAS UNIT	6000	6040	6130	131
42289318520000	FOSSIL STREATER GAS	6185	6230	6313	128
42289318510000	GRESHAM TRUST	6985		7098	113
42289317350000	GOLIE, MILTON GAS UN	6191		6318	127
42289317260000	CHANEY, J. UNIT	6532	6581	6666	133
42289317160000	THORNE-BARKLEY GU 1	6125		6252	127
42289316690000	MINTER	6173	6216	6318	144
42289316320000	FOSSIL WAGNER GAS UN	6245	6300	6377	132
42289316070000	BLACK, F. E.	6827	6870	6958	131
42289313540000	HAYNIE UNIT	6032	6095	6169	137
42289313490000	LTX	5852	5915	5993	141
42289313480000	LTX	5807	5869	5945	138
42289312680000	WARHAWK UNIT	6200	6240	6323	122
42001326390000	HURBROUGH GAS UNIT	6278	6379	6473	195
42073309110000	HOLCOMB	5564	5652	5715	152
42073309030000	HOLCOMB-LITTLE	5654		5731	77
42073309050000	LITTLE	5590	5635	5703	113
42073309060000	LITTLE	5631		5708	76
42073309080000	LITTLE	5531	5587	5660	130
42289310250000	STATE 93003	6997	7033	7115	118
42289310230000	EASTERLING, WARD	7188	7232	7305	116
42289311890000	FLOYD	6553	6587	6677	124
42289310200000	BROWN	6539	6574	6690	151
42289310650000	SULLIVAN A	6796	6832	6927	131
42289310930000	KNIGHT	6918	6963	7037	120

42289310180000	COOK	7044		7165	121
42289311790000	HUBBARD HEIRS	7118		7268	150
42289309860000	FITZGERALD, J.R.	7114	7182	7238	124
42289306330000	SULLIVAN, JOSEPH P.	8311	8335	8419	108
42289306390000	CLIFT, ROY	8007	8038	8098	91
42289311640000	BECHTEL/DAVIS BROS.	8724	8753	8807	83
42289307740000	SULLIVAN, T.A. UNIT	7765	7791	7852	87
42289309230000	PIERCE	7605	7648	7709	104
42313309440000	KETCHUM	8895		8967	72
42225309940000	SEVEN J STOCK FARM	8853	8877	8934	81
42225307460000	EASTHAM STATE FARM	10346	10406	10449	103
42225308170000	ADAMS, JOE	8591	8632	8673	82
42225306390000	BROWN, H.D. ET AL	8681	8709	8766	85
42225307870000	AFGRD UNIT	8335	8368	8415	80
42225308190000	CHAMPION INTERNATION	9709		9789	80
42225309300000	TAYLOR, MADGE GAS UN	6415	6473	6509	94
42225309600000	R. D.-HARRISON	6585	6630	6679	94
42225309630000	MARTIN-DAILEY	6317	6394	6434	116
42225309700000	SHARTLE GAS UNIT	6322	6398	6442	120
42225309790000	MCLEAN ESTATE GAS UN	6152	6250	6297	145
42225309930000	CLINES, M.S.	8634	8666	8726	92
42225310010000	BOBBITT	6358	6408	6463	104
42225310020000	CALVERT	9082	9116	9148	66
42225310100000	SEVEN J STOCK FARM,	9077	9126	9162	85
42225310310000	WHITEHEAD A	6969	7036	7095	126
42225310700000	SEVEN J STOCK FARN,	8871	8916	8952	81
42225310730000	T.I.N.	6375	6496	6544	169
42225310770000	PALMER	6291	6370	6425	134
42225310920000	TEMPLE	7178	7218	7253	75
42225311040000	TEMPLE INLAND A-12	6284	6379	6443	159
42225311090000	OVERSHOWN GAS UNIT	6318	6413	6467	149
42225311200000	CROCKETT, DAVY	6492	6641	6685	194
42225311370000	MAPLES	9187	9228	9272	85
42225311460000	MCFADDIN	7422	7476	7535	113
42225312630000	TODD	10388	10454	10503	115
42225312350000	ABBEY ROAD	9177	9226	9270	93
42225311910000	CARPENTER	9680	9710	9755	75
42225311830000	BLAIR A	10698	10744	10784	86
42225311680000	MOSLEY	9953	9991	10024	71
42225311880000	CROWSON	8914	8952	8998	83
42225312210000	JACKSON	8221	8261	8317	96
42225312240000	BROWN	8477	8517	8570	93
42225312500000	GAMBLE	8716	8752	8800	84

42225312650000	KEDDIE	8625	8651	8709	84
42225312670000	STARNS	8742	8769	8812	71
42225305380000	BROWN, C.W.	7549	7601	7655	106
42225305400000	LANE, G. W.	7245	7300	7344	99
42225305430000	WOLF	7952	8008	8055	103
42225308180000	CANNON, SARA ANN UNI	8693	8747	8793	100
42225304550000	EAST CROCKETT FEDERA	8317	8370	8409	92
42225303970000	HAINY, WILLIAM V.	9320	9373	9403	83
42225303780000	USA-NM-A 19767 (TEX)	8480	8525	8576	97
42225302940000	STRONG, JOSEPHINE S.	8769	8801	8842	72
42225306780000	SCARBOROUGH, G. H.	6935	6986	7047	112
42225306530000	TYER, T. W.	6921	6984	7041	119
42225305420000	MINTER ETAL	7449	7491	7552	103
42225304620000	HARDEN	6582	6702	6769	187
42225303350000	RUNNING DUKE GAS UNI	6575	6650	6712	137
42225303170000	ANDERSON HEIRS	6800	6934	6991	191
42225302980000	PETERS GAS UNIT	6509	6672	6741	232
42225301460000	HENDRICK GAS UNIT	6628	6671	6709	81
42225300630000	SMITH GAS UNIT	6499	6661	6730	231
42313309860000	FORREST C	9366		9447	81
42313312240000	DAVID	9103	9123	9176	73
42313309660000	TALLY HO	10220	10243	10280	60
42073311340000	THRASH, A (CV) GU 1	4676	4778	4821	145
42073311000000	MCELROY	4068	4141	4182	114
42073311190000	JAKUBIK	4558	4625	4670	112
42073311420000	BARNES, DA GU 1	4668		4719	51
42073308860000	NEW BIRMINGHAM MINER	5485	5587	5645	160
42073310220000	MANDY GU 1	5403	5511	5586	183
42073310850000	MCLEOD GAS UNIT	5489	5550	5626	137
42073313710000	HALL	5363	5497	5560	197
42073315080000	NEW BIRMINGHAM GAS U	5544	5637	5695	150
42073315230000	HEMATITE GAS UNIT	5633		5711	77
42001312930000	BISHOP	6673	6715	6752	78
42001322990000	MONNIG B	5935	5976	6028	93
42001323050000	ROBINSON	5887	5946	5984	97
42001324740000	COVINGTON	5929	5996	6040	111
42001325010000	COVINGTON	5978	6039	6076	98
42401310890000	HARRIS -B-	3566	3647	3668	102
42185301980000	SANDERS, M. B.	9871	9884	9922	52
42041313780000	MORGAN	10201	10216	10247	47
42051303300000	VYCHOPEN A UNIT	8716	8743	8800	84
42185302440000	HOLTH, A.	9716	9733	9771	56

42185302030000	POWLEDGE, ESTELLE	9627	9641	9676	49
42185308580000	THE DUKE	10386		10446	60
42185308500000	COMANCHERO	10358	10371	10406	48
42313303820000	SANDERS	8858	8881	8938	80
42313304710000	VICK, M.Y.	9583	9604	9646	63
42313309310000	CONNER	10358	10378	10430	72
42313303550000	MARKS UNIT	9455	9473	9517	62
42313304250000	MORRIS, NORMAN	10049	10070	10121	71
42313001470000	WALTON, J. H., UNIT	9338	9371	9417	79
42313303870000	OSBORNE, G.J.	9535	9556	9606	71
42313304880000	MATHIS, J. F. UNIT	9135	9160	9212	77
42313306870000	CANNON	9198	9224	9286	88
42313302170000	T & H CATTLE CO SOUT	9766		9842	76
42313302320000	HEATH, ORY	10153		10224	71
42313308990000	SANTA ELENA GAS UNIT	10137	10155	10191	55
42313310100000	LAURA UNIT	9945	9961	10004	59
42313306620000	ARTHEL	9593	9614	9659	67
42313309880000	HARGRAVE	9753	9777	9829	76
42313304870000	MANNING	9491	9516	9562	71
42313310460000	HENRY	9677	9693	9745	68
42313310450000	SHOEMAKER	9476	9502	9556	80
42313310290000	GREENE	9590	9616	9671	82
42313310270000	KNIGHT	9765		9830	64
42313309930000	GRISHAM	9829	9851	9901	72
42313309540000	MANNING GAS UNIT	9782	9802	9847	65
42313308880000	BYRD	9428		9504	76
42313310560000	VIVIENNE	9712	9737	9783	70
42313304170000	BARRETT	9987	9999	10038	51
42313312880000	NGR BARRETT	9947	9967	10012	65
42313309380000	SOWELL	9254	9281	9350	96
42313313120000	MORGAN	9065		9142	77
42313313040000	MOSSER	9179		9249	69
42313312990000	LEGGETT	9141		9218	77
42313312980000	GRAY	9152		9227	74
42313312960000	RADER	9287		9360	73
42313305730000	FORREST, W. M.	9005		9084	79
42041312360000	PUTZ, WILLIAM C.	8275	8303	8375	100
42289305430000	BUIE, FORREST ET AL	8177		8275	98
42313310570000	MANNING	9731	9751	9797	66
42313302990000	HENSARLING	8655	8680	8737	82
42225307180000	MORRIS, THELMA	8879	8908	8955	75
42225308760000	TURNER, JULIUS	9453	9495	9541	88
42401349030000	WHITE, GALAN GAS UNI	3552	3612	3631	79

42401307290000	STRICKLAND, J. E., -	3596	3690	3708	111
42000000000000	Watson 55	3626	3709	3730	104
42183306600000	KNOWLES ESTATE	4041	4086	4117	76
42401333010000	CHRISTIAN	3800	3889	3919	119
42401343890000	WOOLLEY	3823		3867	44
42401312180000	MURPHY, W.L.	3826	3898	3932	105
42423320320000	OVERTON GAS UNIT #16	4097	4174	4203	106
42073310800000	BURNS, C. A.	3895	3968	4014	119
42073310900000	MIGL, A.F.	4099	4199	4253	154
42073303560000	BRUNO, D.B. II	4723		4793	70
42073308930000	HUGGER	5398	5545	5608	210
42073309430000	PRIEST	5352	5465	5523	170
42073306330000	TEMPLE-EASTEX A	5698	5766	5833	135
42001326660000	WORLEY	5092	5159	5236	145
42289319530000	SMITH, SHELBY A	7141	7207	7264	123
42289314070000	RED OAK (WOODBINE DE	6513	6552	6589	76
42289314730000	SANDEL-O.K. TAYLOR U	6015	6048	6137	122
42073305470000	MANESS	4629	4704	4765	136
42073304060000	NORMAN, SUMMERS	4394	4476	4540	146
42073306640000	PERKINS UNIT	4835	4940	4999	163
42073307240000	BOLTON ESTATE	5129		5208	79
42073301580000	LESTER, FRANCES	4691	4802	4883	192
42073303240000	CROCKETT, B. L.	4626	4742	4810	184
42073303910000	GILLESPIE	5101	5217	5297	196
42073303430000	BOLTON	5417	5503	5578	161
42073303280000	LONG	5735	5811	5883	149
42073303750000	NEW BIRMINGHAM MINER	5580	5699	5775	195
42401342580000	SEIF-RICHEY	4167	4280	4306	138
42401333800000	STOCKWELL	4909	5025	5055	146
42401318640000	SELPH UNIT NO. 1	4067	4113	4140	73
42401312420000	REKLAW GAS UNIT	4348	4424	4463	115
42401323460000	PERRY	3628	3701	3742	114
42401321710000	DICKERSON, ODIS	3707	3742	3764	58
42423316690000	GUTHRIE	4197		4247	50
42423320620000	ROACH, MARY	4395		4419	24
42423316950000	KICKAPOO CREEK GAS U	4378		4428	50
42423314060000	DEADMON	4420		4466	46
42423314150000	WISENBAKER, ROYCE	5442	5493	5546	104
42423317260000	WARE, J. F.	4310	4378	4438	127
42423319730000	CLOKE	4290	4344	4372	82
42423317600000	CITY OF TYLER	4658	4705	4753	95
42423322000000	JOHNSON, MIKE	5462		5524	62
42073308190000	MAXWELL	5263	5353	5425	162

42073307840000	CURTIS, H. F. A	5931	6001	6074	142
42073308490000	OPAL	5867	5940	6019	151
42073311450000	MCMOYLE	5113	5199	5264	152
42001323990000	M. IVES, ROBERT. JR.	5747	5782	5819	71
42001322200000	FAIRWAY /JAMES LIME/	5966	6005	6047	80
42001325430000	MCGEE	5935	5979	6016	80
42001325390000	GILLESPIE	5550	5577	5614	64
42001323250000	ROYALL NATIONAL BANK	6168	6216	6269	101
42001315930000	POLK, J.K.	6293	6398	6455	162
42161316940000	BURGHER G	4947		5044	97
42161318500000	HILL F	6111		6192	81
42161332890000	MCCAIN	5878		5962	84
42161310380000	CHILDRESS & KNOWLES	5980		6073	93
42161328290000	PICKENS A	5925		6019	94
42289313230000	CARTER A	6386	6429	6446	60
42289319520000	HAMILL FOUNDATION	6661	6703	6763	103
42289304810000	LIPSEY	6141	6191	6230	89
42289314670000	AROC ALLIED	6452	6492	6547	95
42289304480000	MOORE, MAXINE	6353	6394	6442	90
42289304790000	THRASH, AFTON	6454		6544	89
42289310070000	JOHNSON TRUST	6494	6530	6635	141
42423305530000	DENMAN A	4263	4350	4366	103
42423306140000	LURA MAY CHAPMAN G.U	5235		5295	60
42423311370000	RYAN, W. Z.	6129		6188	59
42401318290000	WILSON, AUGUSTA	3943		3988	45
42401320230000	HENRY SEXTON EST., O	3336		3356	20
42401322510000	TORKELSON	3417	3435	3449	32
42401343850000	MCWILLIAMS, J. GAS U	3512	3529	3539	27
42401342940000	CANNON, T. P. GU	3254		3277	22
42401336990000	ROGERS GAS UNIT	3417	3415	3436	19
42401309970000	KANGERGA, MICHAEL ET	3174		3196	22
42001308850000	TEMPLE-EASTEX	5831	5890	5961	130
42001315990000	DAVENPORT, H.S.	6275	6352	6407	132
42289303250000	CURTIS	7221	7253	7330	109
42289301000000	HAGEMEISTER, H. H.	6855	6885	6989	134
42289317940000	NORCOM	6542		6599	57
42289307330000	DONAHOE, JAMES	6486	6549	6658	172
42225300720000	WARNER GAS UNIT	6803	6857	6916	113
42225304140000	MOODY ESTATE	6703	6758	6830	127
42073301430000	SUMMERS	5697		5771	74
42073301500000	KEMPER	5573	5628	5695	122
42347314880000	SACUL A	4414		4466	51
42073313970000	DINGEE	6345	6440	6515	169

42073313660000	CHRONISTER HEIRS	5840	5927	5978	138
42347304470000	MANNING, E. J.	4777	4836	4873	96
42347318650000	CROSSMAN	5252	5272	5298	46
42347313680000	HANNAH, K. UNIT	5202	5256	5281	79
42347307750000	SITTON-MCLAIN	4374	4412	4444	70
42347322870000	TRAWICK GU 20	4041	4088	4114	73
42347316740000	SANDBAR	4582	4613	4635	54
42347331190000	CARGILL #1	4883		4886	3
42347332290000	WALLACE UNIT #2H	5405		5411	6
42347319390000	RED CLOUD #1	5048		5052	4
42005303500000	WINBO #1	7170		7179	9
42373304690000	W.T. CARTER NO. 1	18573		18850	277
42373304880000	ST REGIS PAPER CO	13858	13903	13960	102
42373305180000	JUNE CAIN #1	17555	17770	17829	275
42373305490000	WIRT DAVIS 2	16866		17189	323
42373306030000	TROSTMAN 1	15428		15630	202
42455303000000	JOYCE FOUNDATION NO.	9164	9216	9261	97
42455303120000	ROBINSON 1	8882	8922	8963	82
42455303570000	CAMERON 1	9519	9548	9609	91
42455303360000	M. A. MARTIN 1	10502	10546	10599	97
42455303520000	JOYCE FOUNDATION 1	8310	8361	8400	89
42455304270000	DARNELL ENTERPRISES	10247	10320	10381	134
42005303900000	HOSPITAL GAS UNIT 2	6617	6724	6775	158
42455000590000	ST. REGIS PAPER CO.	10024	10067	10135	111
42455000610000	ST. REGIS PAPER CO.	10211	10261	10317	106
42455300070000	TEMPLE INDUSTRIES	8005	8073	8089	83
42455302930000	RICHARDS, MARY E.	7705	7760	7808	103
42455302970000	TEMPLE 2	7821	7869	7911	90
42455303270000	TRINITY COUNTY LUMBE	11404	11453	11497	93
42455303310000	CAMERON MINERALS #1	10422	10462	10531	108
42455303700000	WOODLAKE	10186	10219	10260	75
42455304040000	BARNES, SAM UNIT	10143	10199	10242	98
42455304420000	USA 1	7760	7817	7849	89
42455304500000	TEMPLE 1	7768	7820	7853	85
42455305070000	TRINITY WALKER TIMBE	11396	11465	11539	143
42455800010000	CAMERON HEIRS 3	10233	10274	10331	98
42225304770000	CROWSON "A"	9033	9068	9109	76
42225305140000	TURNER "D"	6548	6600	6634	86
42225306510000	POTTER	7962	8013	8048	85
42225307080000	RIALS, M & IRA	6704	6740	6796	92
42225307670000	LOVELL, CLYDE	8673	8731	8769	97
42225308690000	GREEN, W.L.	8482	8542	8608	126
42225310300000	TEMPLE-INLAND II	5892	5986	6053	161

42225310550000	TEMPLE INDUSTRIES -B	6337	6430	6484	147
42225311190000	TEMPLE INLAND GAS UN	6477	6609	6658	181
42225313160000	CHANDLER	9473	9517	9600	127
42373300900000	DAVIS, WIRT UNIT	12899	12967	13007	109
42373301070000	CARTER BROS. 1	11861	11913	11963	102
42373301110000	SOUTHLAND PAPER MILL	12873	12958	12996	123
42373301120000	CARTER, W. T. 2	13349	13412	13453	104
42373301400000	DORRANCE 1	9546	9594	9621	75
42373302070000	BAILEY, ARBRA	12950		13087	137
42373303970000	DORRANCE 3	9514	9564	9596	82
42373304070000	DORRANCE 5	9364	9393	9425	61
42373304130000	CARTER, W. L. 8	13163	13220	13265	101
42373304160000	MURPHY, K. S.	9373	9416	9436	63
42373304230000	PLYWOOD, U. S.	9234	9282	9326	92
42373304560000	CARTER, W. T. ET AL	9398	9436	9451	52
42373304970000	DORRANCE 1A	10435	10452	10479	44
42373305100000	LUNSFORD, F. H. UNIT	9927	9955	9990	63
42373305240000	GLOVER, A.D. 1	16502		16783	281
42373305300000	CARTER, W. T. 3	10972	10994	11020	48
42373305550000	CARTER, W.T. "B"	14320	14396	14488	168
42373305560000	CAMERON MINERAL TRUS	10494	10557	10602	108
42373305790000	CAMDEN TIMBER CO.	15273		15488	215
42373305960000	SAGE ET, AL.	11313	11367	11410	97
42373310230000	ANICO UNIT	9144	9204	9221	77
42457300840000	EDWARD J. BRYANT ET	12717	12776	12847	130
42457301010000	CARTER-CAMDON	13229	13309	13378	149
42457301190000	ALLAN SHIVERS	11050	11068	11089	39
42457301380000	BROWN, M. J. FEE O/A	11142	11158	11180	38
42457301460000	MIXON GAS UNIT O/A	11318	11350	11374	56
42457301510000	KIRBY LUMBER CORP.	13250	13303	13347	96
42457302890000	ARCO FEE GAS UNIT	11852	11890	11919	67
42457302960000	CARTER, W.T. & BROS.	13912	13998	14056	144
42457303000000	CARTER, W. T. 2	13317	13384	13431	113
42457303120000	CARTER, W. T. 1	11787		11850	63
42457303150000	ARCO RICE UNIVERSITY	19020		19279	259
42457303220000	BUTTON	12969	13043	13083	114
42457303260000	CARTER, W. T. 2	10984	11002	11023	39
42457303380000	ARCO FEE	17916		18164	248
42457303520000	MCSHANE J.A. TRUST	16371		16618	247
42457303560000	CARTER HEIRS	14759		14960	201
42457303660000	CARTER, W.T. -C-	13710	13773	13838	128
42457303710000	KIRBY FOREST INDUSTR	14135	14222	14259	124
42457303820000	LONG BELL PETROLEUM	13645	13735	13789	144

42457303940000	LONGBELL PETROLEUM	13643	13734	13790	147
42457305420000	MOUTON ET AL	13608	13683	13744	135
42457305460000	HANKS, L.B. ET AL	13303	13361	13397	95
42005300020000	SESSIONS, J. W.	6213	6285	6337	124
42005300140000	CAMERON MINERALS GRO	6265		6271	6
42005300180000	CAMERON MINERALS GRO	6243		6262	19
42005301010000	CARTER BROTHERS ET A	9036		9109	73
42005301060000	OWENS ILLINOIS	6139		6145	7
42005301090000	BRYAN, J.A. GU	7153		7162	9
42005301150000	USA 12064	8805		8828	23
42005301160000	USA 12063	8782		8800	17
42005301350000	CARTER, W. T. EAST	9789		9804	15
42005301380000	CAMERON 1	6160		6167	6
42005301400000	ANGELINA COUNTY LUMB	8819		8834	15
42005301740000	SFM-TEMPLE EASTEX	8039	8089	8110	71
42005301750000	COUSINS, W. R.	7268	7343	7376	109
42005302150000	TEMPLE EASTEX 1	6258	6296	6314	55
42005302200000	ULEN G. MEDFORD UNIT	7499		7514	15
42005302210000	GALLOWAY 1	6104	6148	6174	70
42005302350000	CROSSMAN 1	6487	6575	6614	127
42005302660000	SESSIONS HEIRS 2	6050	6148	6169	119
42005303010000	SESSIONS, J.W. HEIRS	5923	6024	6045	122
42347002200000	WALLACE 1	5178	5248	5286	108
42347304590000	BYRD, J. W. ESTATE	5566	5647	5666	100
42347314660000	CHAMPION INTERNATION	5508	5576	5609	101
42347316460000	DR. WALKER	4056		4061	5
42347325500000	FULLER SALT WATER DI	4549		4559	9
42347329000000	WILL FORESTER GU 1	4747	4788	4808	61
42347329910000	GAMMAGE	4715		4726	11
42347331370000	MURRAY GAS UNIT	5373		5383	10
42347331560000	LEINART UNIT	5600		5605	5
42347332250000	GLASS ONION GU	4867		4875	8
42073303680000	LEWIE BYERS ET AL UN	4522		4667	145
42073304140000	WHITEMAN DECKER GU 1	5584	5652	5700	116
42073304400000	WHITEMAN, ET AL	5677	5773	5836	159
42073305460000	CROSSMAN, P.	6049	6118	6157	108
42073307910000	DECKER, MARSHALL	5750	5806	5860	110
42073312090000	SESSIONS, RUBE GU	6112	6203	6250	137
42073312180000	CHRONISTER HEIRS	5945	6002	6049	104
42073313190000	CROSSMAN, P.	6112	6206	6266	154
42073315560000	MINA 7	5640	5729	5810	170
42001004450000	CITY OF PALESTINE	6148	6237	6305	157

42001025460000	BOWERS	5515	5603	5660	145
42001300030000	JOHNSTON, L. C. UNIT	5366	5455	5517	151
42001312870000	HUEBEL, W. L.	6192	6298	6363	171
42001320020000	INTERNATIONAL PAPER	5378	5462	5517	140
42457304820000	CARTER, W. T.	12120	12175	12222	102
42457303450000	CARTER, W.T. -A-	14053	14134	14171	117
42013006710000	WEGNER ETAL GU	10234		10234	0
42013302760000	GUY S COMBS	6098		6098	0
42013311040000	HENDERSON	10161		10161	0
42013311590000	SMITH T W	9102		9102	0
42013314300000	ALBERT	9328		9328	0
42013317980000	TOM J L /A/ UNIT 2	10120		10120	0
42013318760000	RICHTER H UNIT	10110		10110	0
42013333840000	HENDERSON ETAL GAS U	10224		10225	1
42013333950000	HEINEN D D JR	7218		7219	1
42013334510000	EICHELBERGER E L	7558		7558	0
42013334900000	SMITH MARY CAROL TRU	10343		10343	0
42013335090000	SCHUMANN H A /A/ UNI	10029		10030	1
42013337930000	COUGHRAN THEODORE	7185		7185	0
42013338000000	MCDANIEL	8676		8676	0
42013338310000	STEWART N A ETUX	7222		7222	0
42013339160000	KINSEL	8689		8689	0
42013339240000	TOM J L /A/ UNIT 4	10209		10209	0
42013339260000	CAVAZOS	7261		7261	0
42013339280000	SUMMERS	7640		7640	0
42013339400000	HOWARD-BRAUN	8729		8729	0
42013339790000	KELLNER ETAL GU	10467		10467	0
42013339820000	SCHUMANN `A` UNIT 1	10242		10242	0
42013339890000	WEGNER ETAL GAS UN	10378		10378	0
42013339910000	LIEKE OTTO GAS UNIT	10005		10005	0
42013339920000	TARTT EMMA ETAL	10216		10216	0
42013339930000	KINSEL	8708		8708	0
42013340060000	SCHUMANN H A UNIT /A	10307		10307	0
42013340070000	WISEMAN	6040		6040	0
42013340090000	RICHTER	9948		9948	0
42013340170000	URBANCZYK L T UN 3	9943		9943	0
42013340230000	KING UNIT	9190		9190	0
42013340260000	HENDERSON ETAL UNIT	10328		10328	0
42013340270000	HENDERSON ETAL GAS U	10390		10390	0
42013340300000	URBANCZYK L T GAS UN	9890		9890	0
42013340310000	TOM J L -A- UNIT 2	10000		10000	0
42013340330000	SARAH E FERRY UNIT	7800		7801	1
42013340340000	SCHUMANN H A B UNIT	10341		10341	0

42013340400000	HURT W T ETAL	10416		10416	0
42013340430000	WEGNER ETAL GAS UNIT	10390		10390	0
42013340510000	BURGER T H	7873		7873	0
42013340720000	TARTT EMMA ET AL	10393		10393	0
42013341030000	SMITH M C	10370		10370	0
42013341180000	DE ATLEY M K	10668		10668	0
42013341240000	GEROLD M C	10575		10575	0
42013341420000	HENDERSON ETAL UNIT	10477		10477	0
42013341590000	SCHUMANN ETAL GAS UN	10667		10667	0
42013341900000	SMITH MARY CAROL TRU	10355		10357	2
42013341970000	HURT W T ET AL	10280		10280	0
42013342910000	TARTT EMMA	10601		10600	-1
42013343230099	TOM EDMUND 02 PILOT	10606		10606	0
42013343390099	CHAPMAN PFEIL UNIT	10888		10888	0
42013346057000	WYE RANCH 01	10129		10129	0
42025309060000	J E BOONE ETAL	13105		13106	1
42123302090000	F WARWAS	13648		13655	7
42123308790000	RESPONDEK UNIT	13657		13660	3
42123310090000	MIXON	13847		13855	8
42123310220000	KLAEVEMANN C	13706		13715	9
42123311390000	SCHROEDER A&H	13452		13468	16
42123311620000	MILLER	12007		12030	23
42123311980000	KRAUSE	12581		12605	24
42123317500000	SMITH GAS UNIT #1	13663		13670	7
42123317930000	RED CREST TRUST	13918		13918	0
42123320140000	WAGNER GAS UNIT	13920		13920	0
42123320900000	COSTLOW GAS UNIT	13950		13950	0
42123320980000	MENN GAS UNIT	13748		13752	4
42123321010000	EICHHORN GAS UNIT	14079		14079	0
42123321930000	HOOKS	13068		13088	20
42123322550000	FRIEDRICHS GAS UNIT	13930		13930	0
42123322810000	THIEME GAS UNIT 1	14011		14014	3
42123322847000	KRAUSE	12933		12956	23
42123323097000	MUIR A	12924		12946	22
42123323290099	RESSMAN PILOT	13632		13640	8
42123323780000	GIPS 01	14103		14103	0
42123324067000	LESKE-LOTT UNIT	13149		13168	19
42123324257000	ORMAND A	13679		13694	15
42123324377099	BARROW 01	13903		13909	6
42123325547000	BOENING UNIT	13313		13336	23
42123325907000	PEDRAZA 01	14157		14157	0
42123327187000	MUELLER JO ANN 01	14066		14074	8
42123330520000	JANAK	13062		13085	23

42123338730000	MEDINA UNIT	12696		12720	24
42149304190000	ROBIN UNIT	9308		9331	23
42149304390000	HUFF /A/ UNIT	8829		8850	21
42149304760000	MINYARD UNIT	9968		9997	29
42149304860000	HOLLIEN UNIT	10295		10324	29
42149309920000	ROSABELLE RAY UNIT	8205		8226	21
42149310060000	RIGHTMER /B/	9612		9641	29
42149310190000	WISEMAN-NOVAK UN	9909		9930	21
42149310330000	THEIDE	7117		7131	14
42149311370000	FLORUS	7674		7691	17
42149332307000	PROST UNIT A	11152		11180	28
42149332350000	ARNIM `A` UNIT	10195		10221	26
42149332620000	SANTE UNIT A	11686		11713	27
42149333187000	SANTE NORTH UNIT	11326		11353	27
42149333330000	PROST UNIT O	11455		11481	26
42177302030000	H P ORTS	7758		7767	9
42177303940000	SCHAUER F T ETAL	8151		8160	9
42177305180000	LANG	9027		9048	21
42177305300000	STAMPORT ROBERT	7699		7709	10
42177305480000	SPENCER UNIT	8155		8170	15
42177305540000	THOMPSON UNIT	10367		10390	23
42177305810000	JOHNSON	9454		9472	18
42177305990000	JUDY	10504		10528	24
42177306180000	GATLIN	8622		8635	13
42177306220000	MAGEE MOLLIE	11194		11210	16
42177306450000	HAJEK GEORGE	9971		9992	21
42177306780000	DIXON FOUNDATION	11478		11502	24
42177307020000	HAMILTON R C	7870		7875	5
42177307170000	AUSTIN WILLA W	9873		9895	22
42177307250000	NIXON LILLIE	7994		8004	10
42177307400000	SIEVERS WALTER A	9803		9825	22
42177307800000	HILBRICH EDWIN ETUX	11669		11692	23
42177307820000	HINES UNIT	8564		8578	14
42177307840000	SHEFFIELD	8166		8173	7
42177307900000	CUSACK ANN ETAL OU	10512		10538	26
42177308310000	MANFORD L M	8445		8453	8
42177308440000	BOYSEN	6860		6870	10
42177308840000	DEACON	7885		7898	13
42177308890000	BURT VIVIAN CARTER	10135		10158	23
42177308930000	WOOD UNIT	8031		8042	11
42177308980000	JONES MARY LOU	9142		9160	18
42177309080000	DRESCH	8103		8117	14
42177309200000	KELLY LEONA ETAL	8801		8814	13

42177309390000	CLARK	8587		8600	13
42177309400000	NORRIS T M	7611		7615	4
42177310310000	GANNON UNIT	8415		8428	13
42177310320000	STEFANIE	10842		10868	26
42177310330099	CANNONADE	9476		9494	18
42177310520000	CANNONADE	9359		9378	19
42177310570000	LESSOR J L	9379		9395	16
42177310700000	KALKA ALICE M	7364		7374	10
42177310800000	MOHRMANN UNIT	8315		8333	18
42177311010000	KUHEN ZANIE	9499		9518	19
42177311430000	WARD ETAL	9359		9375	16
42177311580000	WORTHINGTON JEWEL ET	8623		8635	12
42177312540000	JONES	7830		7840	10
42177312620000	LOCKSTEDT UNIT	8376		8391	15
42177312740000	GILBREATH UNIT	8077		8093	16
42177312860000	STEINER UNIT	7820		7831	11
42177313240000	WILSON	7968		7979	11
42177314510000	LESTER J B	8075		8083	8
42177315540000	BAKER SHELBY	8130		8140	10
42177315760000	SPIEKERMANN	11520		11547	27
42177315920000	VALENTA	8672		8688	16
42177315970000	JARMON H T ET AL	11334		11363	29
42177316060000	NAGEL MILDRED ETAL U	8193		8206	13
42177316250000	HARRIS	8502		8517	15
42177316260000	PECK	8925		8943	18
42177316410000	PLOEGER	6938		6943	5
42177316650000	ANDREW /B/	8563		8577	14
42177316750000	DEACON	7948		7960	12
42177316800000	HELGA	10222		10246	24
42177317030000	EILERT MYRTLE K	8843		8860	17
42177317070000	MALAER ETAL GAS UNIT	11555		11581	26
42177317260000	KING HOWARD	8530		8541	11
42177317370000	ALI-O UNIT	8784		8801	17
42177317530000	BARTA /C/	8899		8915	16
42177318460000	CAMPBELL-HAHN UN	11700		11720	20
42177318860000	ALLEN DORIS	10240		10260	20
42177319600000	DUBOSE /A/	11716		11739	23
42177319650000	ALLEN DORIS	9825		9845	20
42177319800000	BORCHERS-HILBRICH-GA	11879		11900	21
42177319910099	GATTI-REILLY UNIT PI	11514		11540	26
42177320180000	PATILLO	8769		8778	9
42177320190000	KOSAREK	8756		8765	9
42177320500000	BAROSH	11180		11207	27

42177320510000	BAKER UNIT	11661		11683	22
42177320800000	KELLY	11177		11202	25
42177320890000	CUSACK-CLAMPIT UNIT	11363		11390	27
42177320940099	KOENNING UNIT	11212		11235	23
42177320977000	BARNHART EF	10066		10090	24
42177320980099	BARNHART EF	9735		9754	19
42177321250099	HAGEN EF	9154		9172	18
42177321540099	BOZKA PILOT	10791		10820	29
42177322667000	CRABB RANCH	9329		9349	20
42177322910099	PATTESON	7436		7440	4
42177323527000	BERGEY-BOENING UNIT	11455		11482	27
42177324460000	CULPEPPER UNIT	9137		9148	11
42177324947000	BARNHART EF	9450		9469	19
42177325310000	WARD E	9103		9118	15
42177325747000	BORCHERS O D	9286		9305	19
42177326677000	WARD F	9717		9735	18
42177326757000	CHILDRESS	8921		8930	9
42177327787000	BROLL	11971		11992	21
42177335780099	BOBCAT	8326		8337	11
42177336987099	CYCLONE PILOT	8913		8929	16
42255302280000	TIPS B B	13372		13372	0
42255305980000	BEN A PAWELEK A	10434		10442	8
42255306570000	IDA P CARROLL	12980		12984	4
42255307140000	PATTON	8168		8168	0
42255307930000	KORTH	9095		9100	5
42255307940000	JARZOMBEK FABIAN L	8668		8668	0
42255308500000	MZYK UNIT	8956		8957	1
42255310430000	RIEDEL	9998		10010	12
42255310680000	FOEGELLE ADRIAN	10628		10636	8
42255310740000	GREEN HIX	13583		13590	7
42255311230000	HENDERSON MARY	10700		10700	0
42255311380000	URBANCZYK	10425		10430	5
42255311400000	KELLNER ETTA L	10420		10420	0
42255311700000	JOHNSON HARDING	12955		12960	5
42255311770000	WIATREK	10769		10780	11
42255311820000	YANTA GUSSIE	10440		10444	4
42255311950000	CARROLL IDA P	12970		12978	8
42255312840000	HANDY SUE	12962		12970	8
42255313100000	EDWARDS	12900		12905	5
42255313140000	ROLF ESTELLE GAS UNI	13021		13021	0
42255313680000	BLACKWELL	13622		13630	8
42255313700000	DAVILA	13714		13720	6
42255313770000	CAMERON-LEE	10621		10621	0

42255314010000	WESSENDORFF	13400		13400	0
42255314380000	KELLNER ETAL GU	10464		10464	0
42255314460000	KELLER ETAL GAS UNIT	10518		10518	0
42255314710000	SAVANNAH -FRIEDA PAR	13053		13060	7
42255314880000	CLARK-HABY UNIT	10809		10810	1
42255315050000	WERNLI GAS UNIT 1	13039		13043	4
42255315520000	YANTA EDWIN	10691		10695	4
42255315640000	FOEGELLE ADRIAN	10664		10670	6
42255315750000	PAWELEK MIKE UNIT	10579		10583	4
42255315770000	WESSENDORFF GAS UNIT	13385		13385	0
42255315860099	KOWALIK228-1 PILOT	11911		11911	0
42255316080099	MILTON PILOT	10568		10579	11
42255316140099	USZYNSKI GAS UNIT 1	13375		13375	0
42255316350000	HANDY	13292		13300	8
42255316510099	JOG UNIT 1 PILOT	10979		10988	9
42255317670000	COATES `A`	9930		9930	0
42255317890099	GEORG EF PILOT	8649		8656	7
42255319480099	MENSIK PILOT	13173		13180	7
42255322020000	VICTORIA UNIT	10415		10423	8
42255326970000	GILLETT SWD	8930		8934	4
42255350240099	JANSEK-ECLETO	10896		10900	4
42285315410000	KREJCI EUGENE	11472		11500	28
42285323317000	OLBRICH UNIT	12722		12746	24
42285335850099	GEORGE HUNTER PILOT	12076		12102	26
42285335910000	WELHAUSEN A	12869		12893	24
42285335980099	STEFANIE UNIT	12759		12783	24
42285336187000	CAROL UNIT	12234		12260	26
42285336707000	OLSOVSKY UNIT	12142		12164	22
42285336790000	FOJTIK UNIT	12159		12187	28
42285337327000	PROST UNIT G	11054		11080	26
42285337337000	PROST UNIT H	11437		11464	27
42285337580000	RONYN UNIT	12423		12451	28
42285337607000	MARCIA UNIT	12958		12982	24
42285338027000	BERGER UNIT	11958		11983	25
42285338077000	ROOSEVELT UNIT	11108		11132	24
42285338540000	NANCY	12877		12901	24
42285339970000	KUDU HUNTER	10605		10629	24
42297318580000	EDWARD B STURCKEN	11452		11452	0
42297346210000	KUNDE 1 GAS UNIT	11664		11664	0
42297347470000	BAKER FAMILY TRUST	12330		12330	0
42297348030000	OLSON MARLENE	12334		12334	0
42297350470000	902 LIMITED UNIT A	11300		11300	0
42493302360000	F W MARTIN	6100		6100	0

42493307200000	EHLER ARTHUR E UNIT	8913		8913	0
42493307360000	MOCZYGEMBA UNIT	8695		8695	0
42493307400000	NOLL EMMETT UNIT	8606		8606	0
42493307530000	KOPECKI C	7407		7407	0
42493307610000	JASKINIA FRED	8341		8341	0
42493307720000	HEINSOHN-KREBS OIL	8448		8449	1
42493308250000	MANFORD	6750		6750	0
42493308410000	ZAIONTZ PETER	8659		8659	0
42493308450000	HIERHOLZER W A	8940		8940	0
42493308810000	HASSEL J F	7383		7383	0
42493309550000	BATES HUBERT L ETAL	6479		6479	0
42493309630000	A D D CORP	8462		8462	0
42493309820000	KOPECKI E M	8417		8417	0
42493309950000	OLD KING COLE UN	6300		6300	0
42493310160000	FLIELLER C	6236		6236	0
42493310240000	MENGDEN P ETAL	8285		8285	0
42493310360000	KOLLODZIEJ	8445		8445	0
42493310610000	SWIENTEK THEODORE	6261		6261	0
42493310770000	FLIELLER CLIFTON	6215		6215	0
42493310960000	DUGOSH FRANK	8529		8529	0
42493311040000	PRUSKI-TALBERT OIL U	8523		8523	0
42493311120000	SCHIFFERS MARY ROSE	6855		6855	0
42493311510000	HAVERLAH WILLIAM C	6198		6198	0
42493312550000	THOMS-WILSON	7742		7742	0
42493312630000	MUTZ PHILLIP	6095		6095	0
42493315130000	DOEGE FELIX	6370		6371	1
42493316000000	COPELAND W E ESTATE	6810		6810	0
42493316210000	KOETHER	8101		8101	0
42493316570000	COPELAND W E ESTATE	6663		6663	0
42493317270000	COMPTON	6446		6446	0
42493317500000	BYRD K W	6385		6385	0
42493317560000	MARTINEZ RENATO	6542		6542	0
42493317790000	BLUEBONNET	6294		6294	0
42493318190000	KOTZUR EDMUND	6765		6765	0
42493318290000	PROSPER LABUS UNIT	7893		7893	0
42493318380000	CASARES UNIT	7618		7618	0
42493318420000	OLENICK	6393		6393	0
42493318520000	JASKINIA FRED	6316		6316	0
42493318670000	WIATREK UNIT	7547		7547	0
42493319100000	SCHIFFERS RANCH	7227		7227	0
42493319370000	SCHIFFERS RANCH	7215		7215	0
42493319620000	CHANDLER E H	6869		6869	0
42493319640000	ESCHENBURG R L II /B	6459		6460	1

42493319680000	HAGEE	7636		7636	0
42493319850000	LDB UNIT	7340		7340	0
42493319920000	WALL DARDEN	7276		7276	0
42493320100000	JARZOMBEK ALICE	7194		7194	0
42493320140000	NOLL	8415		8415	0
42493320180000	SCHIFFERS RANCH	7304		7304	0
42493320410000	COPELAND W E /C/ EST	6825		6826	1
42493320420000	PUNDT	6343		6343	0
42493320550000	CARROLL R J /A/	6647		6647	0
42493320730000	IRVIN	7813		7814	1
42493320900000	CASARES	6430		6430	0
42493320920000	ESCHENBURG R L II /D	6409		6409	0
42493321000000	LEHMANN UNIT	5302		5303	1
42493321410000	PREISS E A	6348		6348	0
42493321600000	KIDD-BROWN UNIT	5304		5304	0
42493321790000	SETLIFF	5600		5600	0
42493321820000	BRYAN	6134		6135	1
42493321830000	THOMS	7690		7690	0
42493321890000	THOMS B	7650		7650	0
42493321900000	THOMS	7604		7604	0
42493322040000	ESCHENBURG R L II	6400		6401	1
42493322060000	LEHMANN UNIT /A/	5279		5279	0
42493322270000	BROLL HENRY JR	6243		6243	0
42493322390000	WIATREK	6918		6918	0
42493323310000	THOMS /C/	7575		7575	0
42493323620000	PROSPER LABUS	7810		7810	0
42493324000000	CARROLL JOHN TRUSTEE	6622		6622	0
4249332550700	WARNKEN	8213		8213	0
42493325560099	HAESE	8315		8315	0
42493325987000	MOCZYGEMBA A-436	8429		8429	0
42493325997000	ZAIONTZ	7869		7869	0
42471303090000	PURE RESOURCES	11299		11425	127
42471302330000	GIBBS BROTHERS	11151		11325	174
42471302680000	CHAMPION INTERNATION	10454		10599	145
42471303670000	LONE RANGER	10932		11051	119
42471303740000	COLBURN UNIT	10507		10631	124
42471000740000	W.D. MCADAMS	10572		10717	146
42407304240000	HORIZON PROPERTIES	12158		12313	154
42407304140000	HORIZON PROPERTIES	12370		12517	147
42347327220000	SCHWIEM 7	5184	5244	5278	95
42471303750000	CHESTER	13750		13904	154
42001313260000	MILLS, J. W.	6316	6399	6454	138
42457305340000	CLEMENTS, HALLY ET A	13423	13448	13498	75

42457305400000	SHEPHERD ET AL	13348	13373	13401	53

VITA

Personal	Joshua Escobedo Davidson Fort Worth, Texas Son of David and Gloria Davidson Brother to Michael Davidson and Danielle Davidson Cubellis
Education	Bachelor of Science in Geology, 2017 Texas Christian University, Fort Worth, Texas
	Master of Science in Geology, 2023 Texas Christian University, Fort Worth, Texas
Experience	Petroleum Landman, Twin Creek Resources June 2017 – Present
	Teaching Assistant, Texas Christian University August 2019 – May 2020

Abstract

Identifying the Sediment Source of The Lower Cenomanian Maness Shale

By Josh Davidson, M.S., 2023

Department of Geological Sciences

Texas Christian University

Thesis Advisor: Richard Denne, Hunter Enis Chair in Petroleum Geology

The Maness Shale is a clay-rich mudrock that marks the transition from a carbonate platform to a siliciclastic-dominated shelf at the inception of the Woodbine succession within the east Texas region of the Gulf Coast Basin. Although the Maness has not traditionally been regarded as a hydrocarbon source or reservoir rock within a lithostratigraphic context, using a sequence stratigraphic approach reveals the possibility of the Maness interval serving as both a source and reservoir rock in specific areas. Prior research investigated the Maness Shale within the vicinity of the San Marcos Arch, the East Texas Basin, and up to the western flank of the Sabine Uplift. However, none of these studies extended to the south of the Sabine Uplift, nor did they definitively identify the sediment source. Therefore, this study aimed to identify the sediment source of the Maness and to evaluate its potential as a source rock based on organic matter content.

Identifying the sediment source involved the analysis of 338 raster well logs spanning nine counties (Rusk, Cherokee, Anderson, Houston, Trinity, Tyler, Polk, Angelina, and Nacogdoches) and the correlation of four horizons (Top of the Buda, Top of the intra-Maness, Top Maness, and Base of the Austin Chalk). The results yielded two structural maps, four isochore maps, three net sandstone maps, and one isochore map that combined the results from this and previous studies of the Maness. The maps indicate that the upper Maness interval, which was previously referred to as the lower Woodbine in studies by Ambrose et al. (2009), is dominated by a coarsening upwards sand package just west of the Sabine Uplift, suggesting a deltaic depositional environment. They also reveal pro-deltaic muds west of the Sabine Uplift in the East Texas Salt Basin, a bypass zone between the Houston Arch and the Lower Cretaceous shelf margin, and sand-rich slope deposits near the shelf margins. Conversely, the lower Maness interval is mainly characterized by shale, which drapes over the Buda Limestone throughout the study area. The results suggest that the sediment source for the lower Maness is located to the north of the study area, whereas the upper Maness has a deltaic sediment source just west of the Sabine Uplift but a primary source to the north, possibly originating from the Ouachita Highlands.

Passey's Δ log R method was applied to estimate organic richness in 5 wells using a sonic/resistivity overlay. TOC wt.% values were estimated by using the local geothermal gradient to estimate effective heating time and the Level of Organic Metamorphism (LOM). The findings indicate some potential within the Maness interval, yet they do not offer sufficient evidence to categorize the Maness as a viable source rock in the examined wells.